

*Physical Properties of Minerals: How and Why to Dive Into their Knowledge*  
Brixen, February 15<sup>th</sup>, 2018

**LONG- VS. SHORT-RANGE PROPERTIES  
ALONG BINARY SOLID SOLUTIONS:  
THE INTERPLAY BETWEEN X-RAY DIFFRACTION  
AND ABSORPTION SPECTROSCOPY**

Matteo Ardit (rdmtt@unife.it)  
*Department of Physics and Earth Sciences*  
*University of Ferrara*

# PREMISE

An understanding of a crystal structure at the atomic scale is a fundamental part of the Mineralogical Sciences.

Experiments at non ambient conditions are routinely employed to investigate the crystal structure of a mineral or a synthetic analogue to interpret their structural variations by means of the so-called “*comparative crystal chemistry*”.

Nevertheless, in addition to the main external variables (*i.e.*, temperature  $T$ , pressure  $P$ , and partial pressure of the atmosphere  $P_{\text{H}_2\text{O}}$ ), **chemical composition** ( $X$ ) –considered as an internal variable also known as "chemical" or "internal" pressure– plays a key role in determining the intrinsic features of a crystal structure.

# BACKGROUND OF THIS LECTURE

*Some year ago...*

... project to explore oxide and silicate structures as ***promising ceramic pigments***.

Enhanced coloring performance (+ lowering of production costs and toxicity) with respect to traditional colorants, by realizing solid solutions of known structures doped with *transition metal ions (TMI e.g., Cr<sup>3+</sup>, Co<sup>2+</sup>)* hosted at 6- or 4-fold coordinated sites.

Investigated structures:

alumoniobite  $(\text{Al}_{1-x}\text{Cr}_x)\text{NbO}_4$ ;

melilite  $(\text{Ca,Sr,Ba})_2(\text{Mg}_{1-x}\text{Co}_x)\text{Si}_2\text{O}_7$ ] or  $[(\text{Ca,Sr})_2(\text{Zn}_{1-x}\text{Co}_x)\text{Si}_2\text{O}_7]$ ;

perovskite  $[\text{Y}(\text{Al}_{1-x}\text{Cr}_x)\text{O}_3]$ ;

pyrophosphate  $\text{Na}(\text{Al}_{1-x}\text{Cr}_x)\text{P}_2\text{O}_7$ ;

spinel  $(\text{Zn}_{1-x}\text{Co}_x)\text{Al}_2\text{O}_4$ ;

willemite  $[(\text{Zn}_{1-x}\text{Co}_x)_2\text{SiO}_4]$ .

# BACKGROUND OF THIS LECTURE

Three fundamental aspects to take into account:

- (I) accommodation process and the structural environment of ***substituting ions*** at specific crystallographic sites (along binary ***solid solutions***);
- (II) ***long-range*** structural investigation of the host structure by means of ***X-ray powder diffraction***;
- (III) ***short-range*** investigation of ions accommodated at coordination polyhedra (*i.e.*, at ***local scale***) by means of ***optical spectroscopy***.

Convolution of the above mentioned aspects: comparison between mean (long-range) and local (short-range) bond lengths (in the “*environment*” at which the substitution takes place) provides information on the **structural relaxation**, *i.e.* by definition:

***“mismatch between mean (diffraction) and local (spectroscopy) bond distances of a crystal structure along a solid solution”***

## SUGGESTED TEXT BOOKS AND READING

- Andrut *et al.* (2004): Optical absorption spectroscopy in geosciences. Part II: Quantitative aspects of crystal fields. In "Spectroscopic methods in mineralogy", *EMU Notes Mineral.*, **6**, 145.
- Burns (1993): Mineralogical applications of crystal field theory (2<sup>nd</sup> Ed). Cambridge University Press, 576 p.
- Faure (1997): Principles and applications of geochemistry (2<sup>nd</sup> Ed). Pearson Education, 625 p.
- Misra (2012): Introduction to geochemistry: Principles and applications. Wiley-Blackwell, 452 p.
- Putnis (1992): Introduction to mineral sciences. Cambridge Univ. Press, 480 p.
- Rossmann (2014): Optical Spectroscopy. *Rev. Mineral. Geochem.*, **78**, 371.
- Wildner *et al.* (2004): Optical absorption spectroscopy in geosciences. Part I: Basic concepts of crystal field theory. In "Spectroscopic methods in mineralogy", *EMU Notes Mineral.*, **6**, 93.

# Part I

- a. Overview on the chemical bonding
  - a1. Ionic bond approximation: potential energy ( $E_p$ )
  - a2. Coordination number
  - a3. Ionic radius ratio
  
- b. Ionic substitutions
  - b1. Goldschmidt's rules
  - b2. Exceptions and Limitations
  - b3. Ringwood's rule
  - b4. Other limitations
  - b5. Classification of solid solutions
    - b5.1. Substitutional ss
    - b5.2. Interstitial ss
    - b5.3. Omission ss

## a. OVERVIEW ON THE CHEMICAL BONDING

Formation of a stable mineral or chemical compound:

*the combination of two or more atoms (ions) is energetically favored with respect to their isolated state*

**Chemical bonds**: interatomic net attractive forces that hold atoms together; usually involve only the *valence electrons*.

Much of the chemical bonds in minerals belong to:

- (i) **ionic bonds** - transferring of one or more electrons between;
- (ii) **covalent bonds** - sharing of electrons between ions (orbitals overlap).

Other types of bonds:

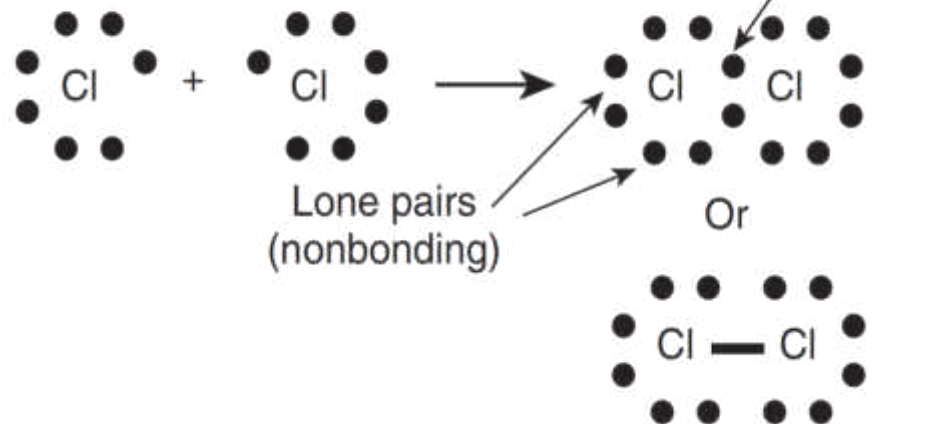
**metallic**, **Van der Waals**, and **hydrogen bonds**.

Lewis dot representation  
•  $e^-$  in the outermost shell

Ionic bonding in NaCl

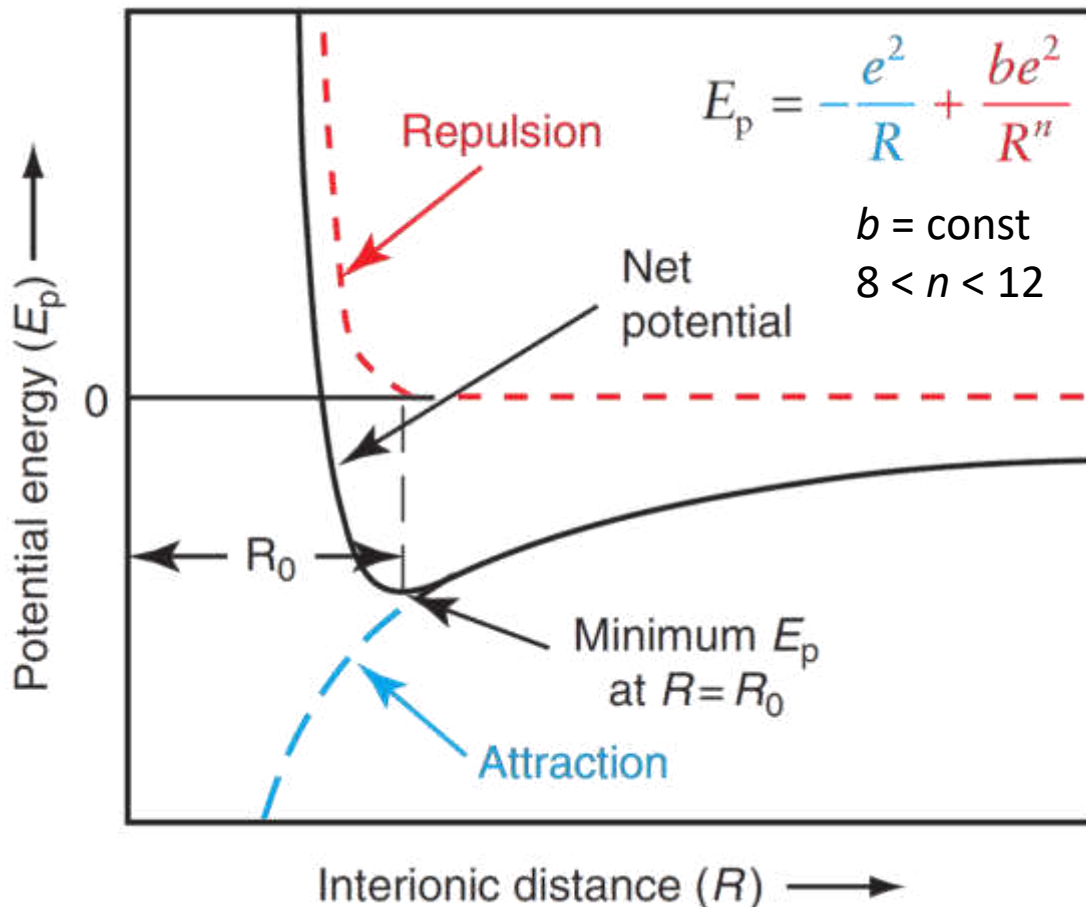


Covalent bonding in  $\text{Cl}_2$



# a1. IONIC BOND APPROXIMATION: POTENTIAL ENERGY ( $E_p$ )

In a cation-anion system, the variation of the **potential energy** ( $E_p$ ) is function of the interatomic distance.



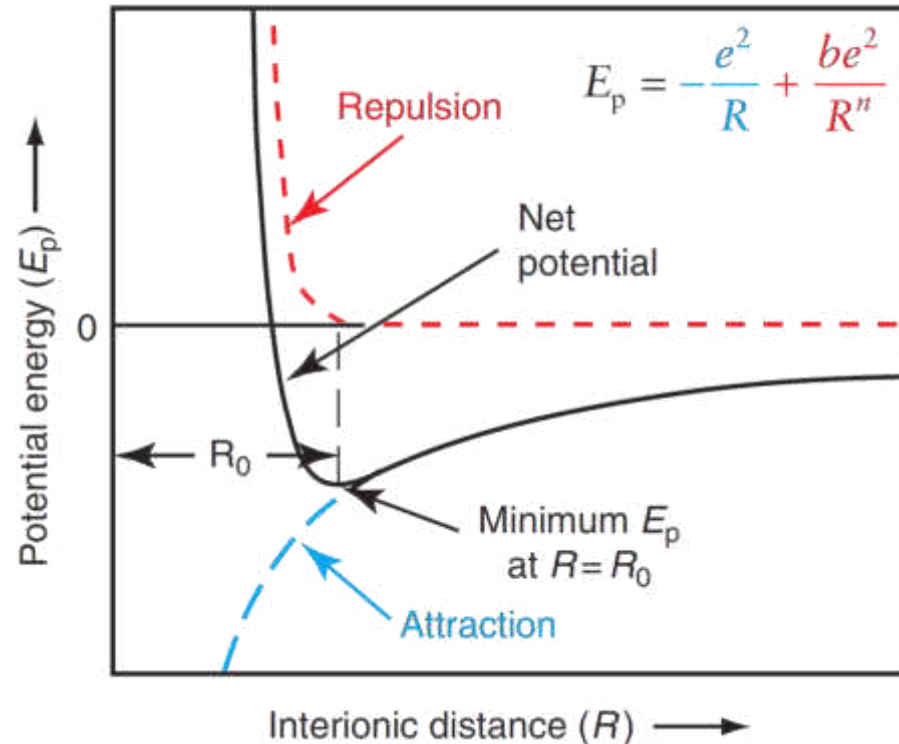
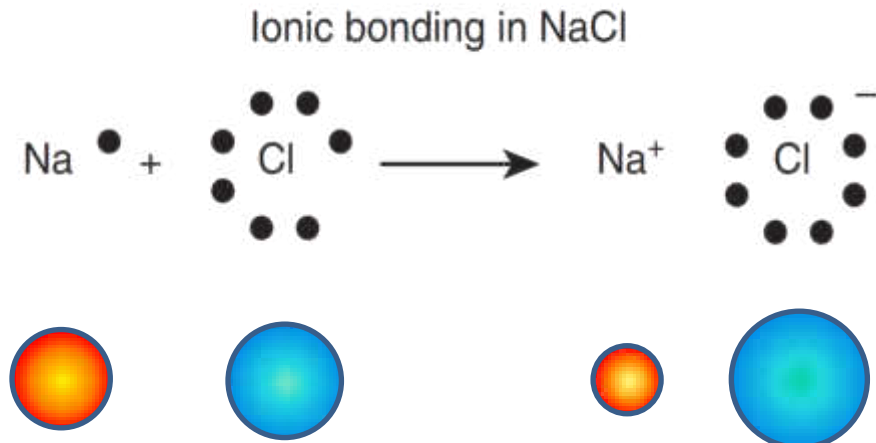
$R_0$  = equilibrium interatomic distance reached at the minimum value of  $E_p$  (i.e., when  $dE/dR = 0$ ).

For  $R > R_0$ ,  $E_p$  is determined by the (Coulomb) attraction between the opposite charges.

For  $R < R_0$   $E_p$  is determined by the (Pauli) repulsion between the nuclei and the electron clouds.

# a1. IONIC BONDING: POTENTIAL ENERGY ( $E_p$ )

The curve for  $E_p$  is typical of all atomic-molecular systems  
introductory concept of interatomic distance and (*lato sensu*) ionic radius.



## a2. COORDINATION NUMBER

For a given set of ions, the most stable arrangement is the one that has the lowest  $E_p$

For a **maximum stabilization** of a crystal **structure**:

- (1) The crystal structure must be electrically neutral;
- (2) The cation–anion separation must be close to the interatomic distance  $R_0$ ;
- (3) The arrangement of the ions treated as spherical balls packed as closely as possible.  
In a given 3D close packing of spheres, the number of oppositely charged nearest neighbors surrounding an ion is called its **coordination number (CN)**.

(e.g., if an ion  $A$  is surrounded by 4 ions of  $B$ ,  $CN_A = 4$  (tetrahedral coordination); if  $A$  is surrounded by six ions of  $B$ ,  $CN_A = 6$  (octahedral coordination), and so on)

Generally, cations are smaller than anions, so the number of anions that can be packed around the smaller cations determines the crystal structures.

### a3. IONIC RADIUS RATIO

The combined influence of cations and anions on coordination number can be predicted by the magnitudes of their radii expressed as *radius ratio* ( $RR$ ).

$$RR = r_c / r_a, \text{ where } r_c \text{ and } r_a \text{ are ionic radius of the cation and the anion, respectively.}$$

On a model based on close packing of spheres, the *critical radius ratios* for different geometrical arrangements of spheres:

$$RR < 0.155 \text{ for } CN = 2;$$

$$0.155 < RR < 0.225 \text{ for } CN = 3 \text{ (trigonal coordination);}$$

$$0.225 < RR < 0.414 \text{ for } CN = 4 \text{ (tetrahedral or square planar coordination);}$$

$$0.414 < RR < 0.732 \text{ for } CN = 6 \text{ (octahedral coordination);}$$

$$0.732 < RR < 1.0 \text{ for } CN = 8 \text{ (body-centered cubic coordination);}$$

$$RR > 1.0 \text{ for } CN = 12 \text{ (edge-centered cubic coordination).}$$

In minerals, the most common anion is  $O^{2-}$ , which has an ionic radius of  $1.40 \text{ \AA}$ , and the ionic radii of most common cations are between  $0.60$  and  $1.10 \text{ \AA}$ . Thus, the  $RR$  with oxygen in minerals mostly lie between  $0.43$  and  $0.79$ , suggesting that the most frequent  $CN = 6$ .



## b. IONIC SUBSTITUTIONS

Most rock-forming minerals are dominantly ionic compounds. They exhibit a considerable range in chemical composition.

**Deviation from their ideal chemical composition occurs due to incorporation of minor amounts of foreign ions into the lattice, primarily by ionic substitutions.**

The ability of different elements to occupy the same lattice position in a particular crystal structure is called *diadochy*.

**Example:** Mg, Fe, Mn, and Sr are diadochic in the structure of calcite ( $\text{CaCO}_3$ ) because they can substitute for Ca in this structure.

The formation of a **solid solution** can be explained by simple rules regarding atomic size, crystal structure, valence, and electronegativity factors.

**note:** equivalent concepts (in this class)

the formation of a solid solution (solid state miscibility) is due to the phenomenon of the diadochy (ionic substitution, vicariance).

## b1. GOLDSCHMIDT'S RULES

Certain elements in minerals show a preferential association (*geochemical coherence*) because ions of such elements substitute easily for each other.

Goldschmidt: the first to propose a series of rules governing the mutual replacement of ions in minerals (under the assumption of a pure ionic bonding).

### *Goldschmidt's rules of substitution*

1. If two ions have the **same radius** and the **same charge**, they would enter into solid solution in a given mineral with equal ease, in amounts roughly proportional to their abundances.

The ionic radii must not differ by more than 15%; substitution is limited or rare if the radii differ by 15% to 30%, and nonexistent if the difference is more than 30%.

**Example:** the common substitution of  $\text{Ta}^{5+}$  (0.64 Å) for  $\text{Nb}^{5+}$  (0.64 Å),  $\text{Hf}^{4+}$  (0.71 Å) for  $\text{Zr}^{4+}$  (0.72 Å),  $\text{Ga}^{3+}$  (0.62 Å) for  $\text{Al}^{3+}$  (0.54 Å), and  $\text{Fe}^{2+}$  (0.78 Å) for  $\text{Mg}^{2+}$  (0.72 Å) in many silicate minerals.

## b1. GOLDSCHMIDT'S RULES

2. When two ions possessing the **same charge** but **different radii** compete for a particular lattice site, the ion with the smaller radius would be incorporated preferentially because it forms a stronger ionic bond.

**Example:** during magmatic crystallization, for example, the earlier formed olivine [(Mg, Fe)<sub>2</sub>SiO<sub>4</sub>] tends to be enriched in Mg<sup>2+</sup> (0.72 Å) relative to Fe<sup>2+</sup> (0.78 Å).

3. When two ions having **similar radii** but **different charges** compete for a particular lattice site, the ion with the higher charge would be incorporated preferentially because it forms a stronger ionic bond.

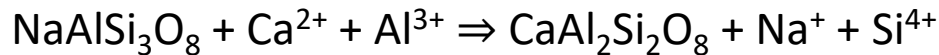
If the substituting ion has a higher charge than the ion in the lattice being substituted, it is said to be **captured** by the crystal structure; if the substituting ion has a lower charge, it is said to be **admitted** by the crystal structure.

**Example:** the K-feldspar structure [KAlSi<sub>3</sub>O<sub>8</sub>] captures Ba<sup>2+</sup> (1.35 Å) for replacement of K<sup>+</sup> (1.38 Å), and the biotite structure [K(Mg,Fe)<sub>3</sub>(AlSi<sub>3</sub>O<sub>10</sub>)(F,OH)<sub>2</sub>] admits Li<sup>+</sup> (0.76 Å) for replacement of Mg<sup>2+</sup> (0.72 Å).

## b1. GOLDSCHMIDT'S RULES

4. Ions whose charges differ by one unit may substitute for one another provided electrical neutrality of the crystal is maintained by *coupled* (or *compensatory*) substitution.

**Example:** concurrent substitution of  $\text{Na}^+$  (1.02 Å) by  $\text{Ca}^{2+}$  (1.00 Å) and of  $\text{Si}^{4+}$  (0.26 Å) by  $\text{Al}^{3+}$  (0.47 Å) in plagioclase feldspars:



In general, very little or no substitution takes place when the difference in charge on the ions is  $> 1$ , even if the size is appropriate.

$\text{Zr}^{4+}$  (0.72 Å) does not substitute for  $\text{Mg}^{2+}$  (0.72 Å) probably because of the difficulty in achieving charge balance by compensatory substitutions.

## b2. EXCEPTIONS AND LIMITATIONS

**Example:** similar in size and charge,  $\text{Mg}^{2+}$  (0.72 Å) and  $\text{Ni}^{2+}$  (0.69 Å) show only a moderately close association, and  $\text{Sr}^{2+}$  (1.18 Å) and  $\text{Hg}^{2+}$  (1.02 Å) show virtually no geochemical coherence.

The major limitation in the Goldschmidt's rules is the assumption of pure ionic bonding because most minerals have a significant component of covalent bonding.

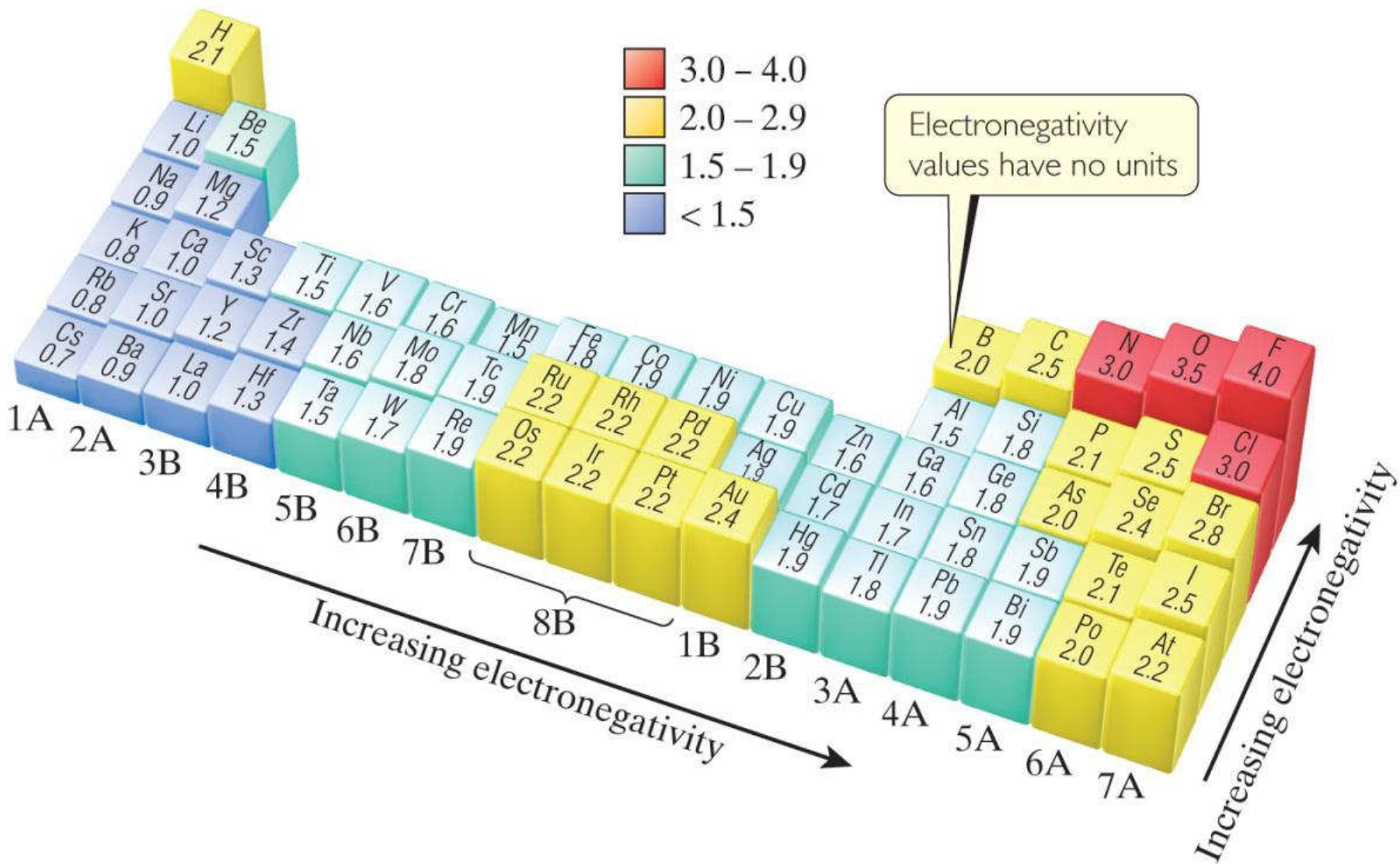
### b3. RINGWOOD'S RULE

Ringwood suggested that substitution may be limited, even when the size and charge criteria are satisfied, if the competing ions have different electronegativities ( $El$ ) and, therefore, form bonds of different strengths.

(*note*: the higher (lower) the  $El$  atomic difference between two atoms the more ionic (more covalent) will be the atomic bonding).

**Example**: although with the same charge and very close size,  $\text{Cu}^{2+}$  (0.73 Å) rarely substitutes for  $\text{Mg}^{2+}$  (0.72 Å) because of the large  $El$  difference (1.90 and 1.31, respectively).

On the contrary, despite a large difference in ionic radius,  $\text{Si}^{4+}$  (0.26 Å;  $El = 1.9$ ) and  $\text{Ge}^{4+}$  (0.73 Å;  $El = 2.01$ ) show strong geochemical coherence because of almost identical values of  $El$ .



## b4. OTHER LIMITATIONS

Other factors that affect the extent of substitution are  $T$  and  $P$  at which the substitution takes place. Elevated  $T$  and lower  $P$  usually favor increased rate of substitution.

**Example:**  $HT$  promote greater atomic vibration and open structures, which are easier to distort locally to accommodate cations of different sizes. Thus, the concentration of minor and trace elements in minerals (*e.g.*, Fe in sphalerite, ZnS) provides a potential means of determining the temperatures of mineral formation (geothermometry).

## b5. CLASSIFICATION OF SOLID SOLUTIONS

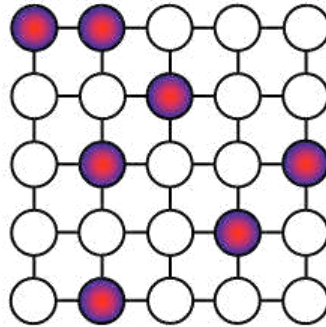
Almost all minerals are solid solutions (ss) to varying degrees. The range of compositions produced by ss in a given mineral is known as a ***solid solution series*** and its compositional extremes as ***end members***.

A ss series may be *continuous*, in which case all intermediate members are possible (*e.g.*, the olivine ss series with  $\text{Mg}_2\text{SiO}_4$  and  $\text{Fe}_2\text{SiO}_4$  as end members) or *discontinuous*, in which case only a restricted range of composition between the end members is found (*e.g.*, the limited ss between ZnS and FeS).

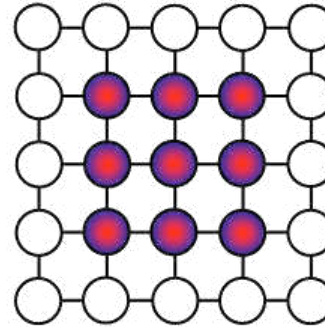
There are three kinds of solid solutions based on the mechanism that causes their chemical composition to vary.

## b5.1. SUBSTITUTIONAL SS

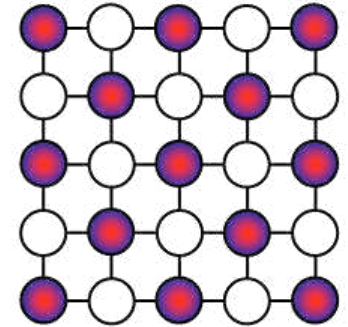
One or more kinds of ions are substituted by other kinds. The most common in minerals.



Random



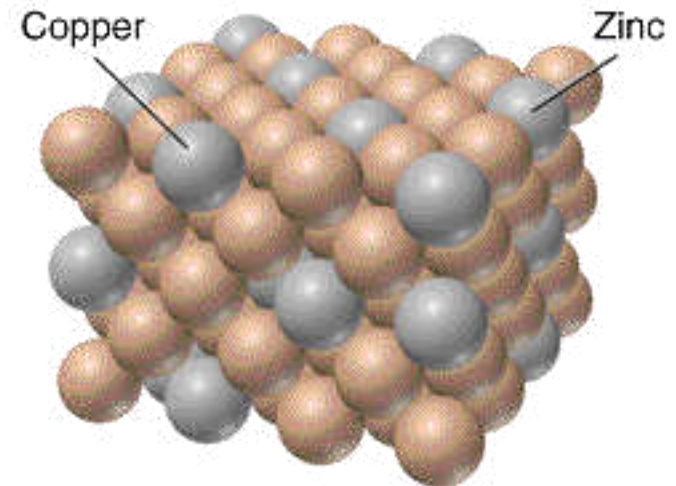
Clustered



Ordered

**Example:** the binary olivine ss series spans all intermediate compositions ranging from the forsterite  $\text{Mg}_2\text{SiO}_4$  to the fayalite  $\text{Fe}_2\text{SiO}_4$  end- members because of diadochic substitution of  $\text{Mg}^{2+}$  by  $\text{Fe}^{2+}$ , which carry the same charge and have similar ionic size.

The plagioclase ss series characterized by progressive coupled substitution of  $\text{Na}^+$  and  $\text{Si}^{4+}$  by  $\text{Ca}^{2+}$  and  $\text{Al}^{3+}$ .



Brass, a substitutional alloy

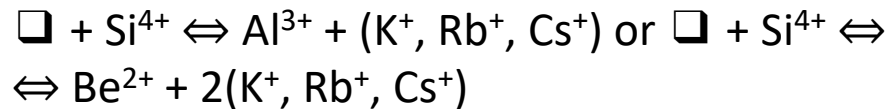
## b5.2. INTERSTITIAL SS

Foreign ions or atoms are added to fill unoccupied interstitial crystal sites ( $\square$ ) that exist between ions or ion groups.

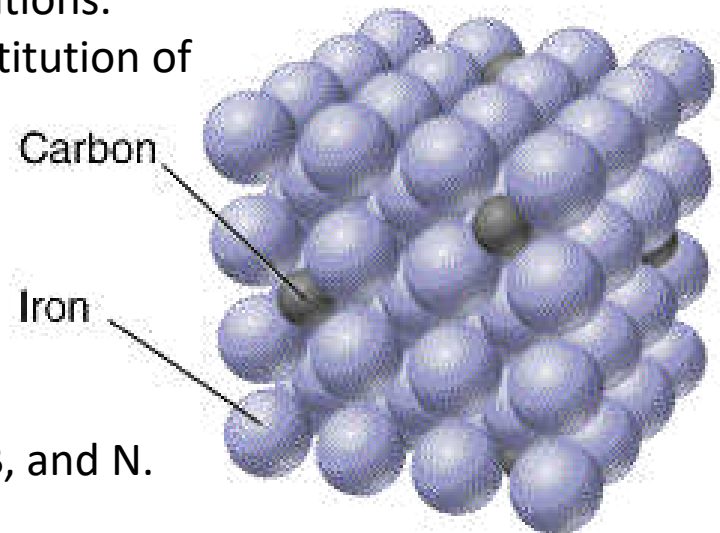
**Example:** the incorporation of  $\text{Na}^+$  into the structure of cristobalite (*HT* quartz polymorph) to compensate for the charge imbalance created by the replacement of a small amount of  $\text{Si}^{4+}$  by  $\text{Al}^{3+}$ .

Minerals such as beryl ( $\text{Be}_3\text{Al}_2\text{Si}_6\text{O}_{18}$ ) whose structure contains large channel-like cavities that can be occupied by relatively large monovalent cations.

The charge balance being maintained by coupled substitution of  $\text{Al}^{3+}$  or  $\text{Be}^{2+}$  for  $\text{Si}^{4+}$  in tetrahedral sites:



This type of solid solution is very common in metals, which easily accommodate small atoms such as H, C, B, and N.



Carbon steel, an interstitial alloy

## b5.3. OMISSION SS

Some ion sites that are normally occupied remain vacant.

**Example:** the monosulfide mineral pyrrhotite. Its chemical analysis always shows more sulfur than its theoretical proportion in FeS. It is now well established that this discrepancy is due to a deficiency of Fe, not an excess of S, in the crystal structure, so that the generalized chemical formula of pyrrhotite is written as  $\text{Fe}_{1-x}\text{S}$ , where  $x$  varies between 0 and 0.125. The electrical neutrality in this structure is maintained by the replacement of three  $\text{Fe}^{2+}$  by only two  $\text{Fe}^{3+}$  leaving one site vacant:



## Part II

- c. Spectroscopy
  - c1. Optical absorption spectroscopy
  - c2. Optical absorption processes
    - c2.1. Charge transfers
    - c2.2. Band gap
    - c2.3. Overtones
    - c2.4. *f*-orbitals of U electronic transitions
    - c2.5. Electron-hole centers
    - c2.6. Crystal-field or ligand-field spectra
  - c3. Crystal-field theory
    - c3.1. *TMI* and CF splitting

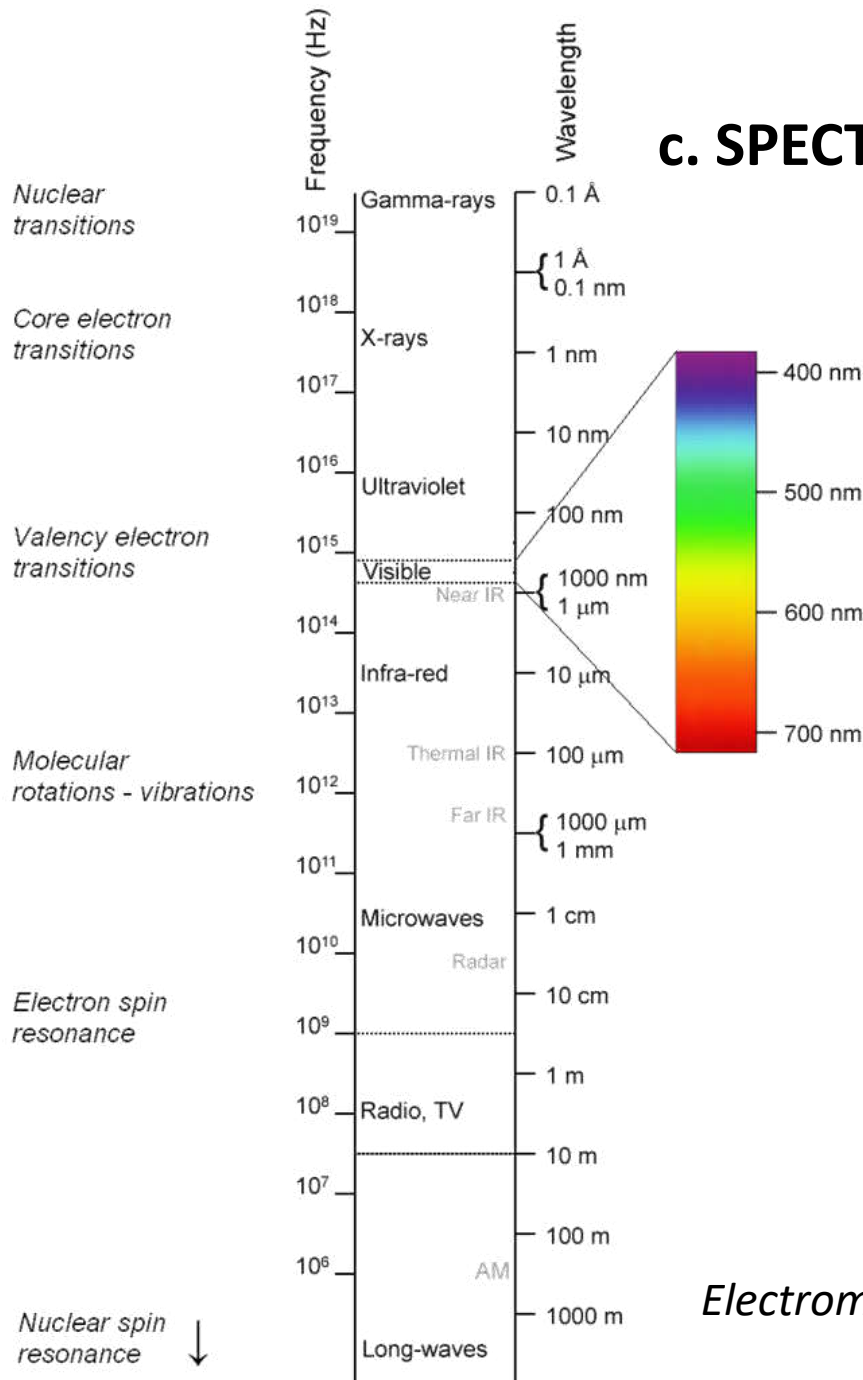
## c. SPECTROSCOPY

Although there are very many different spectroscopic methods they all work on the same basic principle:

*determination of the difference between energy levels in a material by measuring the energy ( $E$ ) of the absorbed or emitted radiation when the material is **excited** to a higher  $E$  state, or as it decays back to the **ground** state.*

Both absorption and emission of energy are provoked when an incident radiation of the appropriate frequency induces changes in the  $E$  levels in the material, and their intensity depends on the number of molecules, atoms, or electrons moving between energy levels.

## c. SPECTROSCOPY



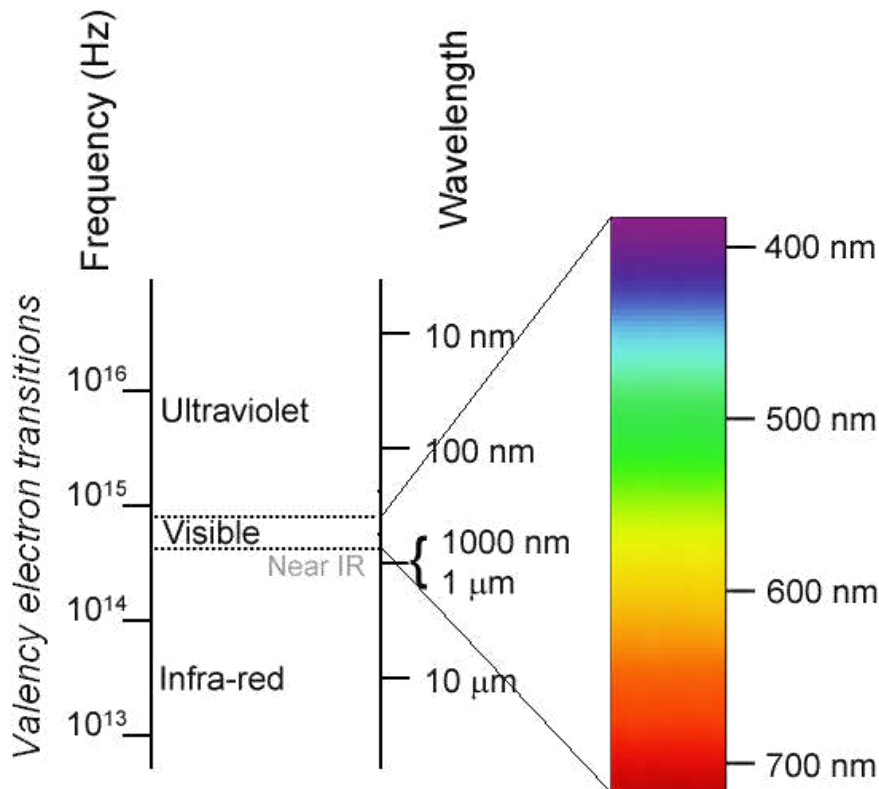
At  $T > 0$  K, a wide range of phenomena (*e.g.*, nuclear spin resonance,  $e^-$  spin resonance, molecular rotations and vibrations, valence  $e^-$  transitions, core  $e^-$  transitions, nuclear transitions, etc.) contribute to the energy of a material, and it is usual to describe these individual phenomena as if they possessed distinct reservoirs of energy.

Each phenomenon is associated with a **range of energy** that varies from the *ground state* (zero  $E$ ) to the *excited states* (higher  $E$ ).

*Electromagnetic spectrum*

# c1. OPTICAL ABSORPTION SPECTROSCOPY

Optical spectroscopy is concerned with qualitative and quantitative measurements of the absorption, reflection, and emission of light on single crystals or powder samples in the spectral range ( $26300$  to  $12800\text{ cm}^{-1}$ ), *i.e.*, from near ultra-violet, through visible, to near infrared portions of the electromagnetic spectrum, in which the ***transitions between electronic states*** occur.



Optical spectroscopy area can be broadly divided into three subareas:

- (1) Absorption spectra in transmission;
- (2) Reflection measurements;
- (3) Emission spectroscopy.

## c2. OPTICAL ABSORPTION PROCESSES

Processes which contribute to the absorption spectra of minerals in the optical spectral range can be categorized as:

**c2.1.** Electronic transitions which involve displacement of charge density (*charge transfer, CT*) from one ion to another.

**a. CT between anion and cation.** It usually requires higher energies than CF transitions and produce absorption bands centered in the UV region.

**Example:** transfer of  $e^-$  density from a filled O orbital to a partially occupied  $Fe^{3+}$  orbital. In the case of highly oxidized ions (*e.g.*,  $Fe^{3+}$  and  $Cr^{6+}$ ), the wing of the absorption band will extend into the visible part of the spectrum giving back a yellow-brown color.

**b. Intervalence charge transfer (IVCT).** It involves movement of electron density between metal ions in different oxidation states. The pairs or clusters of cations typically share edges or faces of coordination polyhedra.

**Example:** the deep blue of sapphire is a familiar example of color caused by this type of transition. The  $Fe^{2+}$ - $Fe^{3+}$  and  $Fe^{2+}$ - $Ti^{4+}$  intervalence interactions are common. In some meteoritic minerals, the  $Ti^{3+}$ - $Ti^{4+}$  interaction is also prominent.

## c2. OPTICAL ABSORPTION PROCESSES

**c2.2.** Absorption edges result from electronic transitions between the top of a valence band and the bottom of the conduction band. Any photon with energy greater than this **band gap** will be absorbed.

These types of absorption bands are usually encountered in sulfides.

**Example:** the red color of cinnabar is the result of a band gap which allows light with wavelength longer than 600 nm to pass while absorbing shorter wavelengths.

**c2.3. Overtones** of vibrational transitions. The most commonly encountered bands in the near-infrared are the overtones of OH and H<sub>2</sub>O groups. Vibrational overtones are readily recognized because they have much smaller widths than electronic transitions which can occur in the same spectral region.

**Example:** the spectrum of beryl contains both absorption from Fe<sup>2+</sup> and from the vibrational modes of H<sub>2</sub>O molecules.

The blue color of thick layers of glacial ice is the result of absorption of light by these transitions.

## c2. OPTICAL ABSORPTION PROCESSES

### c2.4. Electronic transitions involving *f-orbitals of uranium* and the rare earth elements.

These electronic transitions involve electrons in inner orbitals that are shielded from the coordination sphere of the central metal ion. Thus, absorption bands from the trivalent REE tend to be much sharper than most of the bands from the third-row transition metals and tend to have only small shifts in wavelength with changes in the coordination number and geometry of the cation.

c2.5. In many minerals, absorption of light is associated with *electron-hole centers* and molecular ions produced by ionizing radiation.

The spectra of these centers can often be quite difficult to interpret. Often, color in minerals arises from the combined action of *d*-orbital transitions from metal ions together with color centers from natural irradiation.

**Example:** smoky quartz, blue feldspar, green diamonds and blue calcite are examples of this process.

## c2. OPTICAL ABSORPTION PROCESSES

c2.6. the process will focus on:

Electronic transitions involving electrons in the  $d$ -orbitals of ions of the first row transition elements (*TMI*) such as  $\text{Cr}^{3+}$ ,  $\text{Mn}^{3+}$ ,  $\text{Co}^{2+}$ ,  $\text{Fe}^{2+}$  and  $\text{Fe}^{3+}$  that give rise to absorption in the visible and near-infrared region.

The spectra they produce are called ***crystal-field (CF) spectra***.

### c3. CRYSTAL-FIELD THEORY

Among the many processes which contribute to the absorption spectra of investigated materials crystal-field  $d-d$  transitions process plays a decisive role.

Pioneered by Bethe (1929) and van Vleck (1932), the ***crystal-field theory (CFT)*** is a model of chemical bonding applicable to *TMI* and lanthanides, and it describes the origin and consequences of interactions between the  $d$  (or  $f$ ) orbitals with the electrostatic fields originating from negatively charged anions or dipolar groups coordinating the central ion.

***CFT in geosciences:*** colour and pleochroism, interpretation of electronic structure and bonding, partitioning of *TMI*, evaluation of thermodynamic properties of minerals influenced by CFSE (*e.g.*, electronic entropy or enthalpy of mixing), mantle geochemistry of transition elements (*e.g.*, polyhedral bulk moduli from high-pressure spectra, and phase transition), detection of structural details (*e.g.*, cation ordering, and dynamic or static Jahn-Teller distortions).

## c3.2. TMI AND CF SPLITTING

TMI are characterized by incompletely filled inner  $d$  orbitals.

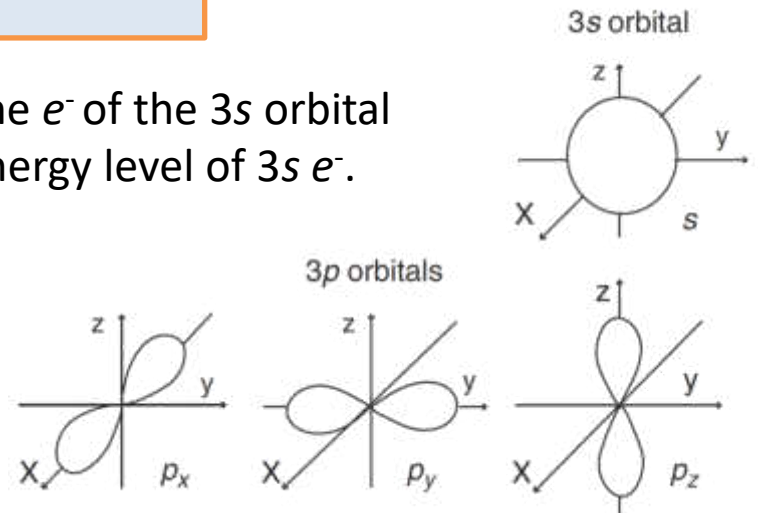
First transition series ( $3d$  orbitals): the electronic structures are of the general form [Ar core ( $1s^2 2s^2 2p^6 3s^2 3p^6$ )  $3d^{1 \text{ to } 10} 4s^1 \text{ or } 2$ ].

**Ions are formed when the  $4s$  electrons ( $e^-$ ), and in some cases  $3d e^-$ , are removed from the metal atom.**

**Example: TMI into a hypothetical field of negative charges evenly distributed on a sphere.**

The increased repulsion between the ligands and the  $e^-$  of the  $3s$  orbital (spherical symmetry) results simply in raising the energy level of  $3s e^-$ .

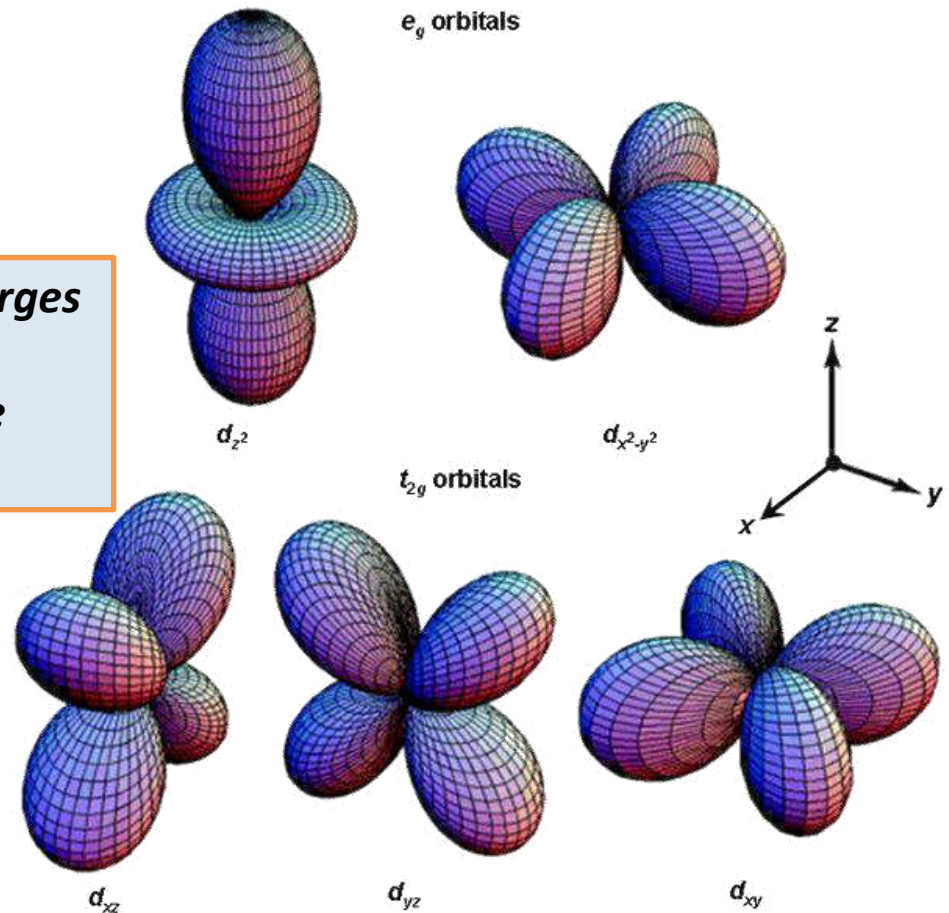
The threefold degenerated  $3p$  orbitals of the metal pointing directly towards the negative charges are also raised to a higher energy level because of increased repulsion between the ligands and  $3p e^-$ , but remain degenerate.



## c3.2. TMI AND CF SPLITTING

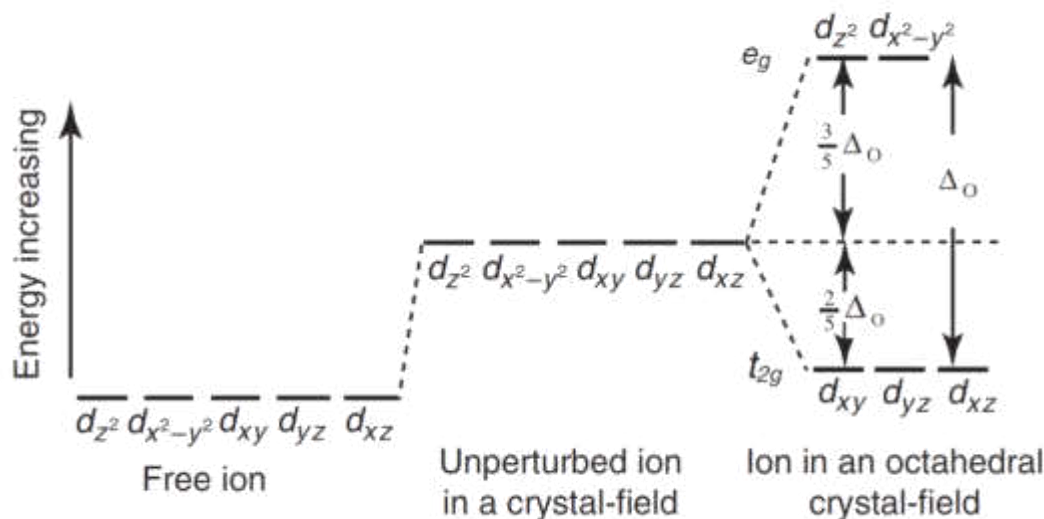
The main effect of ligands on the TMI arises from interaction with  $3d e^-$ . Also the  $3d$  orbitals ( $3d_{z^2}$ ,  $3d_{x^2-y^2}$ ,  $3d_{xy}$ ,  $3d_{xz}$ ,  $3d_{yz}$ ) are fivefold degenerate (i.e., they are energetically equivalent and the  $d e^-$  have equal probability of being located in any of the five  $3d$  orbitals).

*from a hypothetical field of negative charges evenly distributed on a sphere to an octahedral distribution of negative charges*



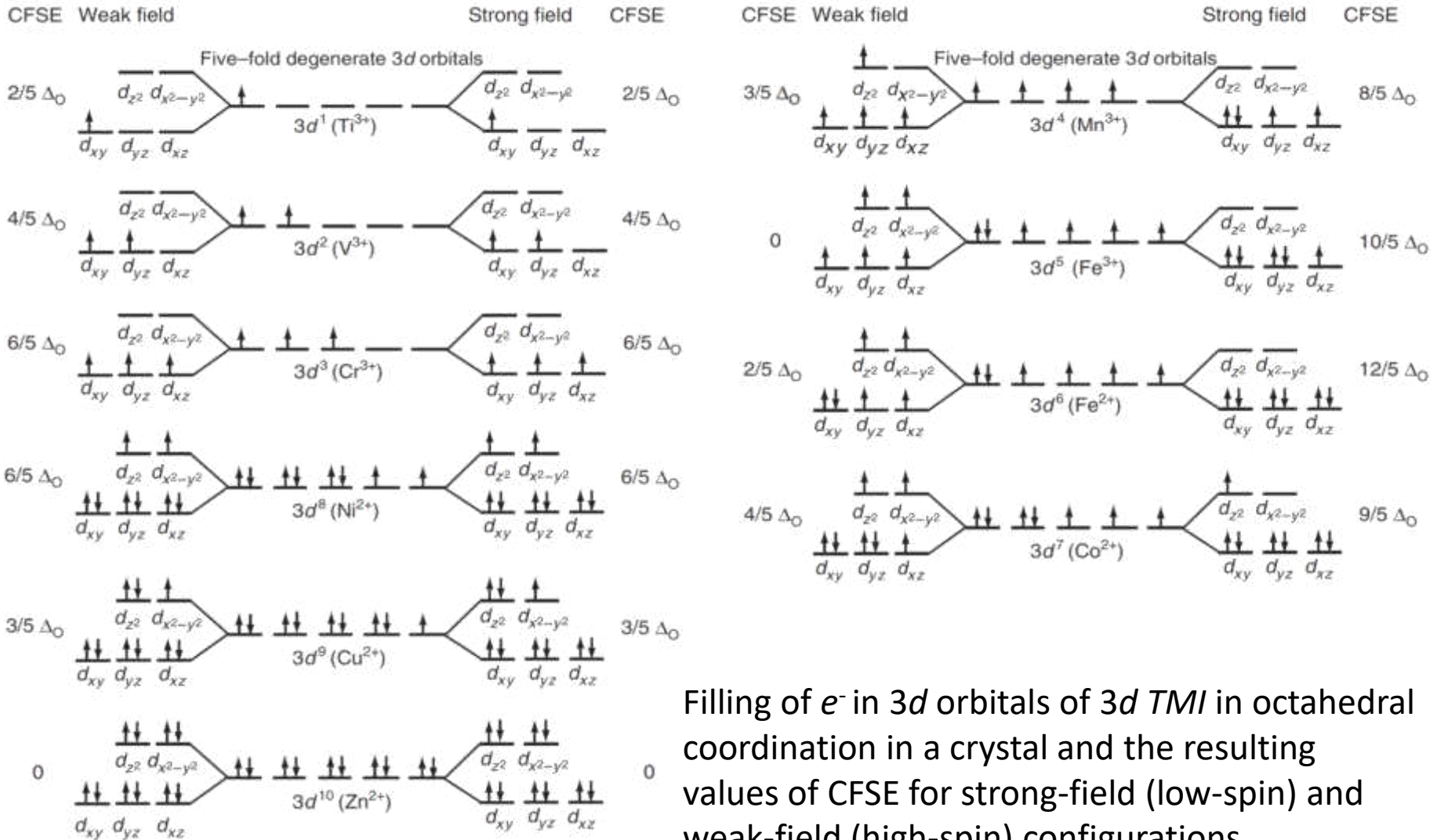
## c3.2. TMI AND CF SPLITTING

The 3d orbitals can no longer remain degenerate, and they split into two groups that have different levels of energy. The energy separation between  $t_{2g}$  and  $e_g$  orbitals is termed the **crystal-field splitting** parameter ( $\Delta_o$  or **10Dq**).



Each  $e^-$  in a  $t_{2g}$  orbital lowers the energy of the TMI (and thus increases its stability), whereas each  $e^-$  in the  $e_g$  orbital undergoes an energy increasing (it diminishes the stability). The resultant net energy, which depends on the number of  $e^-$  and how they fill the orbitals, is called **crystal field stabilization energy (CFSE)**, the magnitude of which can be estimated from **absorption spectra measurements**.

## c3.2. TMI AND CF SPLITTING



Filling of  $e^-$  in 3d orbitals of 3d TMI in octahedral coordination in a crystal and the resulting values of CFSE for strong-field (low-spin) and weak-field (high-spin) configurations.

## Part III

- d. From the Vegard's law to the Virtual Crystal Approximation
  - d1. Structural relaxation coefficient
  - d2. Local distances from EAS
  - d3. Local distances: XRD VS. EAS

## d. FROM THE VEGARD'S LAW TO THE VCA

**Goldschmidt:** theory about the replacement of elements by means of simple concepts such as ion size, valence, electronegativity... ..at the same time...

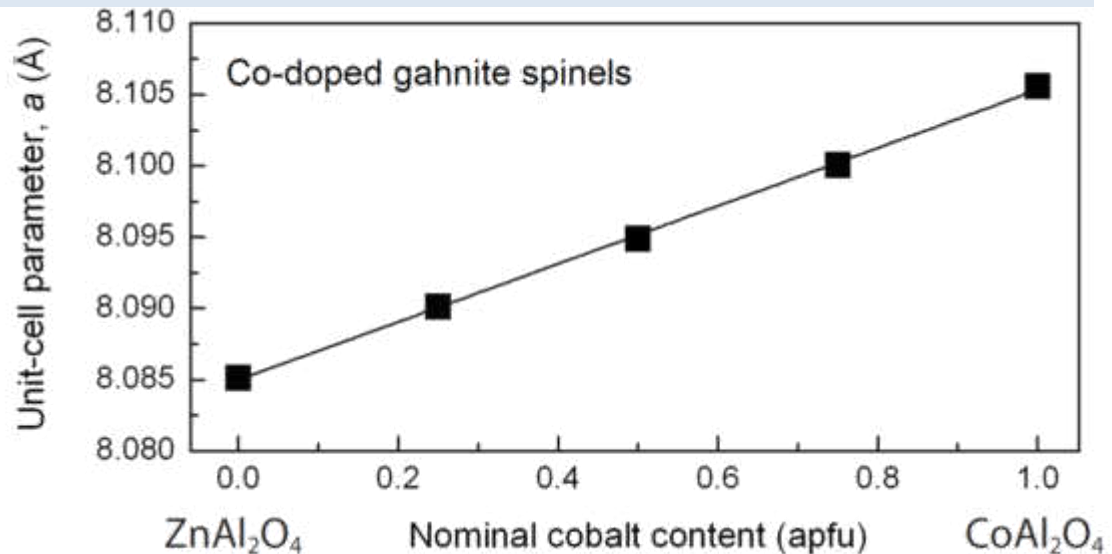
**Vegard:** at  $T = \text{const}$ , the lattice constants of an alloy linearly scale with the concentration of its constituent elements.

⇒ for a hypothetical binary  $A_{1-x}B_xO$  solid solution the lattice constant  $a(x)$  is:

$$a(x) = [(1-x) a_{AO} + (x a_{BO})]$$

$a_{AO}$  and  $a_{BO}$  are the constant values assumed by AO and BO end-members, respectively.

The validity of the previous empirical relationship was extended to the bond lengths of binary solid solutions and it is known as "**Virtual Crystal Approximation**" model, VCA.



# d1. STRUCTURAL RELAXATION COEFFICIENT

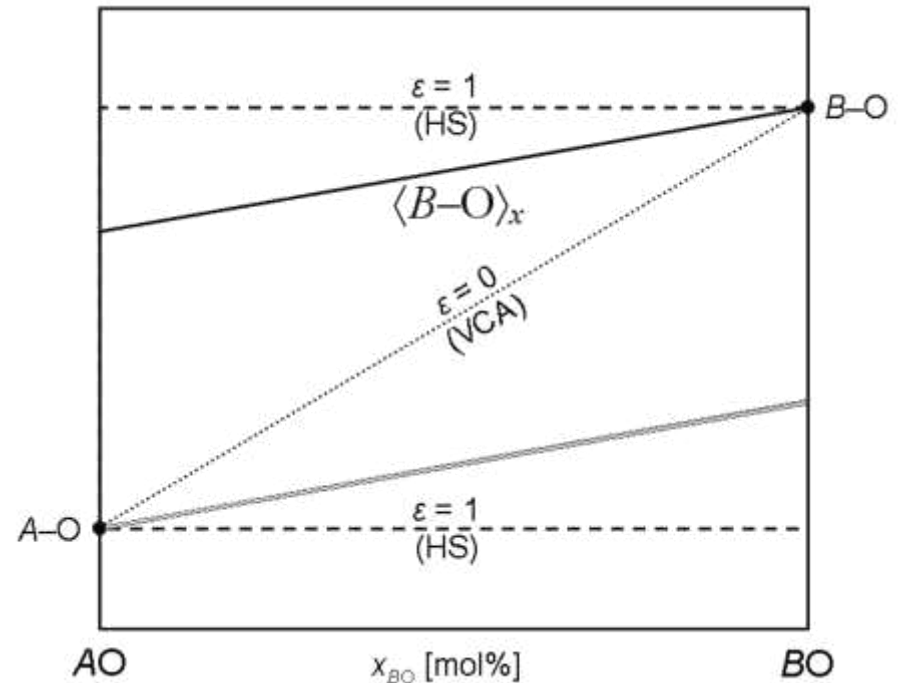
Numerous studies revealed that local bond distances achieved by spectroscopic techniques (*short-range*) depart from those obtained by averaging diffraction methods (deviations from the VCA model).

The *mismatch between long- vs. short-range bond distances of a crystal structure along a binary join* can be parameterized by the *structural relaxation coefficient* ( $\epsilon$ ):

$$\epsilon = (\langle B-O \rangle^{local} - \langle A-O \rangle) / (\langle B-O \rangle - \langle A-O \rangle)$$

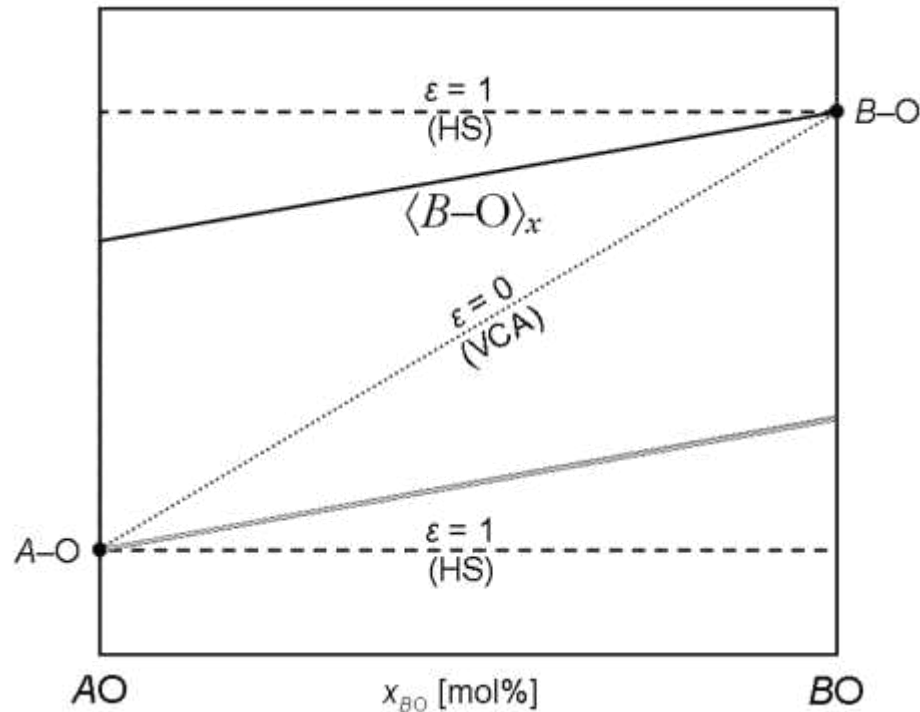
$\langle A-O \rangle$  &  $\langle B-O \rangle$ : mean bond lengths for AO and BO end-members (by XRD);

$\langle B-O \rangle^{local}$ : local distance for the  $A_{1-x}B_xO$  join derived by EAS as infinite dilution of B (TMI)



## d1. STRUCTURAL RELAXATION COEFFICIENT

The rationale of this approach is that the relaxation coefficient can range from  $\varepsilon = 0$ , when the *VCA* model is verified, to  $\varepsilon = 1$  in the case of the Hard Sphere (*HS*) model, which implies that all atoms in the solid solution retain their initial sizes. In other words,  $\varepsilon$  can span from absent (*VCA*) or full (*HS*) lattice relaxation.

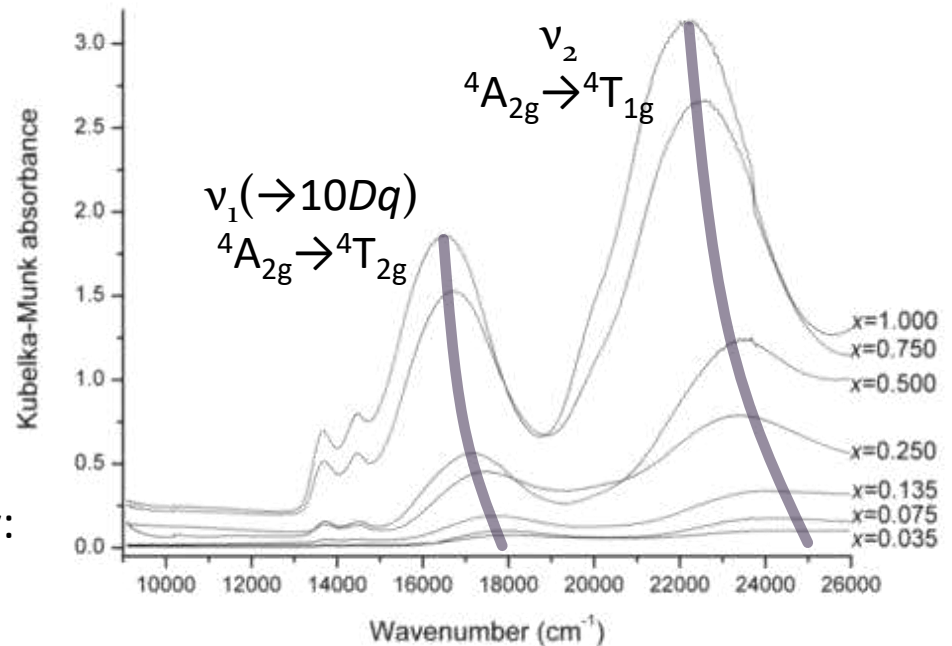


## d2. LOCAL DISTANCES FROM EAS

During EAS measurements of samples belonging to isostructural solid solutions, the lengthening of polyhedral mean bond distances, caused by the replacement of a *TMI* for another ion, entails a gradual shift of the *TMI* absorption bands as well as a band absorbance increasing.

**Example:** in the case of octahedrally coordinated  $\text{Cr}^{3+}$ , the most intense bands are those attributed to:

- parity-forbidden transitions [at low energy:  $\nu_1 = {}^4A_{2g}({}^4F) \rightarrow {}^4T_{2g}({}^4F) = 10Dq$ ]
- &
- spin-allowed transitions [at high energy:  $\nu_2 = {}^4A_{2g}({}^4F) \rightarrow {}^4T_{1g}({}^4F)$ ]



## d2. LOCAL DISTANCES FROM EAS

According to the Crystal Field Theory, in an oxygen based structure, the crystal field parameter  $10Dq$  depends on the mean metal-oxygen bond distances:

$$10Dq = 5/3 \times q \times \langle r^4 \rangle \times \langle A_{1-x}B_x-O \rangle^{-5}$$

$q$ : effective charge of the ligand

$\langle r^4 \rangle$ : mean of the fourth power of the  $d$ -electron–core distance

$\langle A_{1-x}B_x-O \rangle$ : mean distance at the metal-centred ion by XRD.

This eq. has several restrictions because it considers only one type of ligand as a point electric charge, when the  $\langle B-O \rangle$  bond could be not strictly ionic.

However, in the roughest way, the crystal field strength is inversely correlated with the fifth power of the mean central ion–ligand distance ( $\rightarrow$  **Point Charge Approximation** model):

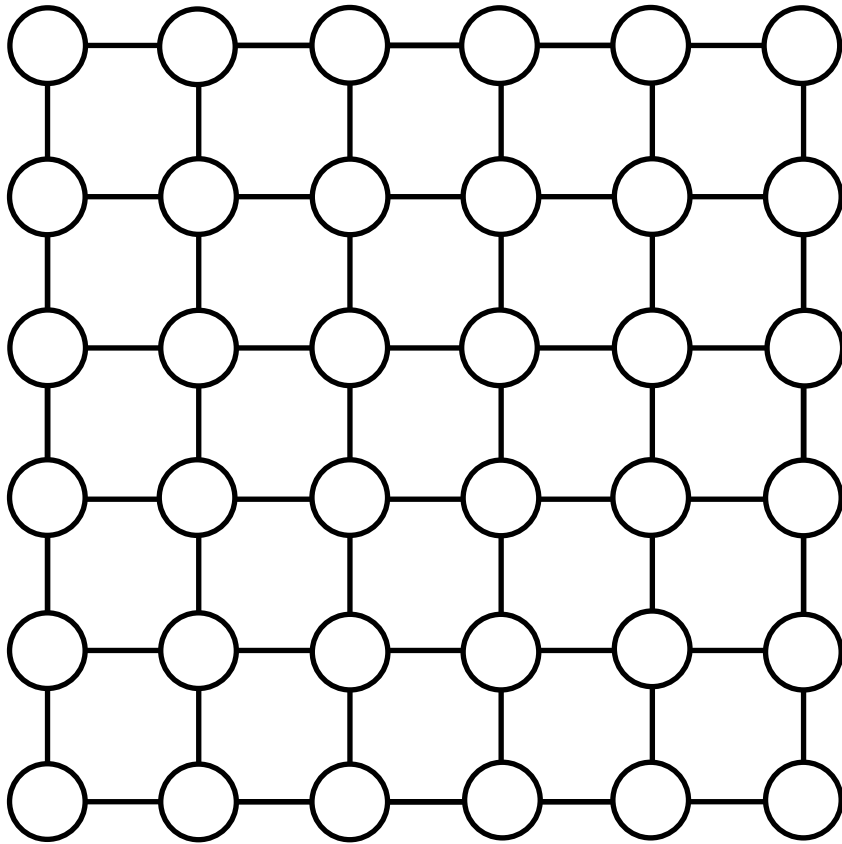
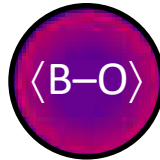
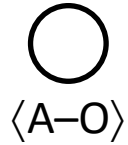
$$10Dq = \text{const} \times \langle A_{1-x}B_x-O \rangle^{-5}$$

The local ion-oxygen distance  $\langle B-O \rangle_x^{local}$ , can be calculated for each composition of the  $A_{1-x}B_xO$  solid solution by:

$$\langle B-O \rangle_x^{local} = \langle B-O \rangle_{x=1} \times [(10DqB)_{x=1} / (10DqB)_x]^{1/5}$$

### d3. LOCAL DISTANCES: XRD VS. EAS

$A_{1-x}B_xO$  solid solution



*TMI*  
%

XRD  
[VCA]

EAS  
[VCA] vs. [HS]

0



25

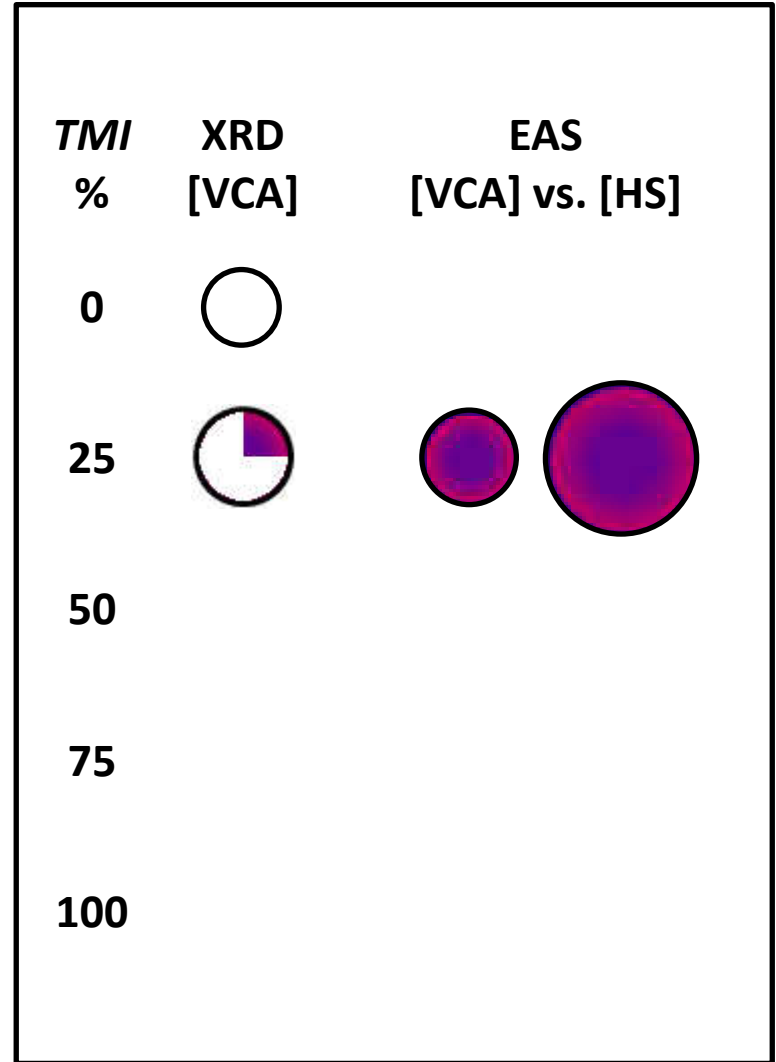
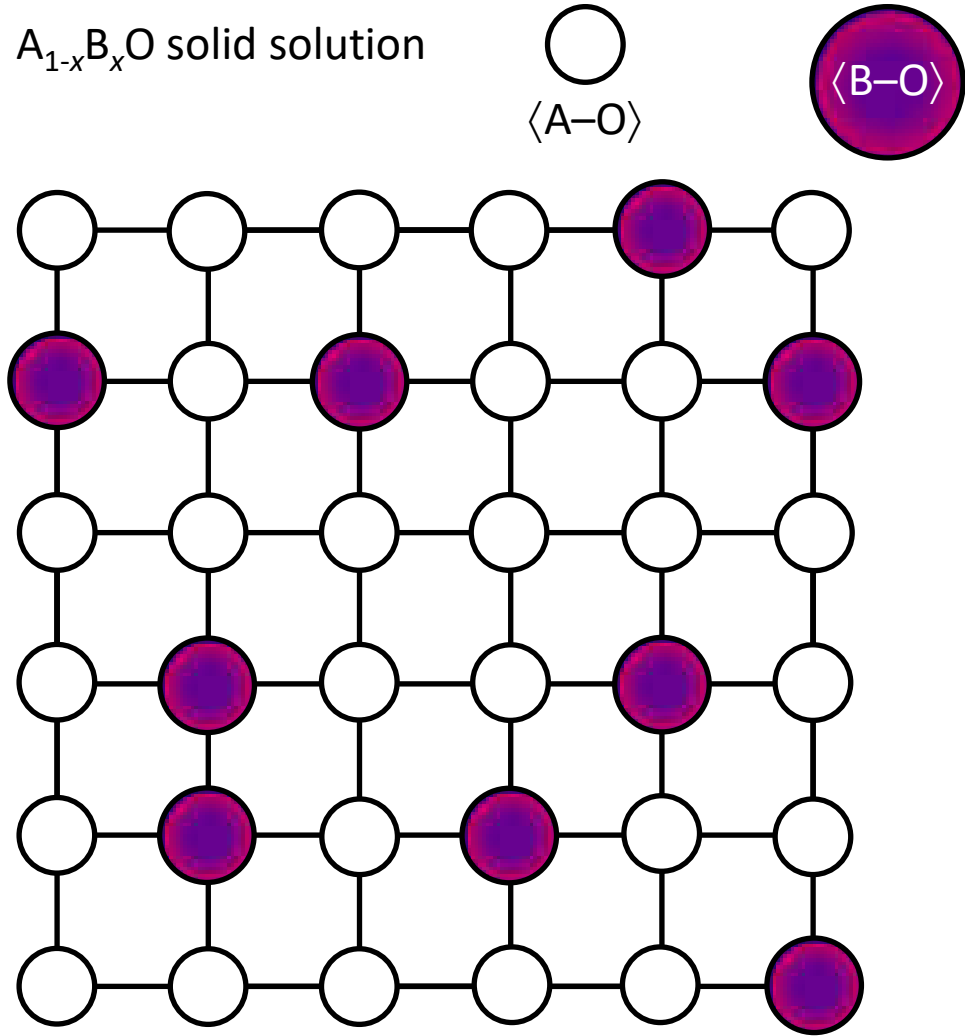
50

75

100

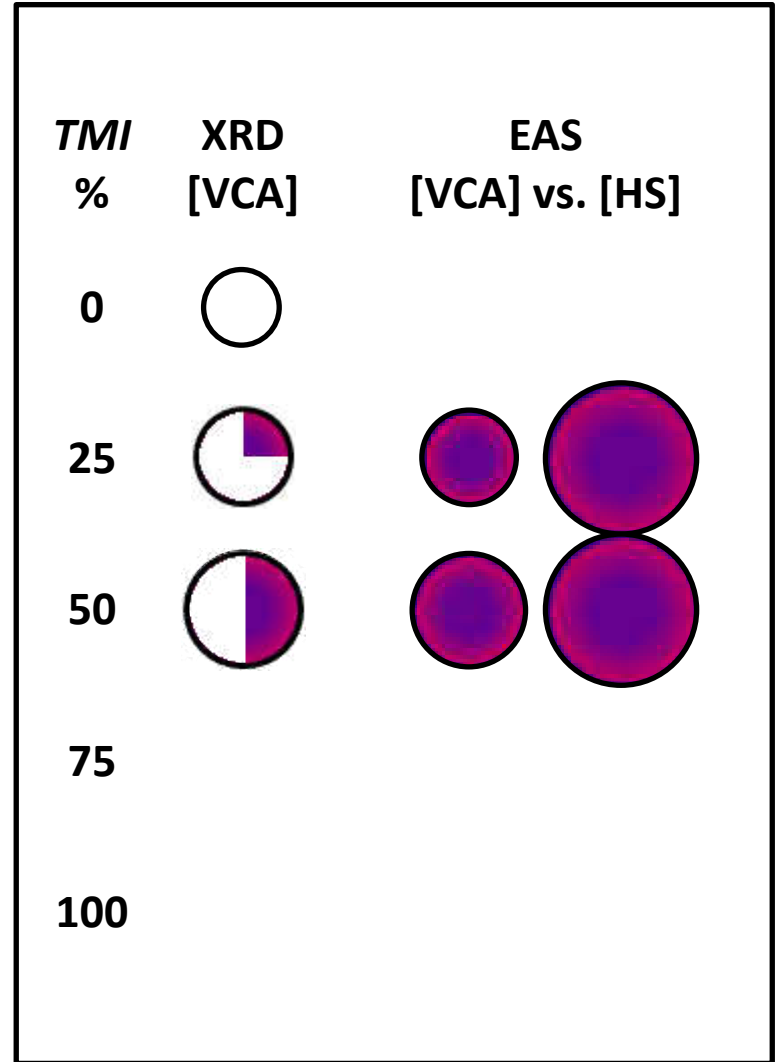
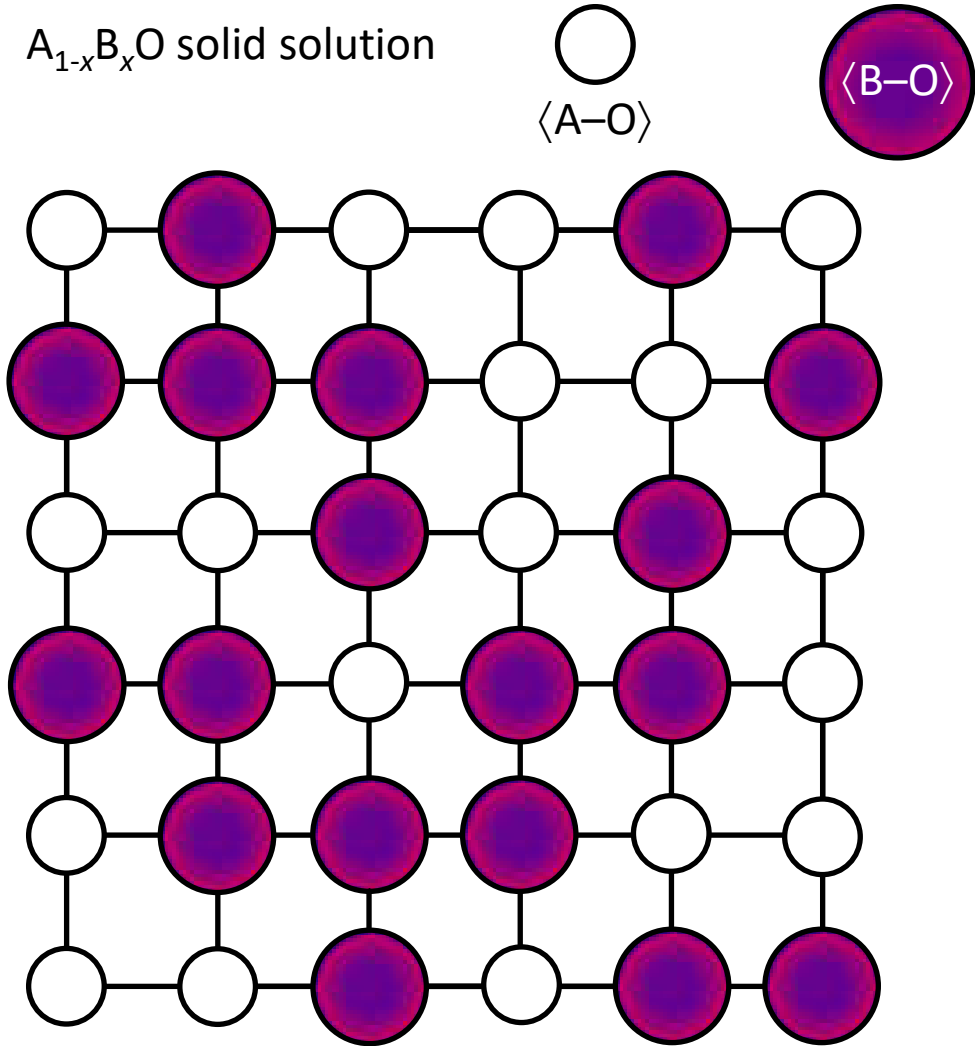
### d3. LOCAL DISTANCES: XRD VS. EAS

$A_{1-x}B_xO$  solid solution



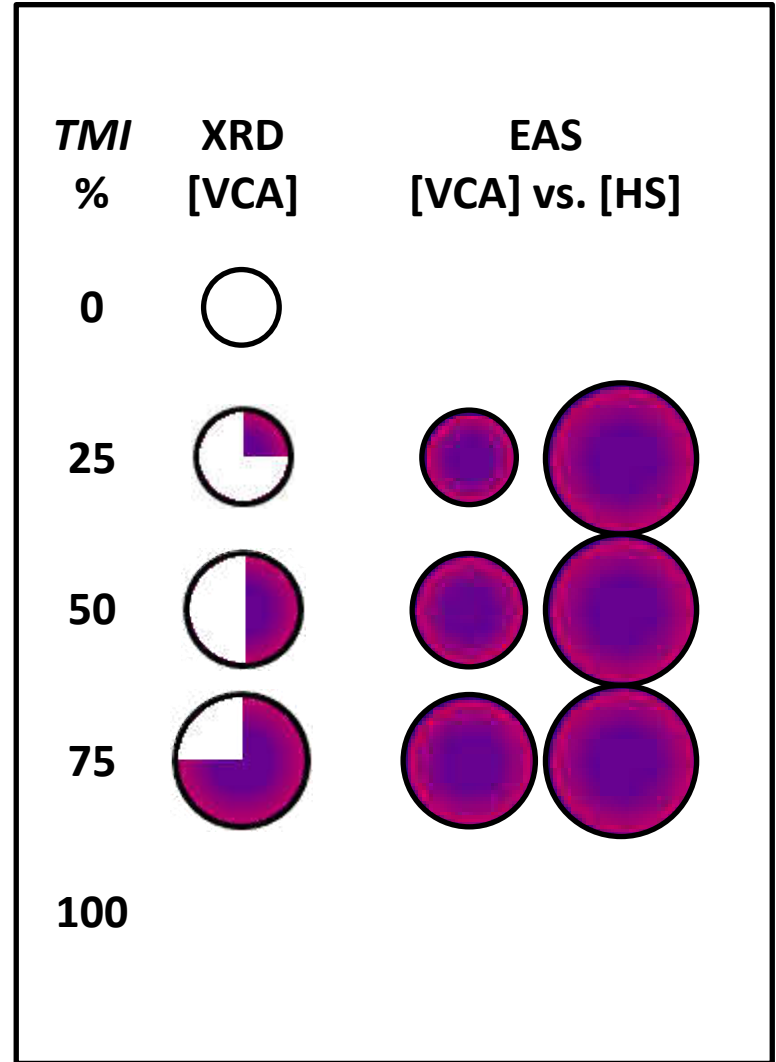
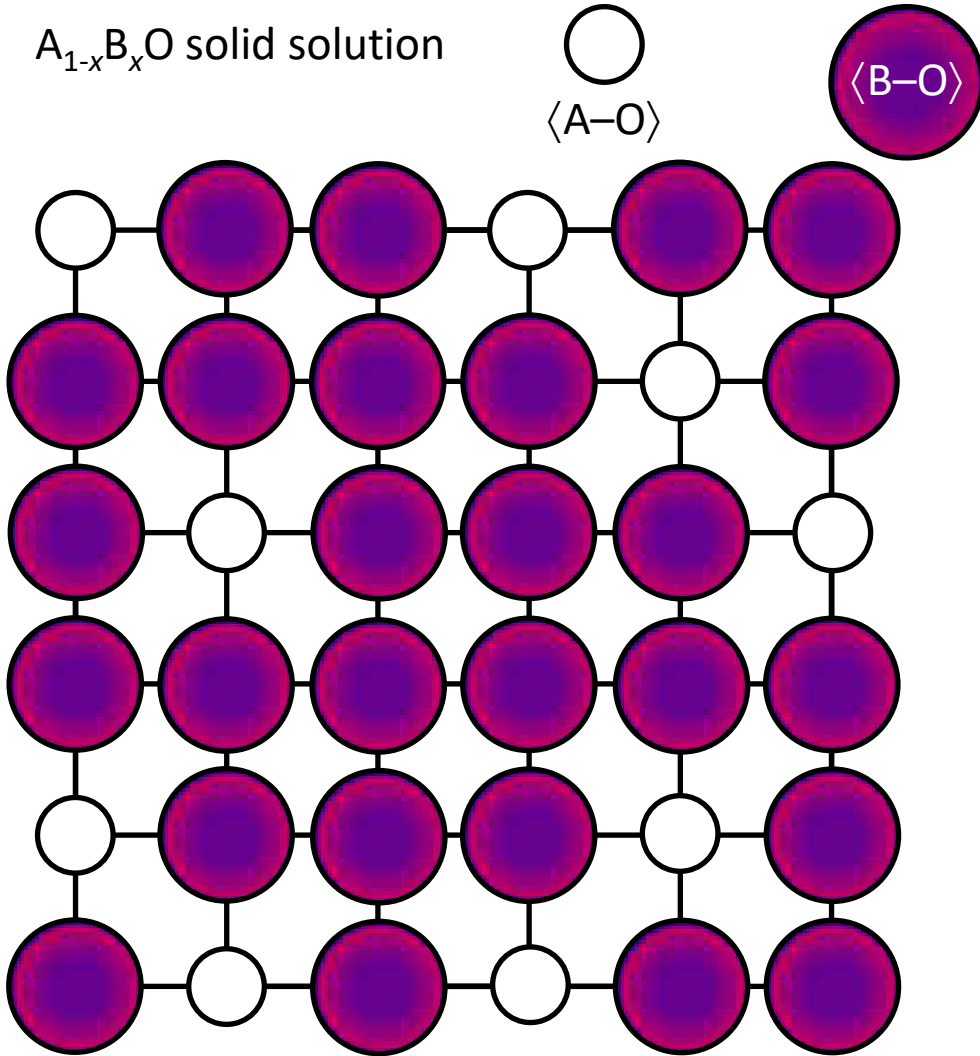
### d3. LOCAL DISTANCES: XRD VS. EAS

$A_{1-x}B_xO$  solid solution



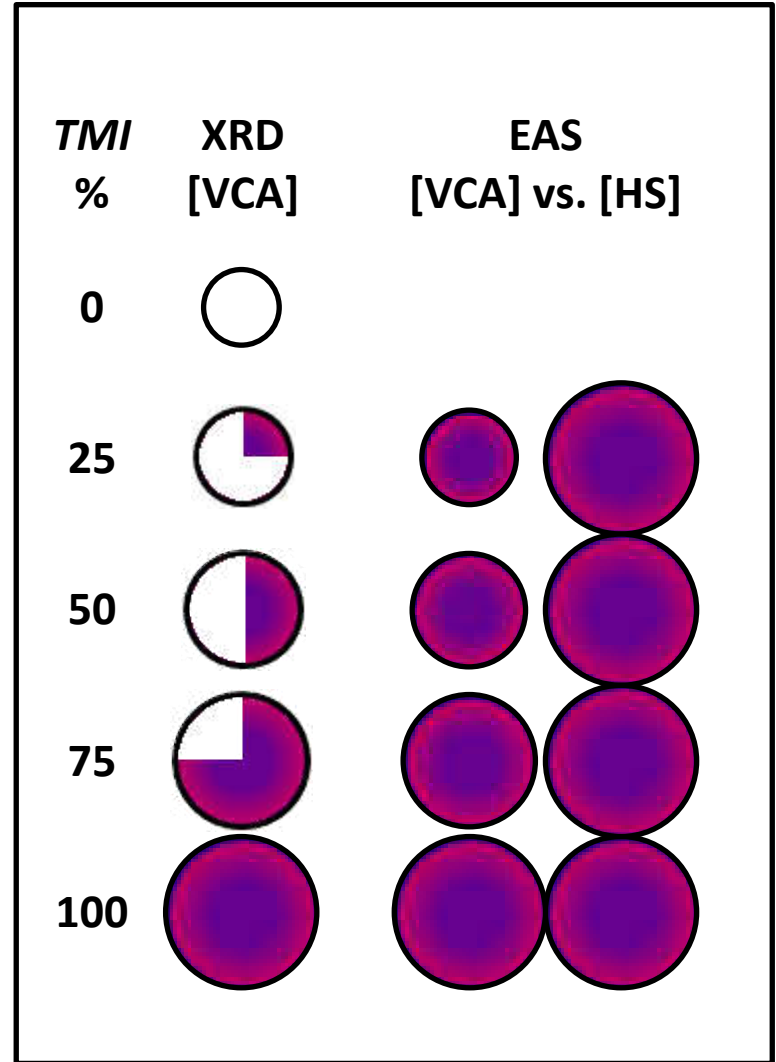
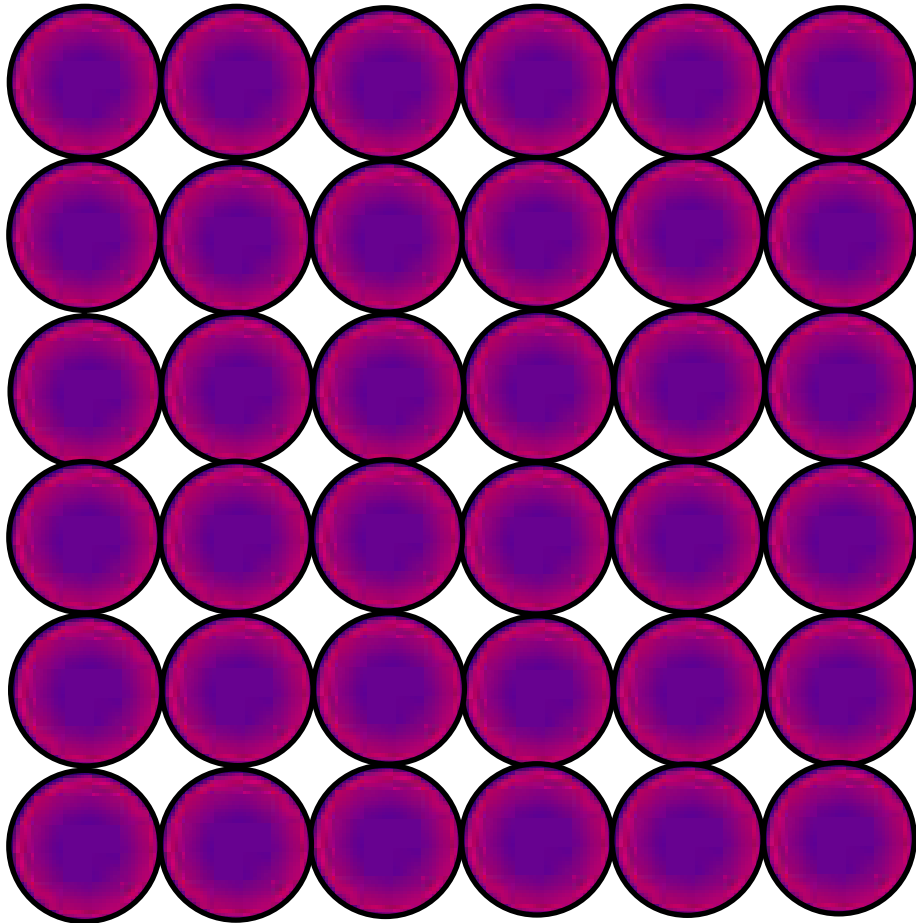
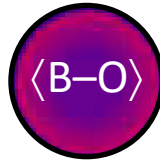
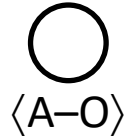
### d3. LOCAL DISTANCES: XRD VS. EAS

$A_{1-x}B_xO$  solid solution

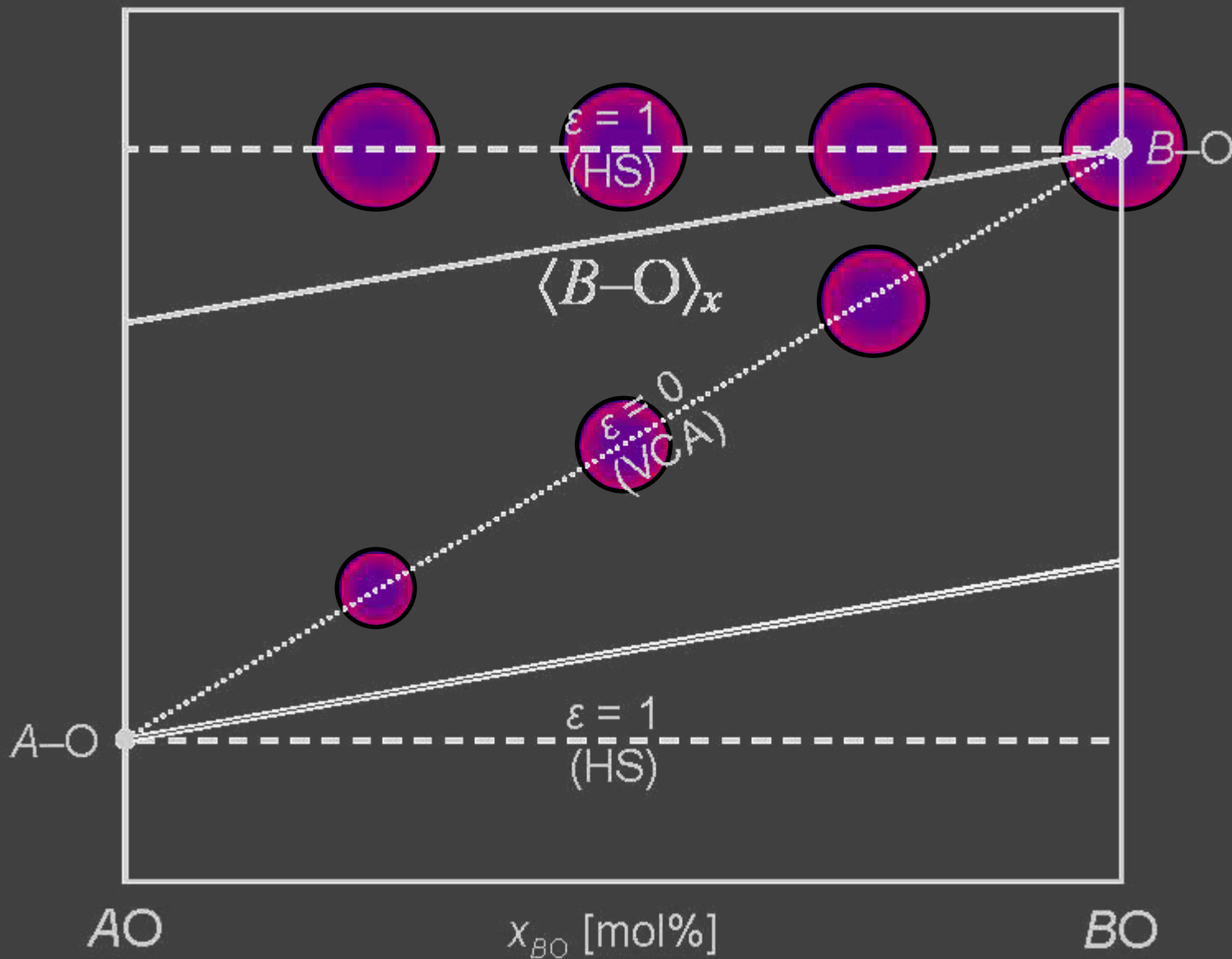


### d3. LOCAL DISTANCES: XRD VS. EAS

$A_{1-x}B_xO$  solid solution



### d3. LOCAL DISTANCES: XRD VS. EAS



## Part IV

e. Structural relaxation examples

e1. spinel  $(\text{Zn}_{1-x}\text{Co}_x)\text{Al}_2\text{O}_4$

e2. perovskite  $\text{Y}(\text{Al}_{1-x}\text{Cr}_x)\text{O}_3$

e3. melilite  $\text{Ca}_2(\text{Zn}_{1-x}\text{Co}_x)\text{Si}_2\text{O}_7$ ;

e4. pyrophosphate  $\text{Na}(\text{Al}_{1-x}\text{Cr}_x)\text{P}_2\text{O}_7$

f. replacement of  $\text{Cr}^{3+}$  for  $\text{Al}^{3+}$  at octahedral site in compounds of mineralogical interest

## SUGGESTED READING

- Andrut *et al.* (2004): Optical absorption spectroscopy in geosciences. Part II: Quantitative aspects of crystal fields. In "Spectroscopic methods in mineralogy", *EMU Notes Mineral.*, **6**, 145.
- Ardit *et al.* (2012): Structural relaxation in tetrahedrally coordinated  $\text{Co}^{2+}$  along the gahnite-Co-aluminate spinel solid solution. *Am. Mineral.*, **97**, 1394.
- Ardit *et al.* (2012): Local structural relaxation around  $\text{Co}^{2+}$  along the hardystonite-Co-åkermanite melilite solid solution. *Phys. Chem. Minerals*, **39**, 713.
- Ardit *et al.* (2012): Structural stability, cation ordering, and local relaxation along the  $\text{AlNbO}_4\text{-Al}_{0.5}\text{Cr}_{0.5}\text{NbO}_4$  join. *Am. Mineral.*, **97**, 910.
- Ardit *et al.* (2014): On the structural relaxation around  $\text{Cr}^{3+}$  along binary solid solutions. *Eur. J. Mineral.*, **26**, 359.
- Ardit *et al.* (2014): Structural relaxation around  $\text{Cr}^{3+}$  at the  $\text{Na}(\text{Al}_{1-x}\text{Cr}_x)\text{P}_2\text{O}_7$  octahedral site: an XRPD and EAS study. *Z. Kristallogr.*, **229**, 687.
- Ardit *et al.* (2016): Pigments based on perovskite. In: *Perovskite and related mixed oxides: Concepts and applications.*, **12**, 259.
- Boyce & Mikkelsen (1985): Local structure of ionic solid solutions: Extended x-ray absorption fine-structure study. *Phys. Rev. B*, **31**, 6903.
- Burns (1993): Mineralogical applications of crystal field theory (2<sup>nd</sup> Ed). Cambridge University Press, 576 p.

## SUGGESTED READING

- Cruciani *et al.* (2009): Structural relaxation around Cr<sup>3+</sup> in YAlO<sub>3</sub>–YCrO<sub>3</sub> perovskites from electron absorption spectra. *J. Phys. Chem. A*, **113**, 13772.
- Denton & Ashcroft (1991): Vegard's law. *Phys. Rev. A*, **43**, 3161.
- Dondi *et al.* (2013): Next neighbors effect along the Ca-Sr-Ba-åkermanite join: Long-range vs. short-range structural features. *J. Solid State Chem.*, **202**, 134.
- Dondi *et al.* (2014): Tetrahedrally coordinated Co<sup>2+</sup> in oxides and silicates: Effect of local environment on optical properties. *Am. Mineral.*, **99**, 1736.
- Dunn *et al.* (1965): Some aspects of crystal field theory. Harper & Row Eds., 115p.
- Galoisy (1996): Local versus average structure around cations in minerals from spectroscopic and diffraction measurements. *Phys. Chem. Minerals*, **23**, 217.
- Gaudry *et al.* (2003): Structural and electronic relaxations around substitutional Cr<sup>3+</sup> and Fe<sup>3+</sup> ions in corundum. *Phys. Rev. B*, **67**, 094108.
- Gaudry *et al.* (2005): Structural relaxations around Ti, Cr and Fe impurities in  $\alpha$ -Al<sub>2</sub>O<sub>3</sub> probed by x-ray absorption near-edge structure combined with first-principles calculations. *J. Phys.: Condens. Matter*, **17**, 5467.
- Gaudry *et al.* (2006): From the green color of eskolaite to the red color of ruby: an X-ray absorption spectroscopy study. *Phys. Chem. Minerals*, **32**, 710.

## SUGGESTED READING

- Gaudry *et al.* (2007): Relaxations around the substitutional chromium site in emerald: X-ray absorption experiments and density functional calculations. *Phys. Rev. B*, **76**, 094110.
- Hålenius *et al.* (2010): Structural relaxation around Cr<sup>3+</sup> and the red-green color change in the spinel (sensu stricto)-magnesiochromite (MgAl<sub>2</sub>O<sub>4</sub>-MgCr<sub>2</sub>O<sub>4</sub>) and gahnite-zincochromite (ZnAl<sub>2</sub>O<sub>4</sub>-ZnCr<sub>2</sub>O<sub>4</sub>) solid solution series. *Am. Mineral.*, **95**, 456.
- Hålenius *et al.* (2011): A first record of strong structural relaxation of TO<sub>4</sub> tetrahedra in a spinel solid solution. *Am. Mineral.*, **96**, 617.
- Juhin *et al.* (2007): Structural relaxation around substitutional Cr<sup>3+</sup> in MgAl<sub>2</sub>O<sub>4</sub>. *Phys. Rev. B*, **76**, 054105.
- Juhin *et al.* (2008): Structural relaxation around substitutional Cr<sup>3+</sup> in pyrope garnet. *Am. Mineral.*, **93**, 800.
- Khomenko & Platonov (1985): Electronic absorption spectra of Cr<sup>3+</sup> ions in natural clinopyroxenes. *Phys. Chem. Minerals*, **11**, 261.
- Kizler *et al.* (1996): Structural relaxation around substitutional Cr<sup>3+</sup> ions in sapphire. *J. Am. Ceram. Soc.*, **79**, 3.
- Langer (2001): A note on mean distances,  $R_{[MO_6]}$ , in substituted polyhedra, [(M<sub>1-x</sub>M<sub>x</sub>')O<sub>6</sub>], in the crystal structures of oxygen based solid solutions: local *versus* crystal averaging methods. *Z. Kristallogr.*, **216**, 87.

## SUGGESTED READING

- Langer *et al.* (2004): Local mean chromium–oxygen distances in Cr<sup>3+</sup>-centered octahedra of natural grossular-uvarovite garnet solid solution from electronic absorption spectra. *Z. Kristallogr.*, **219**, 272.
- Langer *et al.* (2006): Electronic absorption spectra of phosphate minerals with olivine-type structures: I. Members of the triphylite-lithiophilite series,  $M1^{[6]}Li^{M2[6]}(Fe_x^{2+}Mn_{1-x}^{2+})[PO_4]$ . *Eur. J. Mineral.*, **18**, 337.
- Lever (1984): Inorganic electronic spectroscopy (2<sup>nd</sup> Ed). Elsevier, 420 p.
- Marfunin (1979): Physics of minerals and inorganic materials. Springer, 340 p.
- Martins & Zunger (1984): Bond lengths around isovalent impurities and in semiconductor solid solutions. *Phys. Rev. B*, **30**, 6217.
- Mikkelsen & Boyce (1983): Extended x-ray-absorption fine-structure study of Ga<sub>1-x</sub>In<sub>x</sub>As random solid solutions. *Phys. Rev. B*, **28**, 7130.
- Poole & Itzel (1963): Optical reflection spectra of chromia-alumina. *J. Chem. Phys.*, **39**, 3445.
- Tanabe & Sugano (1954): On the absorption spectra of complex ions. I and II. *J. Phys. Soc. Jpn.*, **9**, 753 and 767.
- Taran *et al.* (2004): Local relaxation around  $[6]Cr^{3+}$  in synthetic pyrope–knorringite garnets,  $[8]Mg_3^{[6]}(Al_{1-x}Cr_x^{3+})_2[4]Si_3O_{12}$ , from electronic absorption spectra. *Phys. Chem. Minerals*, **31**, 650.

## SUGGESTED READING

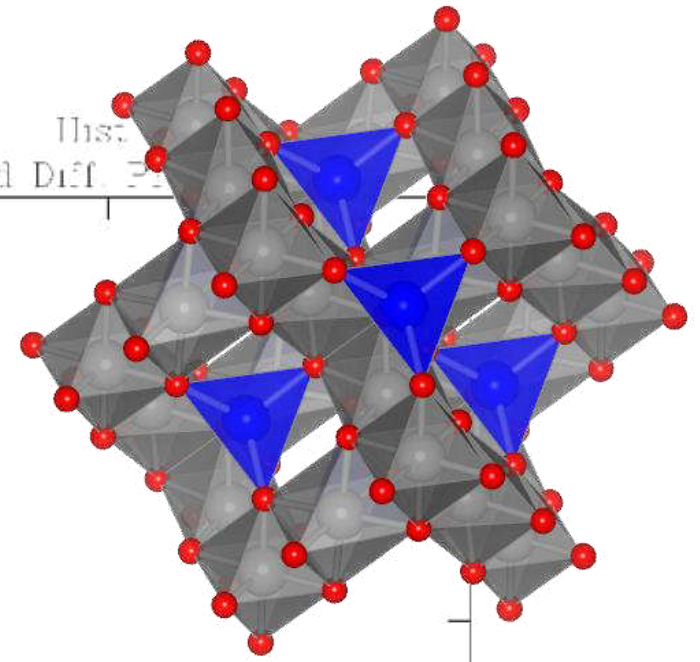
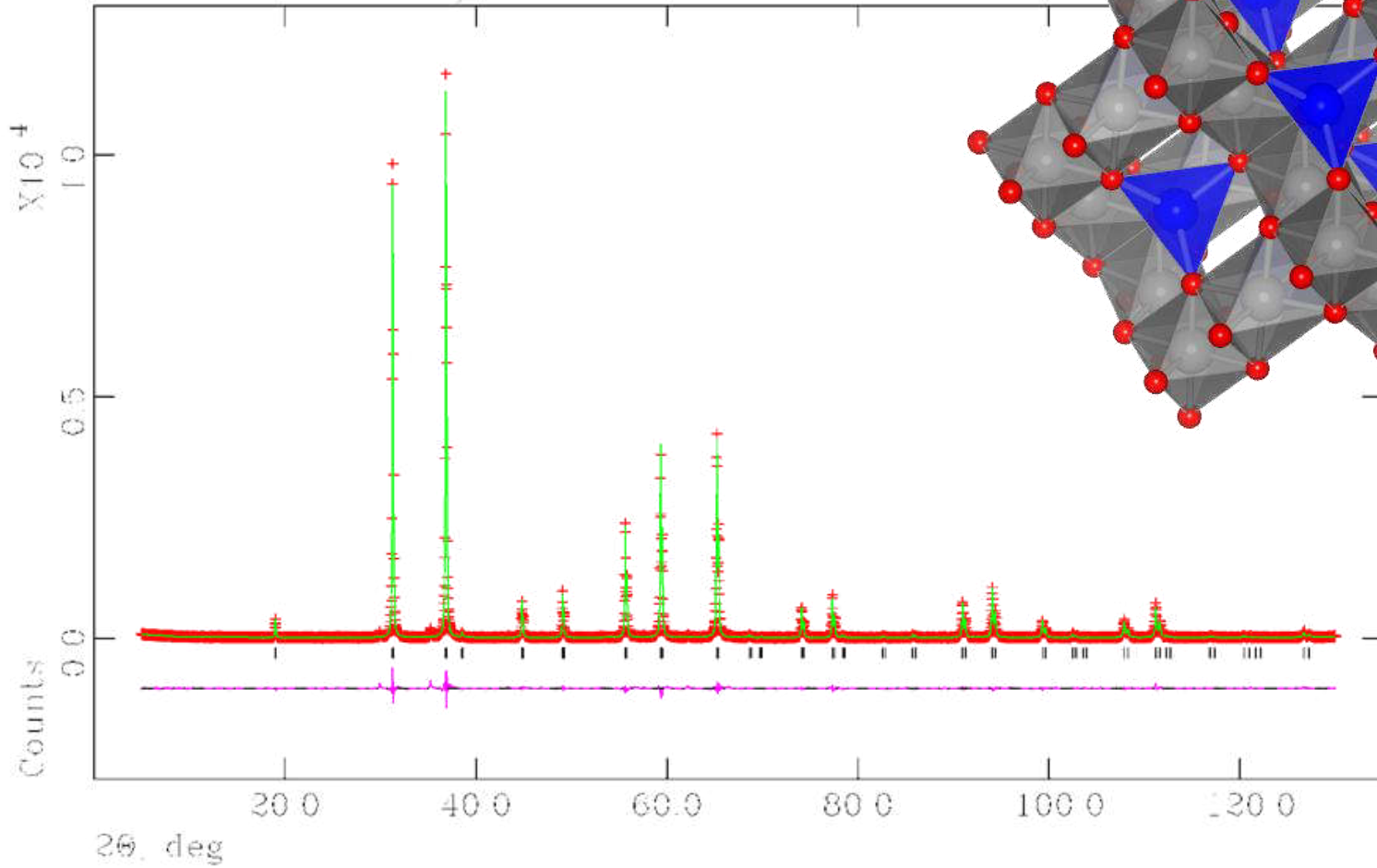
- Taran *et al.* (2011): High-pressure electronic absorption spectroscopy of natural and synthetic Cr<sup>3+</sup>-bearing clinopyroxenes. *Phys. Chem. Minerals*, **38**, 345.
- Urusov (1992): A geometric model of deviation from Vegard's rule. *J. Solid State Chem.*, **98**, 223.
- Urusov (2001): The phenomenological theory of solid solutions. In "Solid solutions in silicate and oxide systems". *EMU Notes Mineral.*, **3**, 121.
- Urusov & Taran (2012): Structural relaxation and crystal field stabilization in Cr<sup>3+</sup>-containing oxides and silicates. *Phys. Chem. Minerals*, **39**, 17.
- Vegard (1921): Die Konstitution der Mischkristalle und die Raumfüllung der Atome. *Z. Phys.*, **5**, 17.
- Wildner *et al.* (2004): Optical absorption spectroscopy in geosciences. Part I: Basic concepts of crystal field theory. In "Spectroscopic methods in mineralogy". *EMU Notes Mineral.*, **6**, 93.
- Zen (1956): Validity of "Vegard's law". *Am. Mineral.*, **41**, 523.

# e1. SPINEL

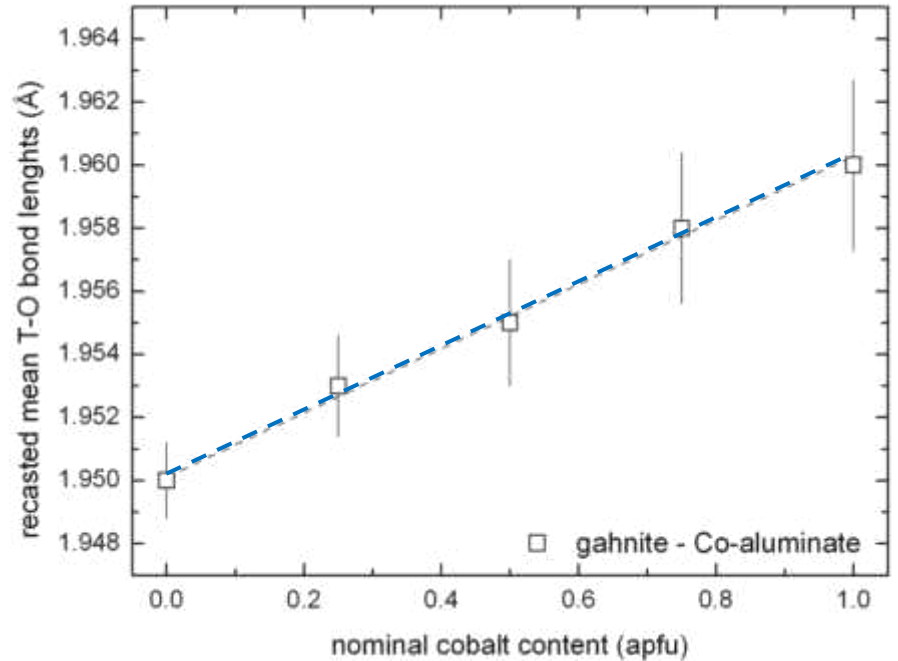
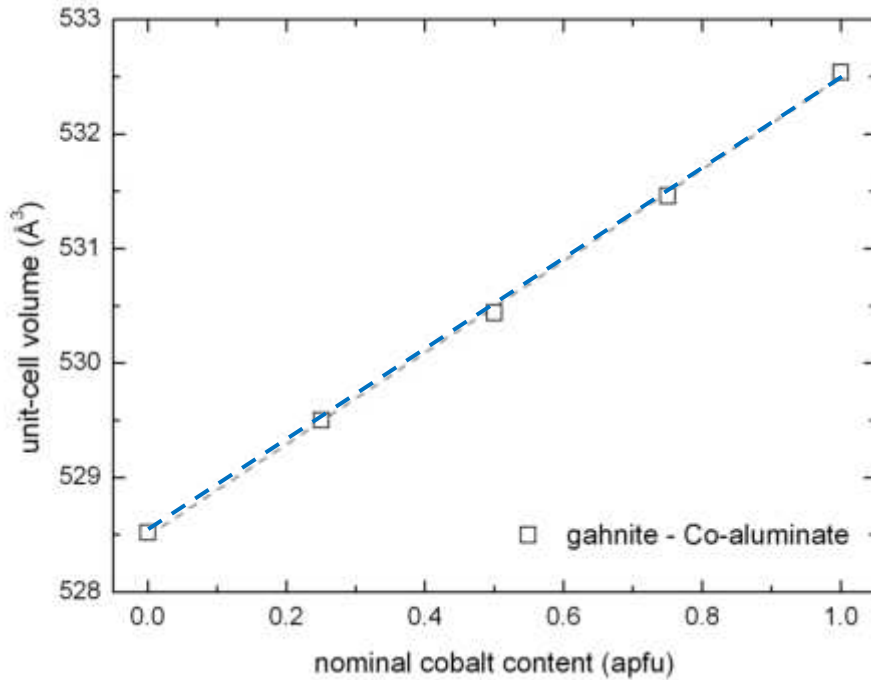
ZnAl<sub>2</sub>O<sub>4</sub>

Lambda = 5405 A L S cycle 3263

Obsd. and Diff.  $\chi^2$



# e1. SPINEL



Agreement with the Vegard's law from the linear trends of:

- unit cell parameters;
- mean bond lengths.

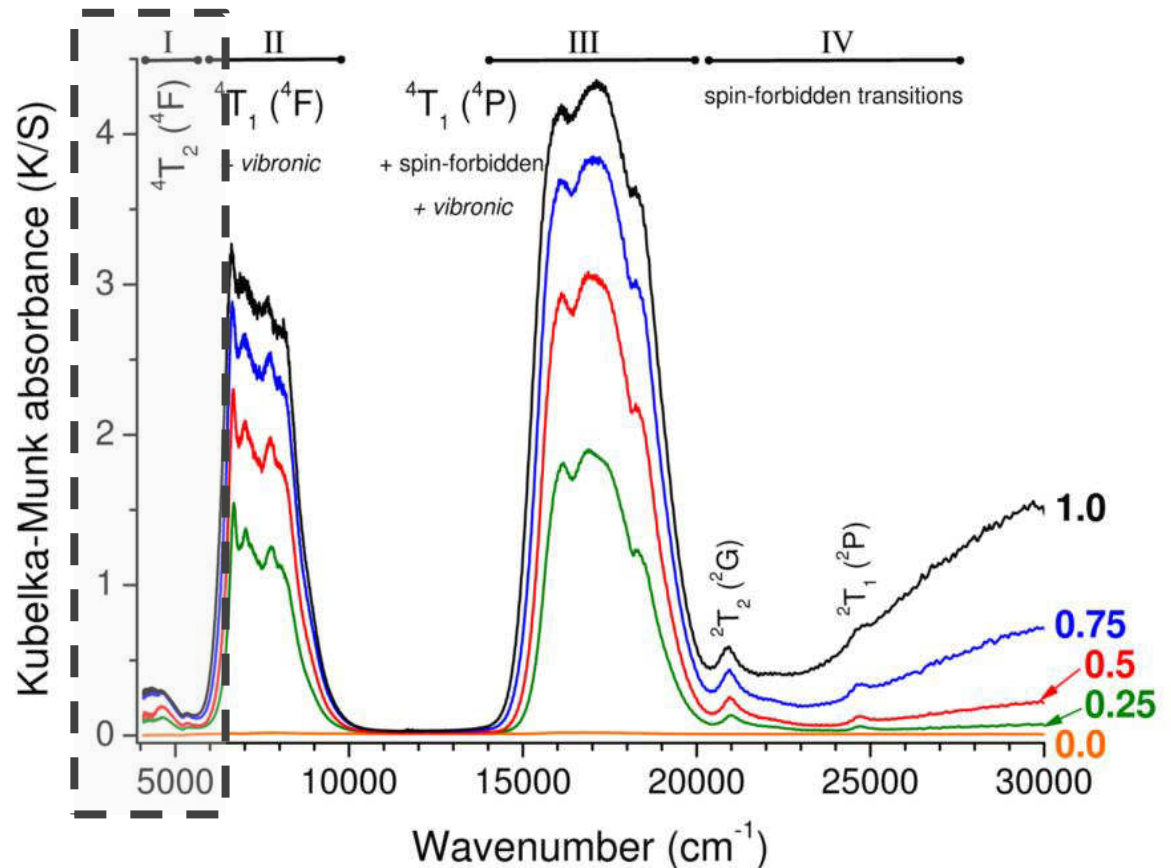
progressive and linear increase (although  $i.r.^{[IV]Zn^{2+}} > i.r.^{[IV]Co^{2+}}$ )

# e1. SPINEL

Several absorption band originate from different phenomena

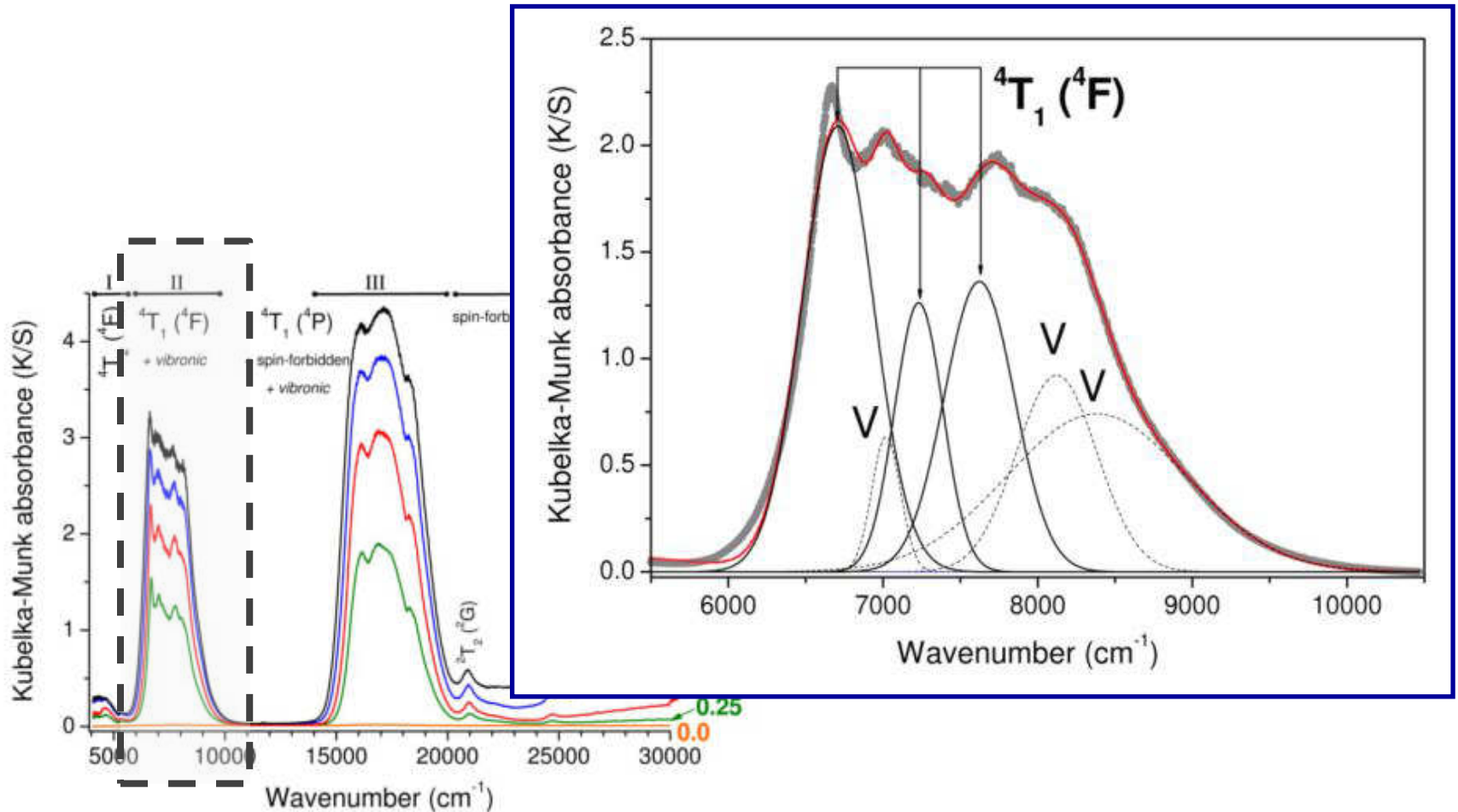
**note:** A strong spin-orbit coupling, expect for  $d^7$  ions, leads to a conspicuous splitting of the  $\text{Co}^{2+}$  bands.

[I]  $4000\text{--}6000\text{ cm}^{-1}$ :  ${}^4T_2({}^4F)$  spin-allowed transitions is split into two bands at  $4150\text{ cm}^{-1}$  and around  $4000\text{ cm}^{-1}$ ) + vibronic effects.



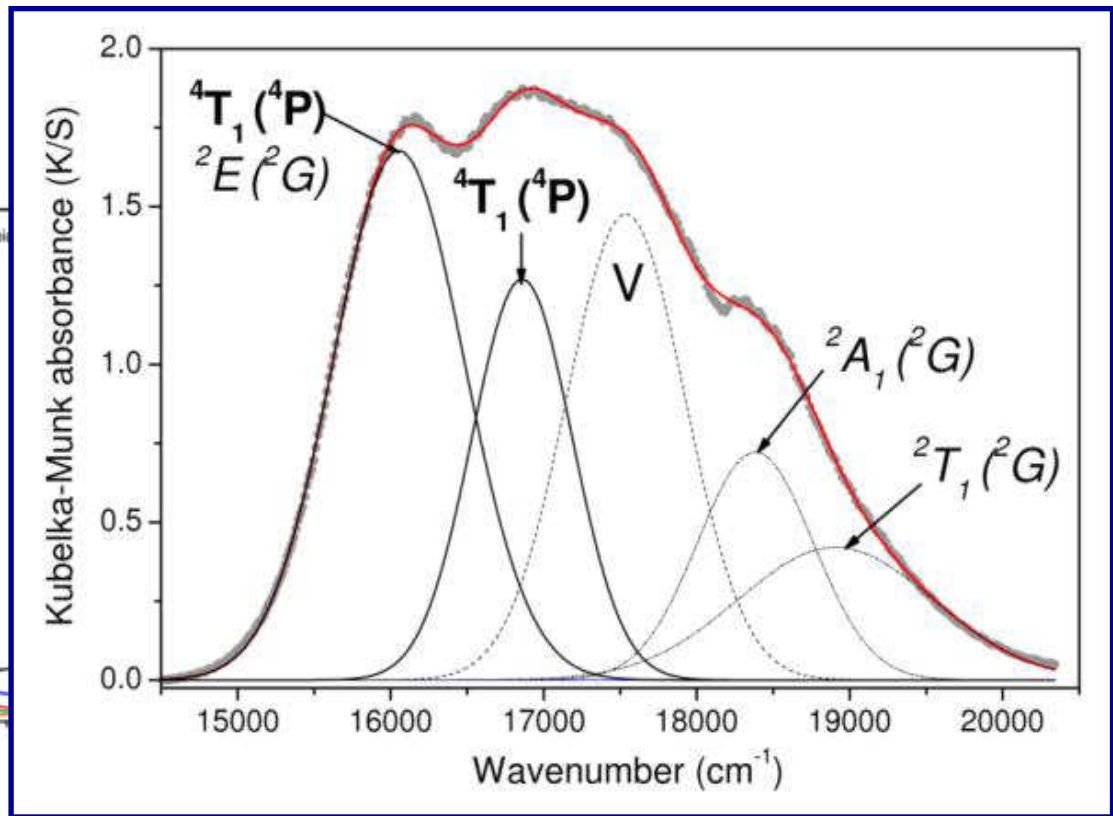
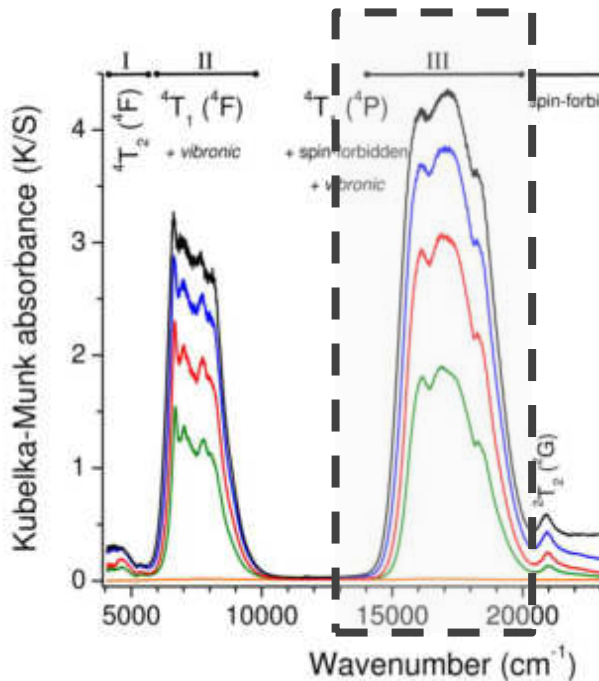
# e1. SPINEL

[II] 6000–9000  $\text{cm}^{-1}$ : the  ${}^4T_1({}^4F)$  spin-allowed transition is split into three components (around 6700, 7200 and 7600  $\text{cm}^{-1}$ , respectively) which are associated to various vibronic sidebands



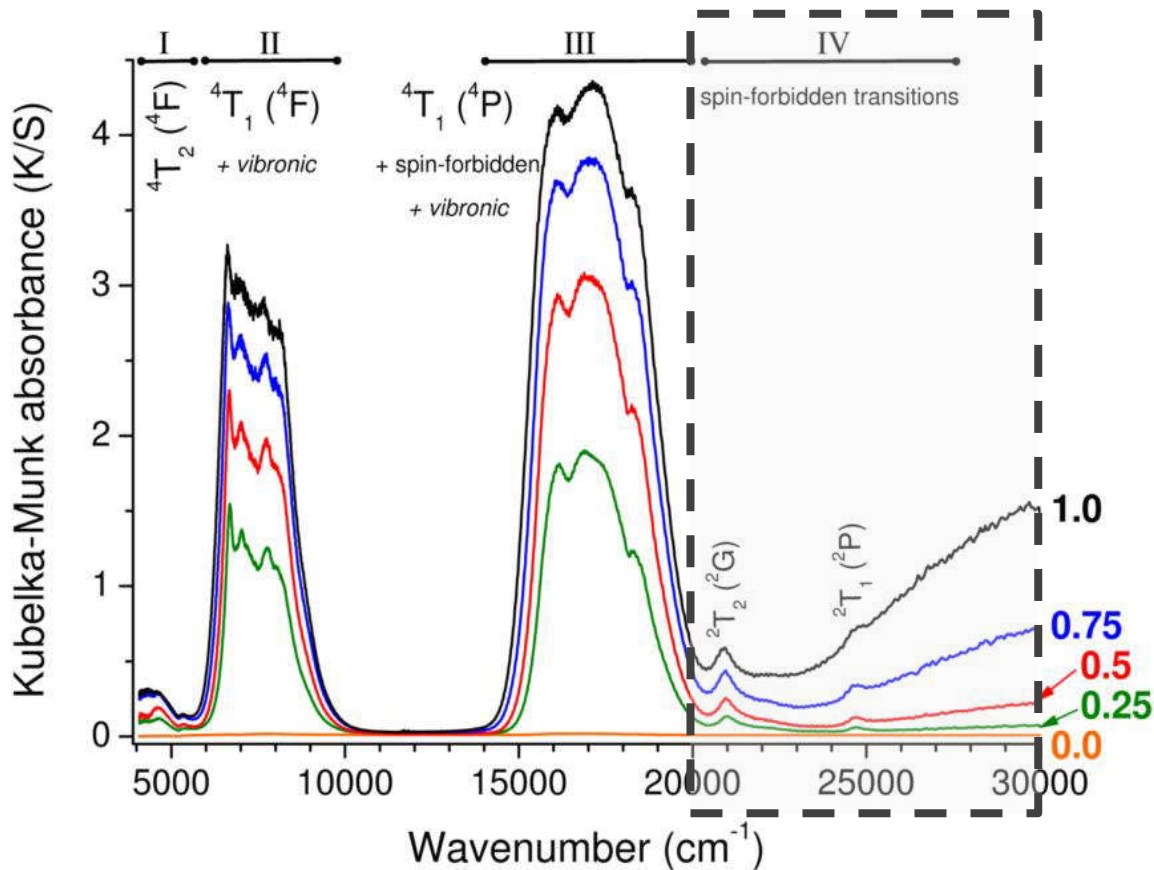
# e1. SPINEL

[III] 15000–20000  $\text{cm}^{-1}$ : quadruplet  ${}^4T_1({}^4P)$  transition overlaps four doublet transitions. The  ${}^4T_1$  transition is three-fold split into the 16000–17000  $\text{cm}^{-1}$  range, where only two bands are clearly distinguished, although the first one is strongly mixed with the  ${}^2E$  and  ${}^2T_1$  states. A third band at about 18500  $\text{cm}^{-1}$  is attributed to both the  ${}^2A_1$  and  ${}^2T_2$  spin-allowed transitions, whose anomalous intensity stems from vibronic effects in the 17000–18000  $\text{cm}^{-1}$  interval.



# e1. SPINEL

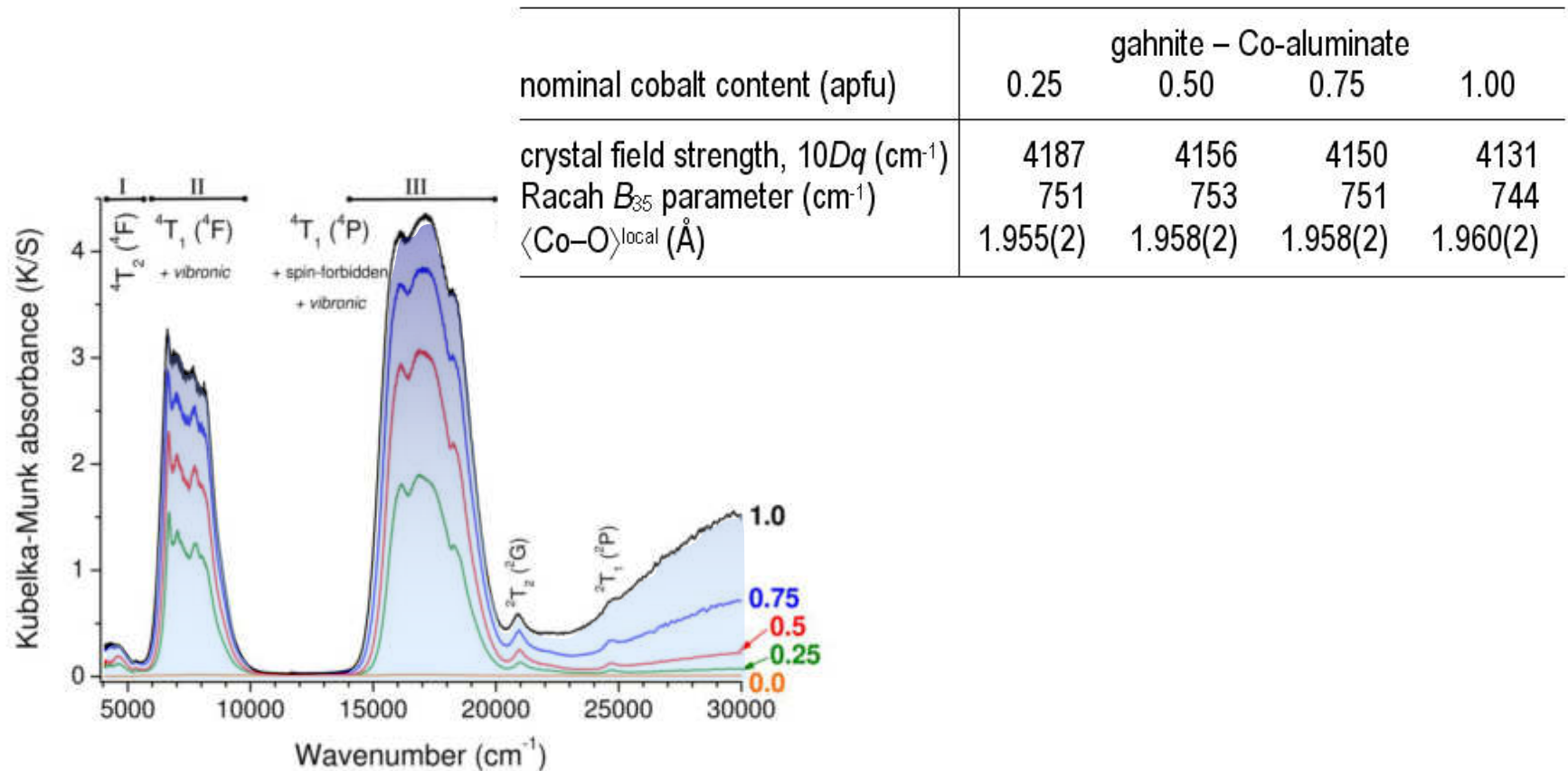
[IV] over  $20000\text{ cm}^{-1}$ : spin-forbidden transitions occur in the high energy part of spectra. Only two weak bands are discernible and attributed to  ${}^2T_1({}^2P)$  at  $\sim 21000\text{ cm}^{-1}$  and  ${}^2T_1({}^2H)$  at  $\sim 24500\text{ cm}^{-1}$ .



# e1. SPINEL

Typical optical spectra of  $\text{Co}^{2+}$  in tetrahedral coordination ( $d-d$  electronic transitions):

- band absorbance increase with cobalt content;
- band energy shifted.



# e1. SPINEL

Point Charge Approximation

$$10Dq = \text{const} \times \langle \text{Co-O} \rangle^{-5}$$

const: effective charge on the ligand (Q) and av. radius of the *d* orbital  $\langle r \rangle^4$

$$\langle \text{Co-O} \rangle_x^{\text{local}} = \langle \text{Co-O} \rangle_{x=1} \times [(10Dq_{\text{Co}})_{x=1} / (10Dq_{\text{Co}})_x]^{1/5}$$

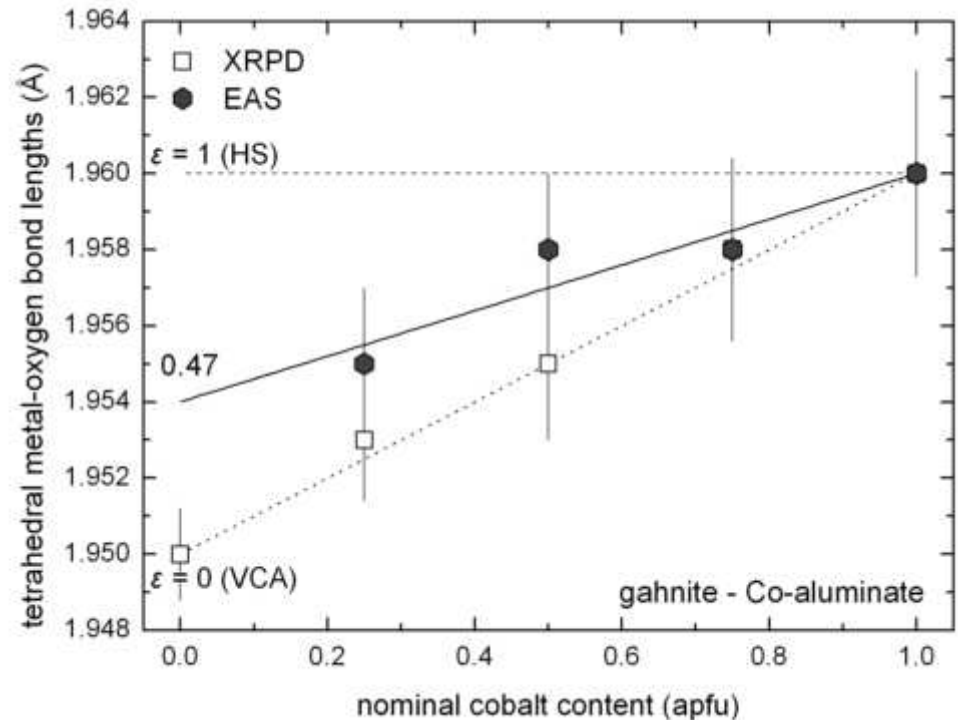
Thus:

$$\varepsilon = (\langle \text{Co-O} \rangle_x^{\text{local}} - \langle \text{Zn-O} \rangle) \times (\langle \text{Co-O} \rangle - \langle \text{Zn-O} \rangle)^{-1}$$

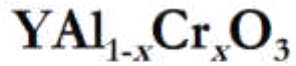
Relaxation coefficient

$$\varepsilon(\lim_{x_{\text{Co}} \rightarrow 0}) = 0.47,$$

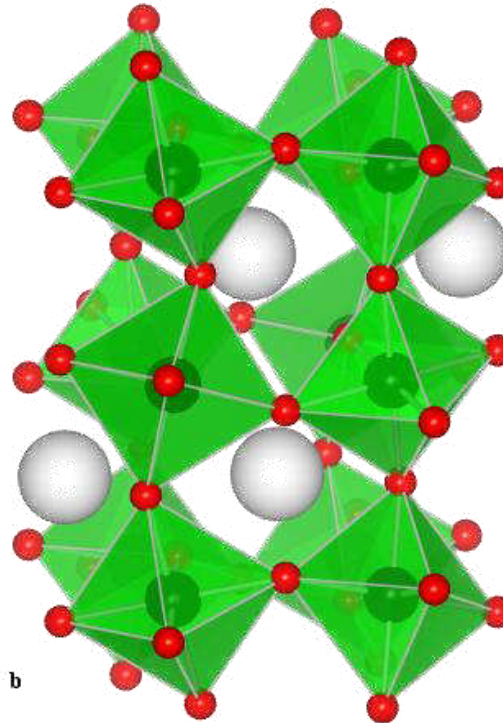
not so far from the Vegard's law  
where the structural  
relaxation is absent ( $\varepsilon = 0$ ).



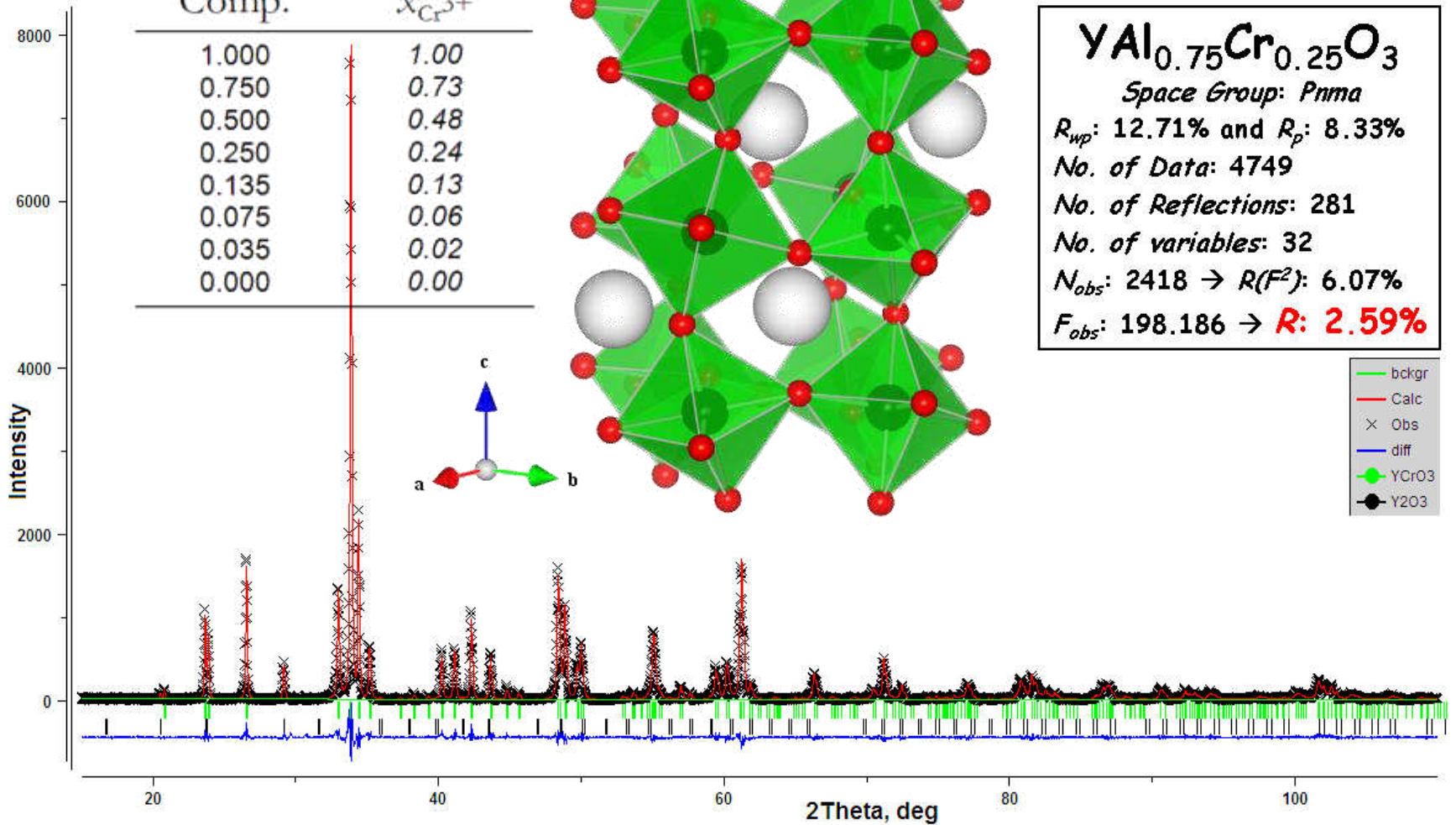
## e2. PEROVSKITE



Cr <sup>3+</sup> Batch Comp.	Refined $x_{\text{Cr}^{3+}}$
1.000	1.00
0.750	0.73
0.500	0.48
0.250	0.24
0.135	0.13
0.075	0.06
0.035	0.02
0.000	0.00



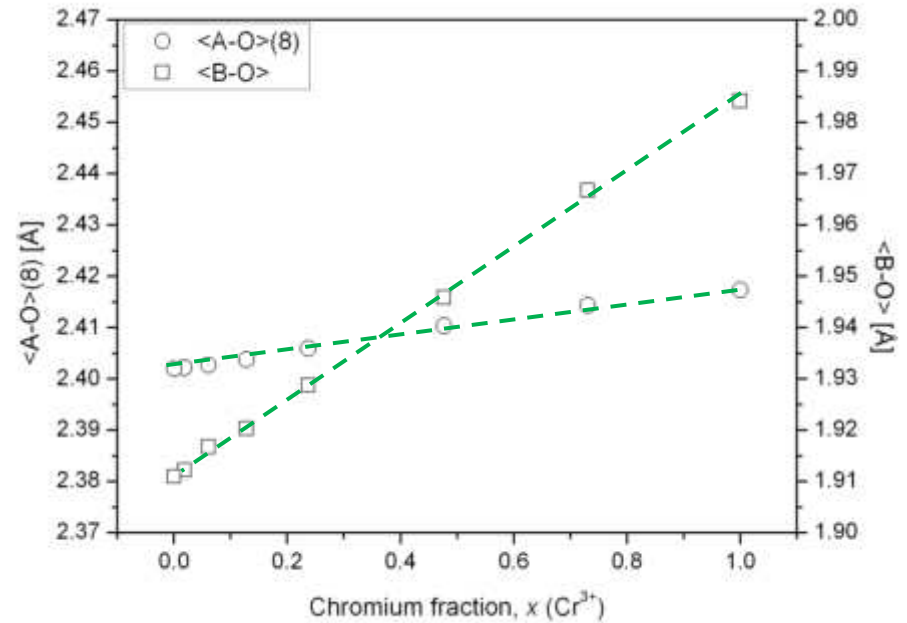
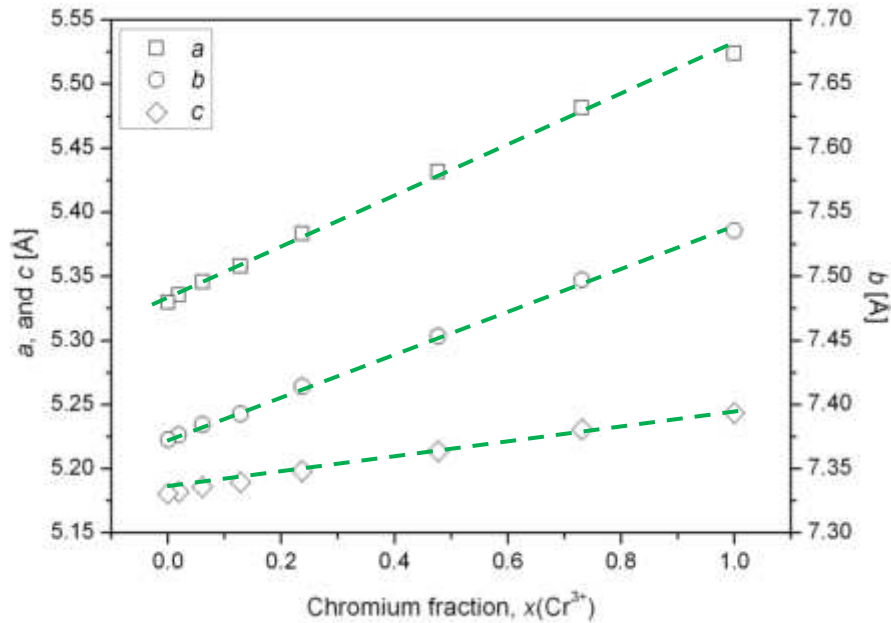
$\text{YAl}_{0.75}\text{Cr}_{0.25}\text{O}_3$   
 Space Group: *Pnma*  
 $R_{wp}$ : 12.71% and  $R_p$ : 8.33%  
 No. of Data: 4749  
 No. of Reflections: 281  
 No. of variables: 32  
 $N_{obs}$ : 2418  $\rightarrow R(F^2)$ : 6.07%  
 $F_{obs}$ : 198.186  $\rightarrow R$ : **2.59%**



## e2. PEROVSKITE

Agreement with the Vegard's law from the linear trends of:

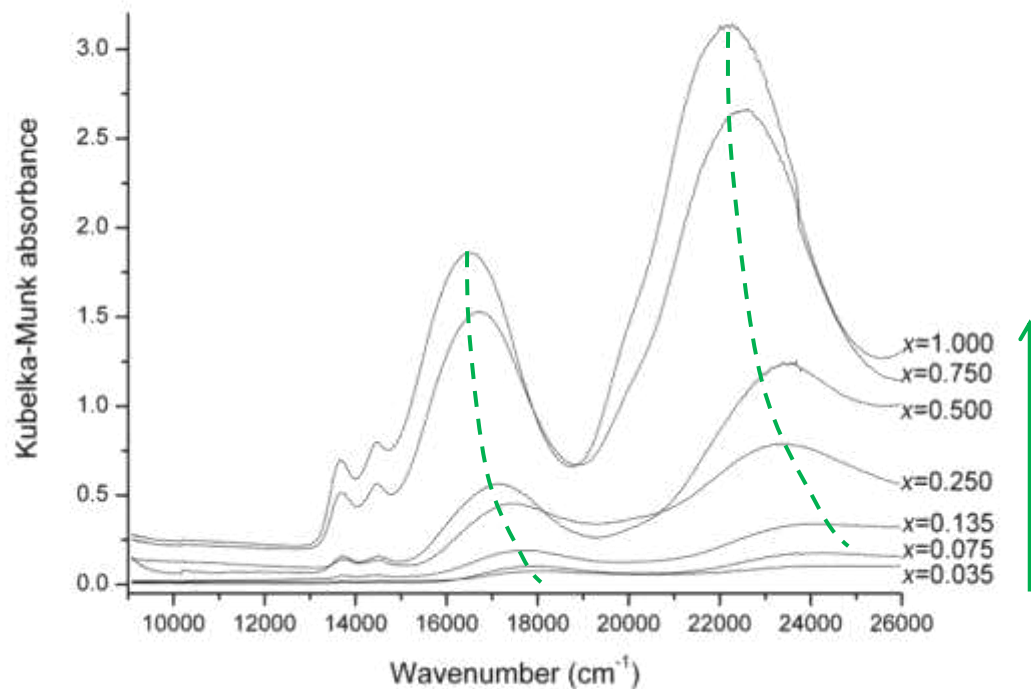
- unit cell parameters;
- mean bond lengths.



## e2. PEROVSKITE

Typical optical spectra of  $\text{Cr}^{3+}$  in octahedral coordination ( $d-d$  electronic transitions):

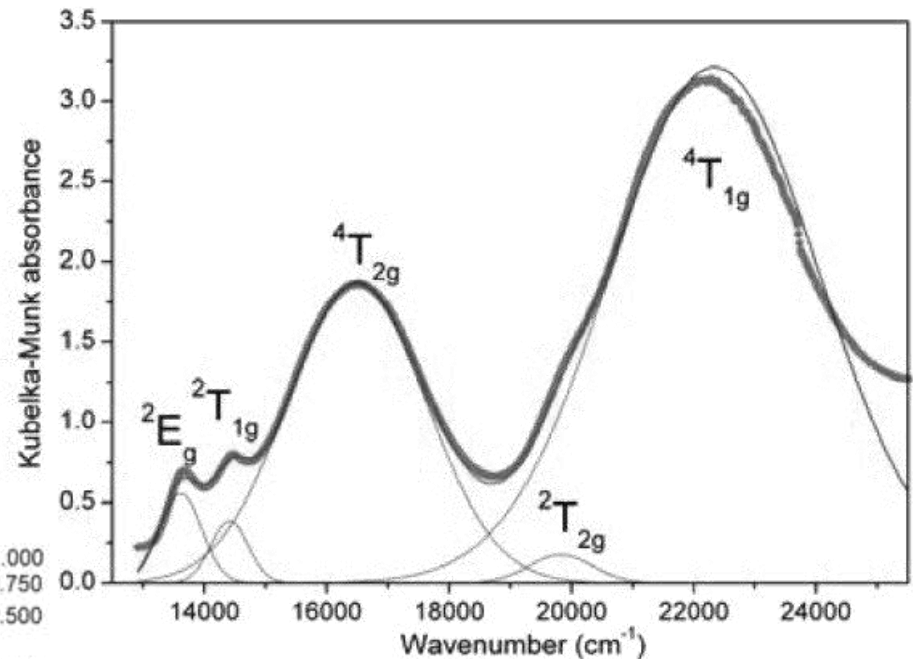
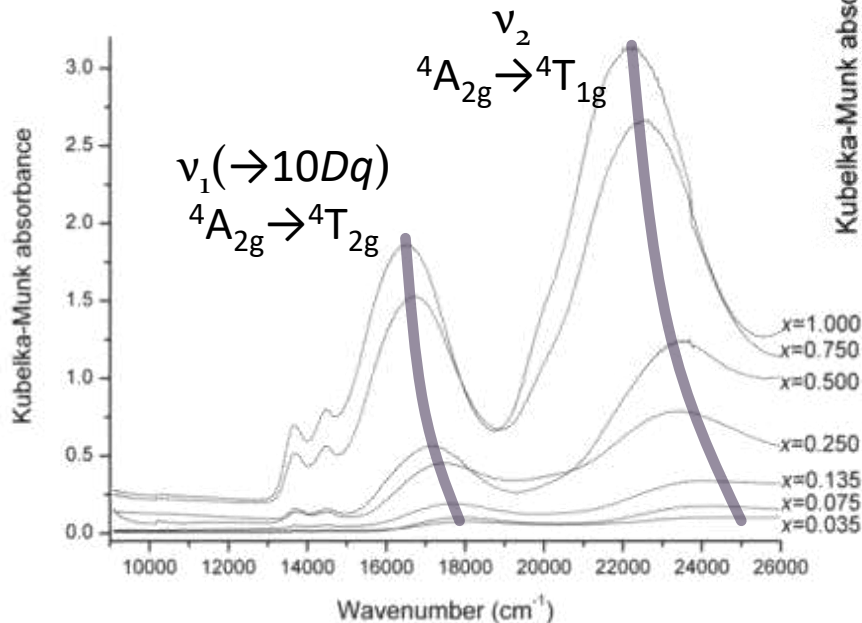
- band absorbance increase with chromium content;
- band energy shifted because of changing in crystal field strength in the Cr–O bond length.



## e2. PEROVSKITE

16000–18000  $\text{cm}^{-1}$  & 22000–24000  $\text{cm}^{-1}$ : intense bands attributed to the parity-forbidden and spin-allowed transitions from the ground level  ${}^4A_{2g}({}^4F)$  to  ${}^4T_{2g}({}^4F)$  and  ${}^4T_{1g}({}^4F)$ , respectively.

13700  $\text{cm}^{-1}$ , 14300  $\text{cm}^{-1}$  and 19500  $\text{cm}^{-1}$ : Minor bands due to parity- and spin-forbidden transitions  ${}^4A_{2g}({}^4F) \rightarrow {}^2E_g({}^2G)$ ,  $\rightarrow {}^2T_{1g}({}^2G)$  and  $\rightarrow {}^2T_{2g}({}^2G)$ , respectively.

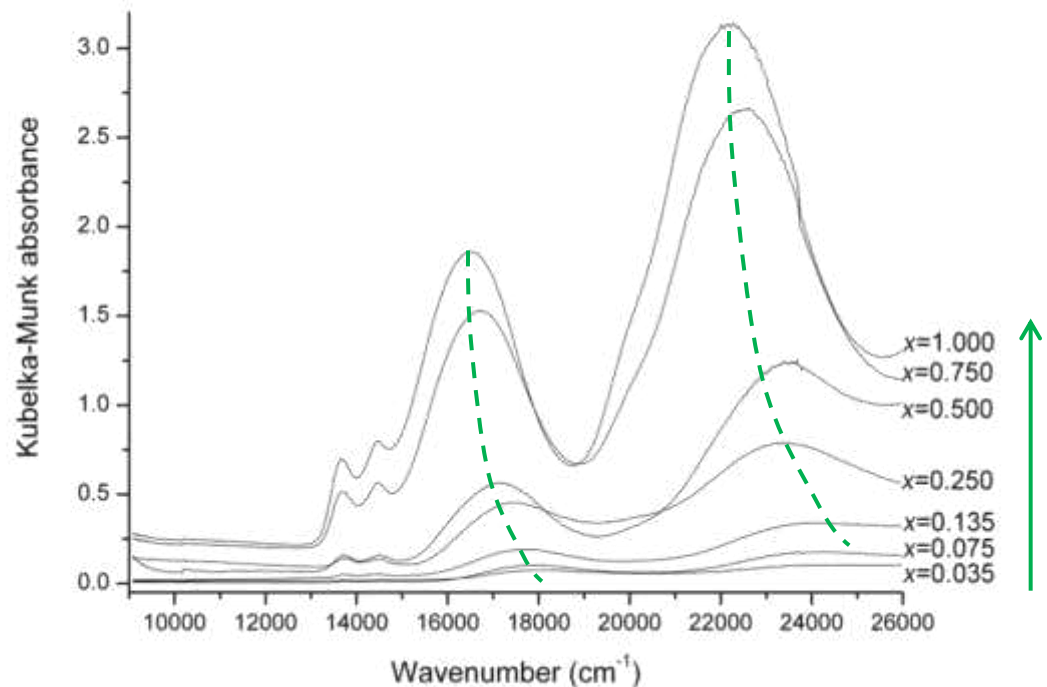


## e2. PEROVSKITE

Typical optical spectra of Cr<sup>3+</sup> in octahedral coordination (*d-d* electronic transitions):

- band absorbance increase with chromium content;
- band energy shifted.

Sample	10Dq (cm <sup>-1</sup> )	<Cr-O> <sup>local</sup> (Å)
Cr35	17867	1.950
Cr75	17864	1.950
Cr135	17616	1.956
Cr250	17349	1.962
Cr500	16968	1.971
Cr750	16627	1.979
Cr1000	16405	1.984



## e2. PEROVSKITE

Point Charge Approximation

$$10Dq = \text{const} \times \langle \text{Cr-O} \rangle^{-5}$$

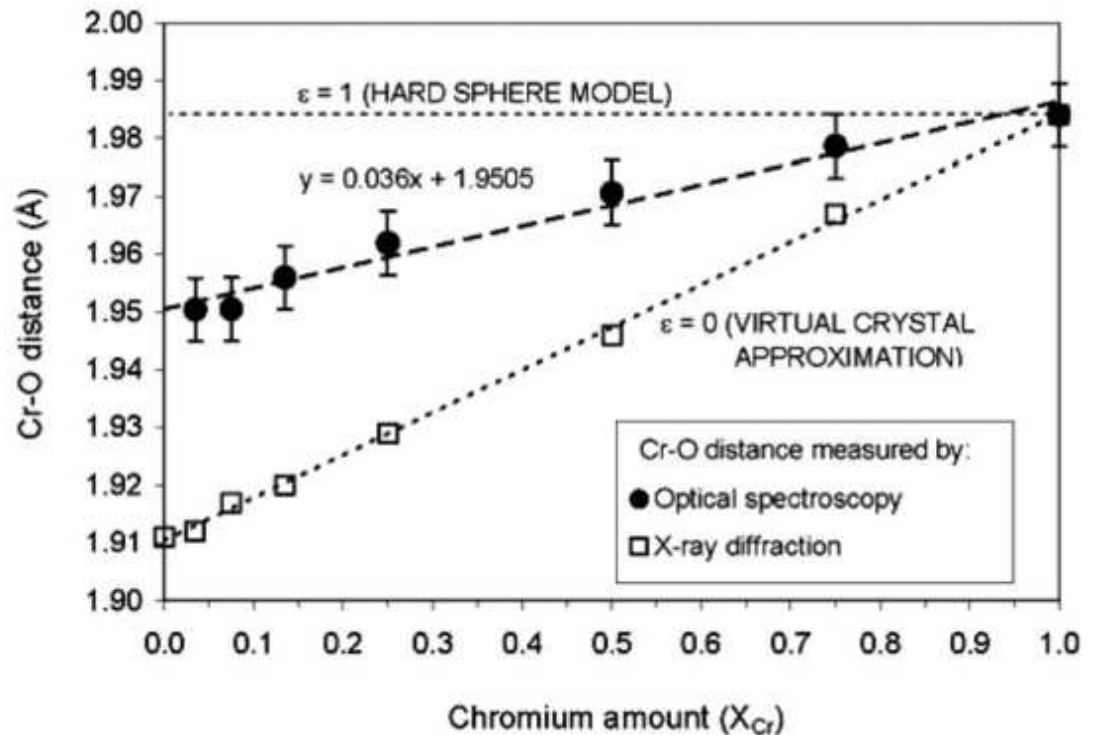
const: effective charge on the ligand (Q) and av. radius of the *d* orbital  $\langle r \rangle^4$

$$\langle \text{Cr-O} \rangle_x^{\text{local}} = \langle \text{Cr-O} \rangle_{x=1} \times [(10Dq_{\text{Cr}})_{x=1} / (10Dq_{\text{Cr}})_x]^{1/5}$$

Thus:

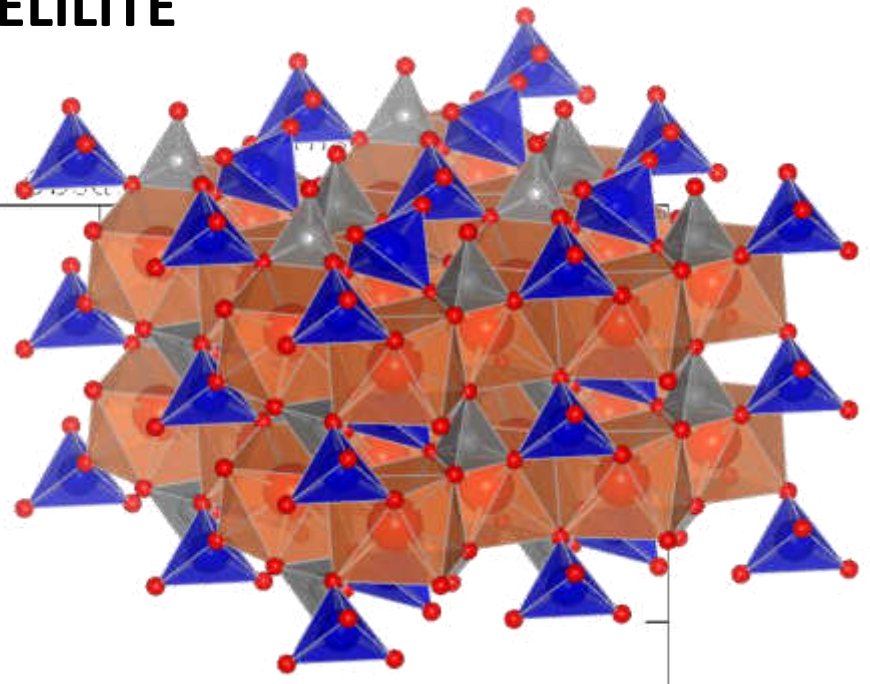
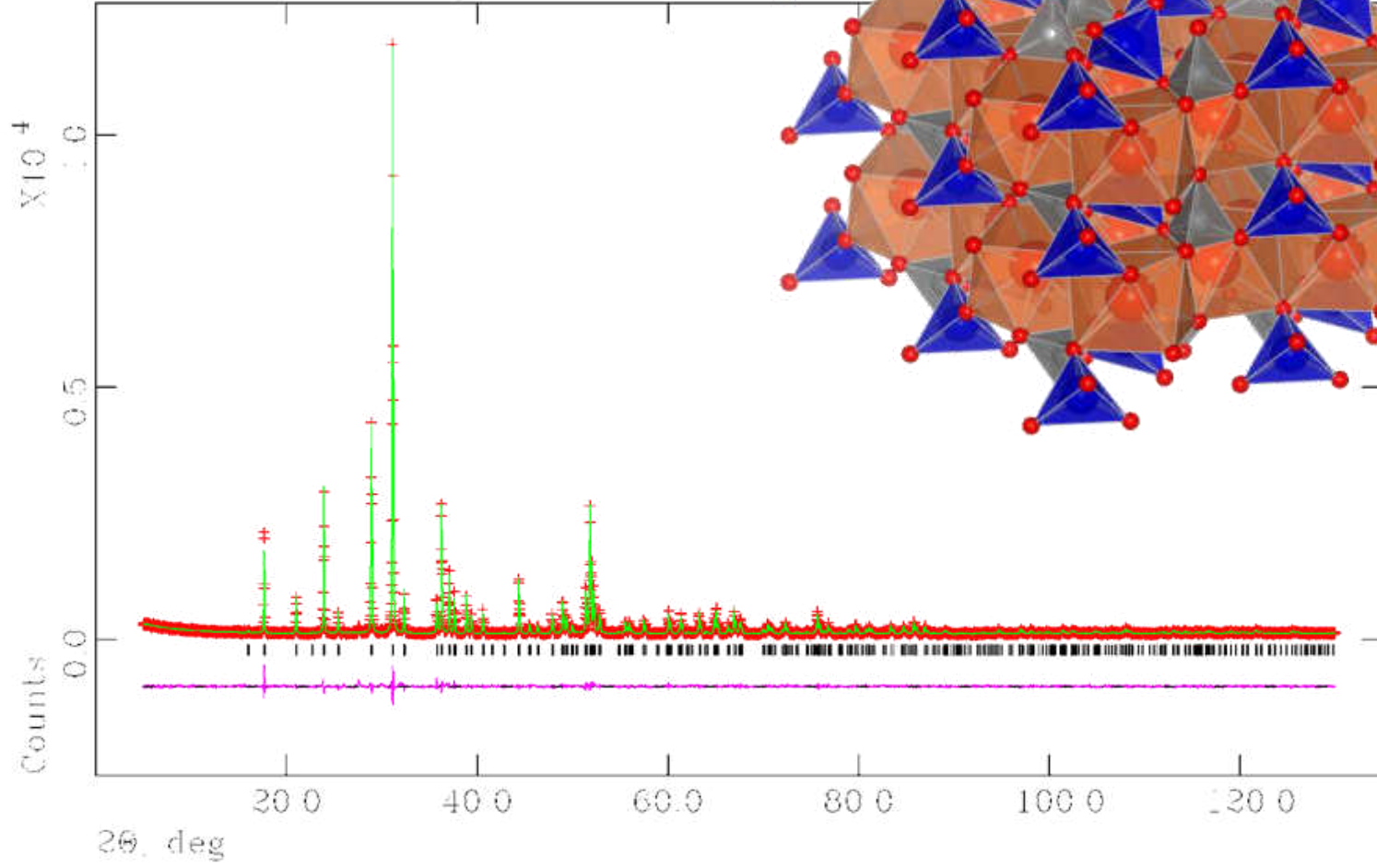
$$\varepsilon = (\langle \text{Cr-O} \rangle_x - \langle \text{Al-O} \rangle) \times (\langle \text{Cr-O} \rangle - \langle \text{Al-O} \rangle)^{-1}$$

Relaxation coefficient  
 $\varepsilon(\lim x_{\text{Cr}} \rightarrow 0) = 0.54$ ,  
 between the HS and  
 the VCA models.

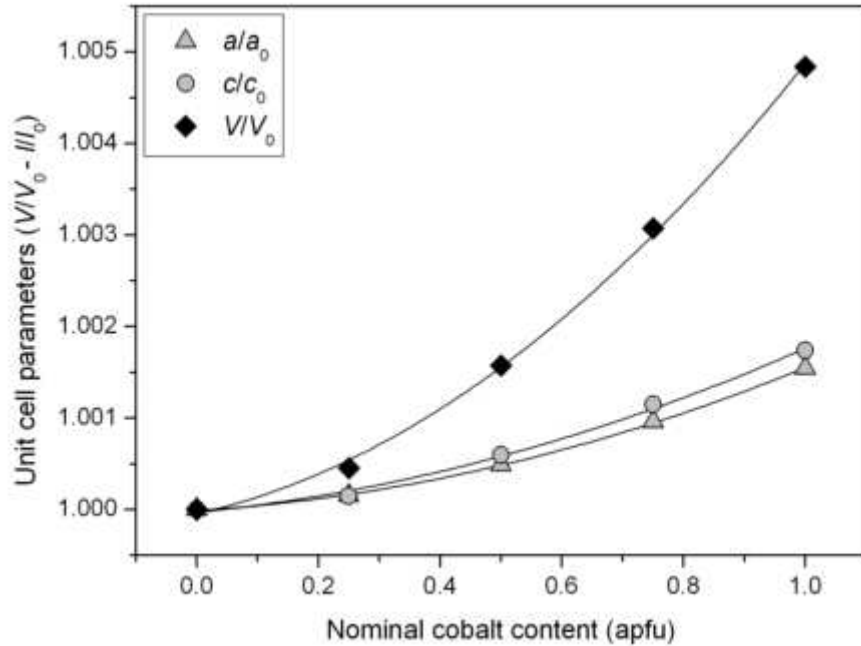


# e3. MELILITE

Ca<sub>27</sub>n<sub>0.35</sub>Co<sub>0.75</sub>Si<sub>207</sub>  
Lambda 1.5405 A L S cycle 3854



### e3. MELILITE

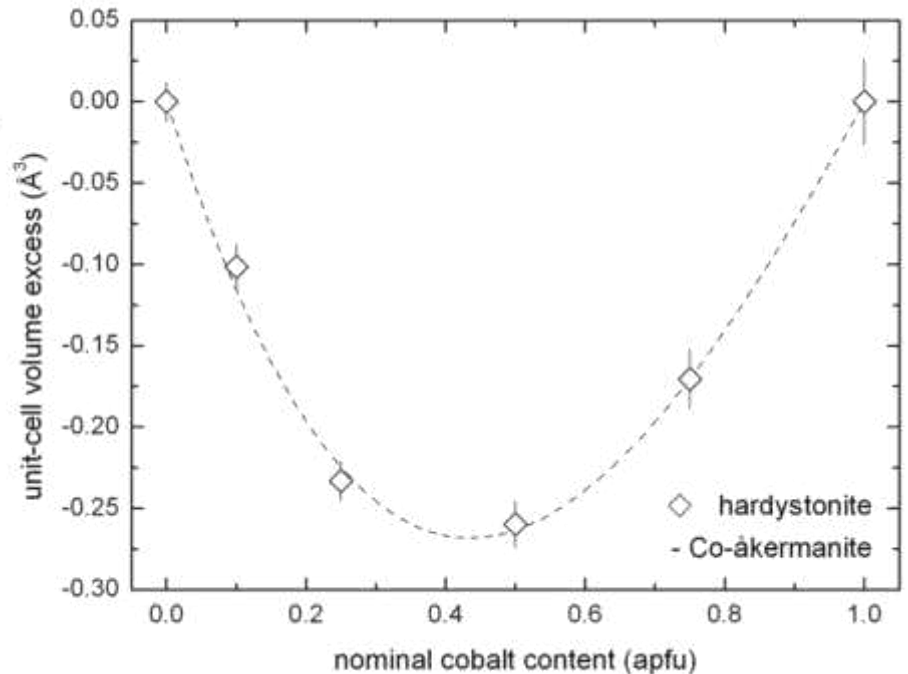


hardystonite–Co-åkermanite

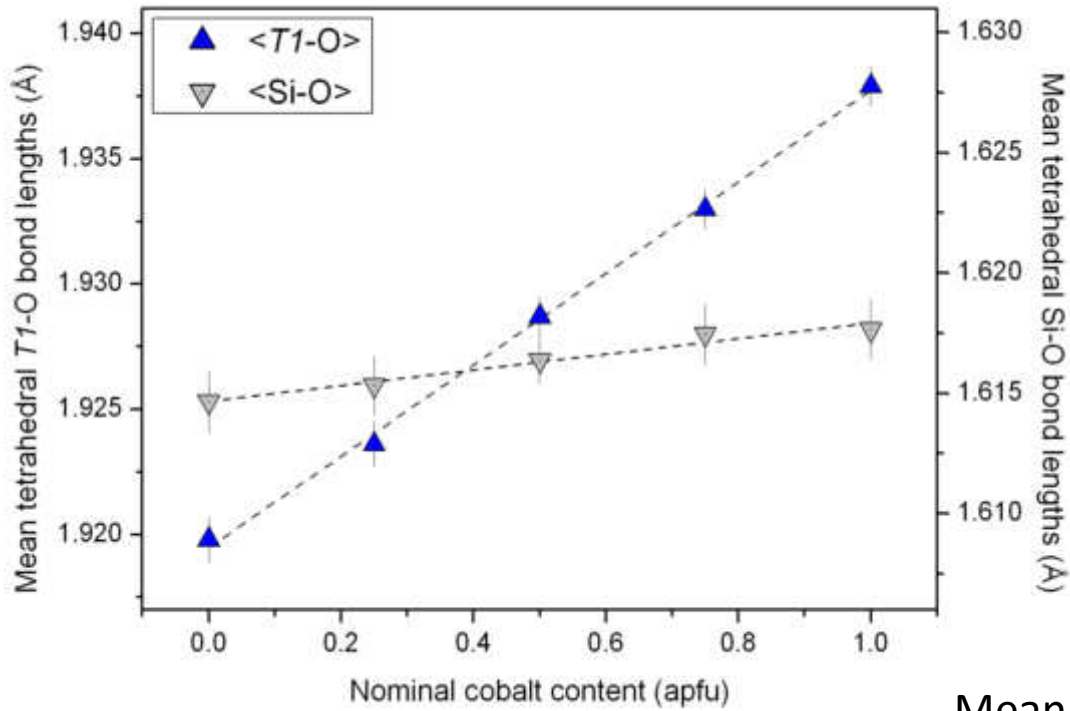
- Lattice parameters do not follow the Vegard'law (quadratic fitting);
- The dotted line represents a 3<sup>rd</sup> order polynomial fitting (i.e., the biparametric Margules eq.):

$$V^{ex} = W_A x(1-x)^2 + W_B x^2(1-x),$$

with  $W_A = -1.34(6) \text{ \AA}^3$  and  $W_B = -0.76(8) \text{ \AA}^3$ .



### e3. MELILITE

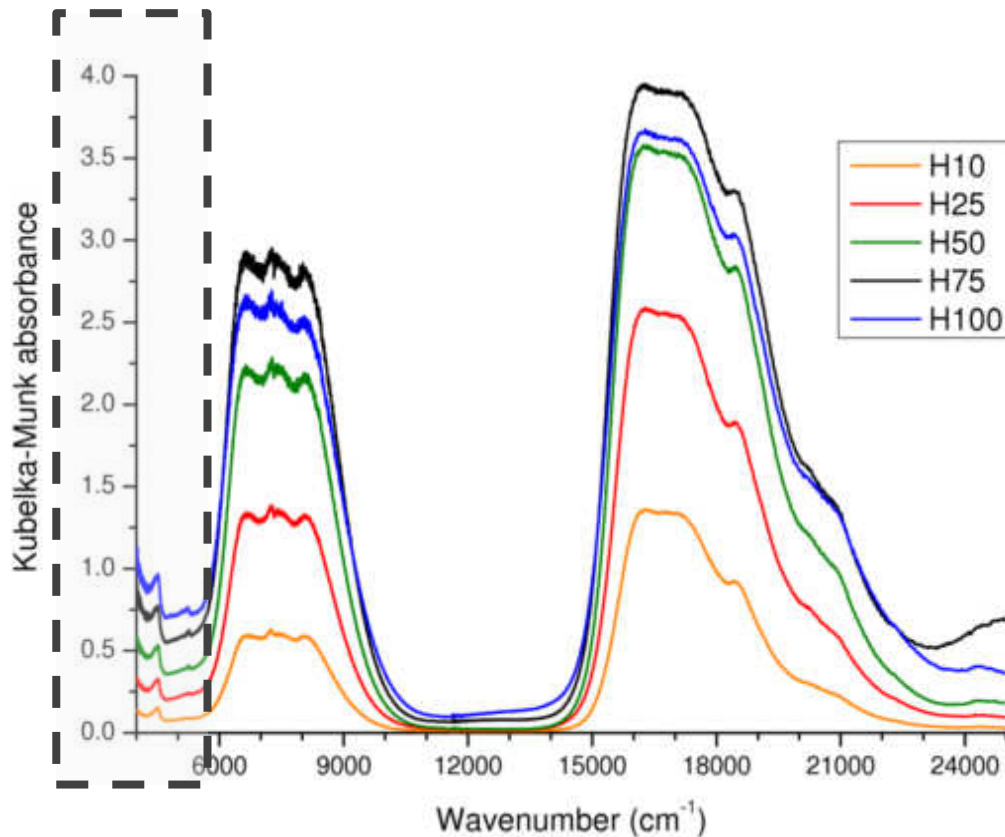


- Mean tetrahedral bond lengths scale linearly as a function of Co increasing.

### e3. MELILITE

Optical density increases as a function of the  $\text{Co}^{2+}$  content.

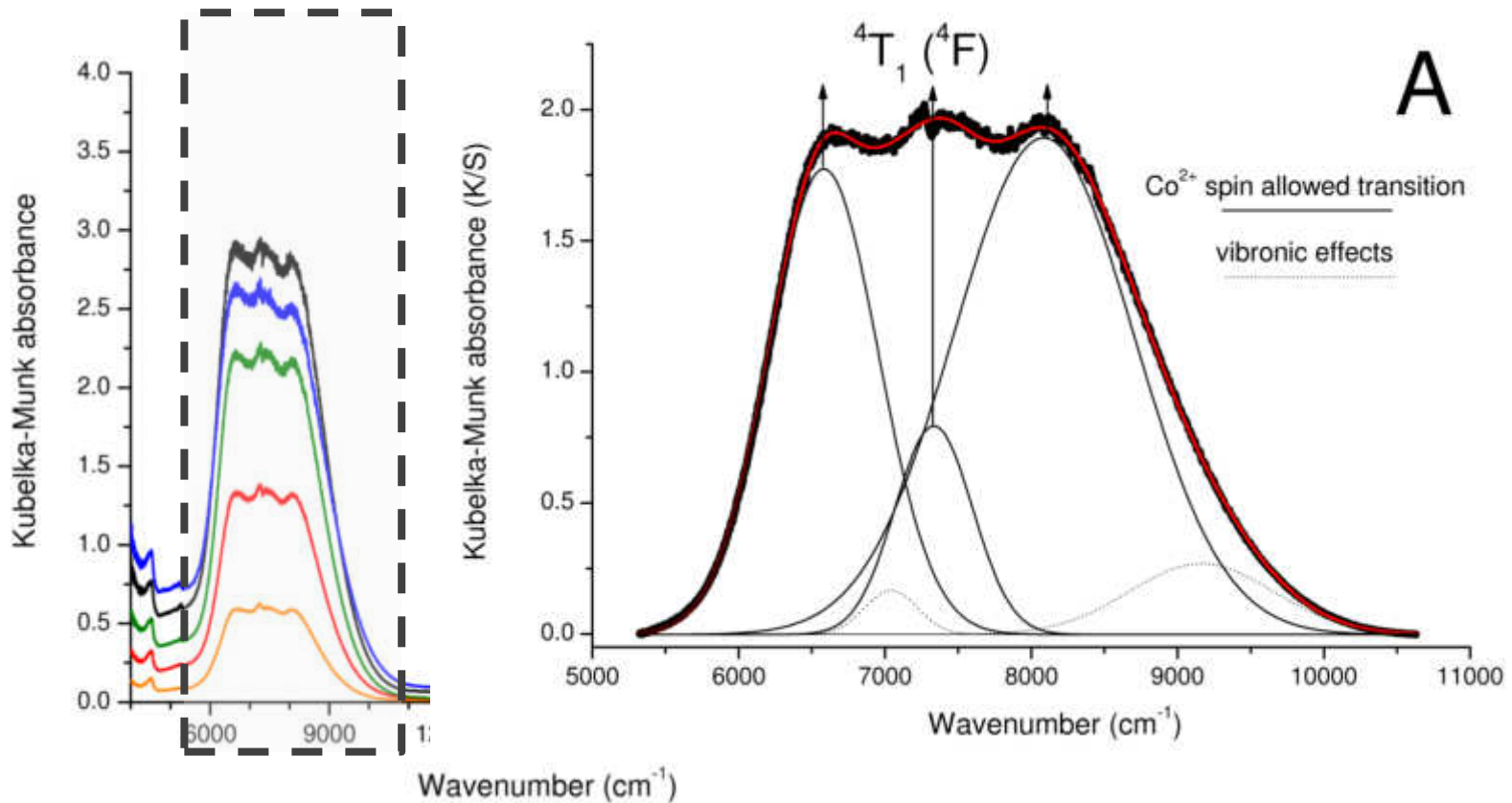
Absorption bands from tetrahedral coordinated  $\text{Co}^{2+}$  ( $d-d$  electronic transition).



4000–5500  $\text{cm}^{-1}$ : low intensity bands  
consequence of vibronic transitions  
and one of the three subbands  
(4500  $\text{cm}^{-1}$ ) caused by the splitting  
of the  ${}^4\text{T}_2$  ( ${}^4\text{F}$ ) transition.

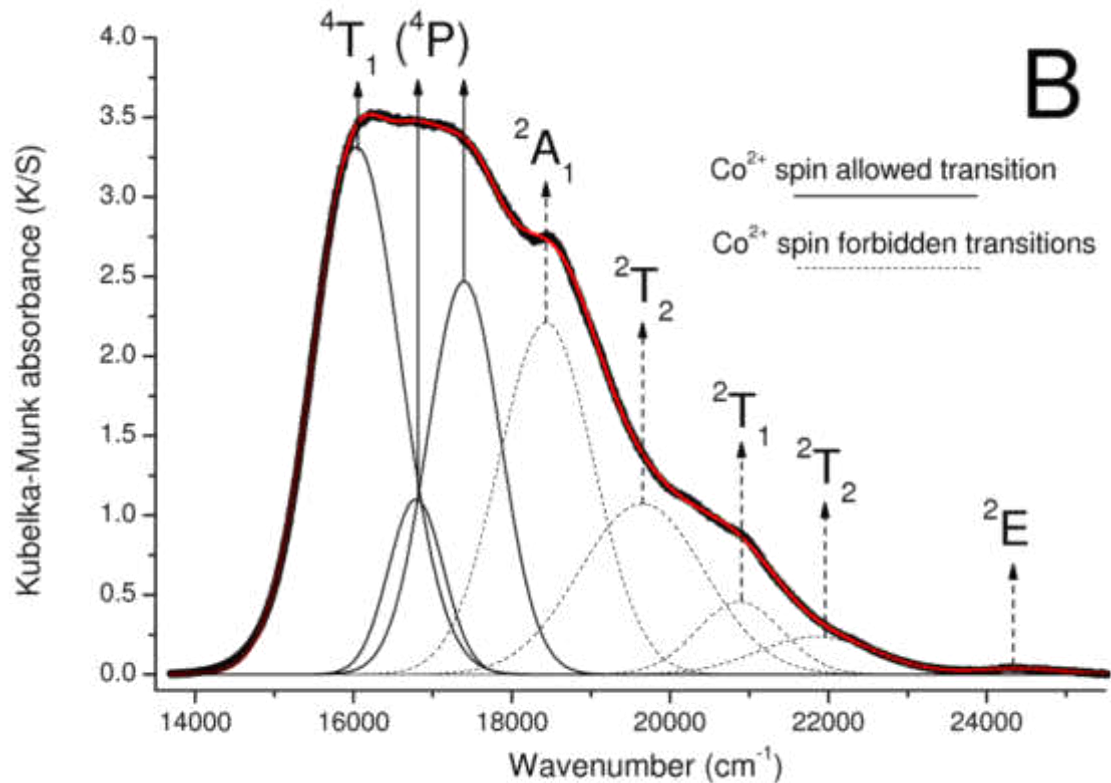
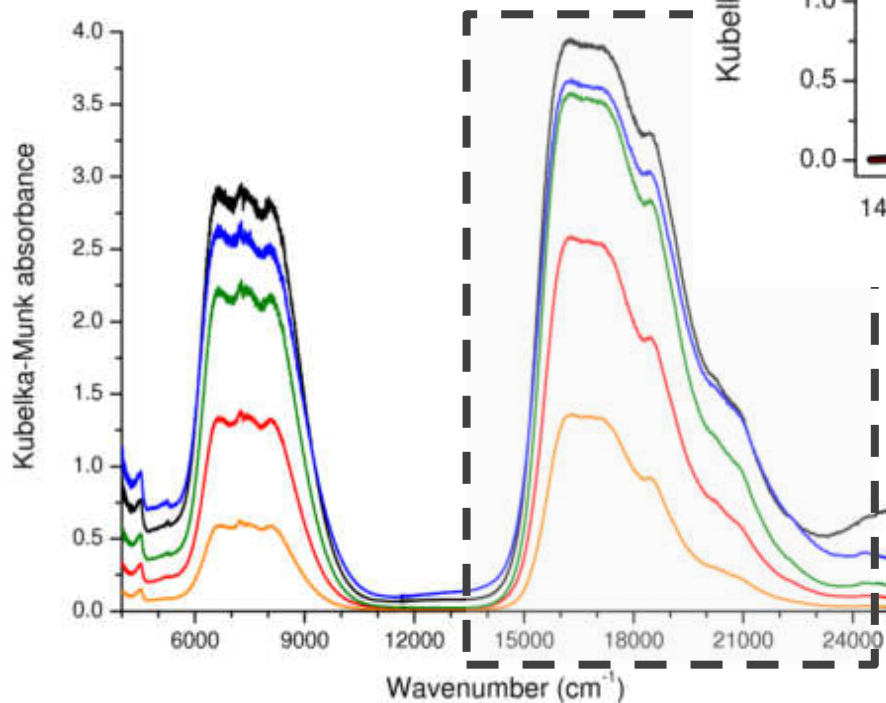
### e3. MELILITE

5500–10500  $\text{cm}^{-1}$ : the  ${}^4T_1({}^4F)$  transition is three-fold split  
+ some vibronic sidebands at higher energy



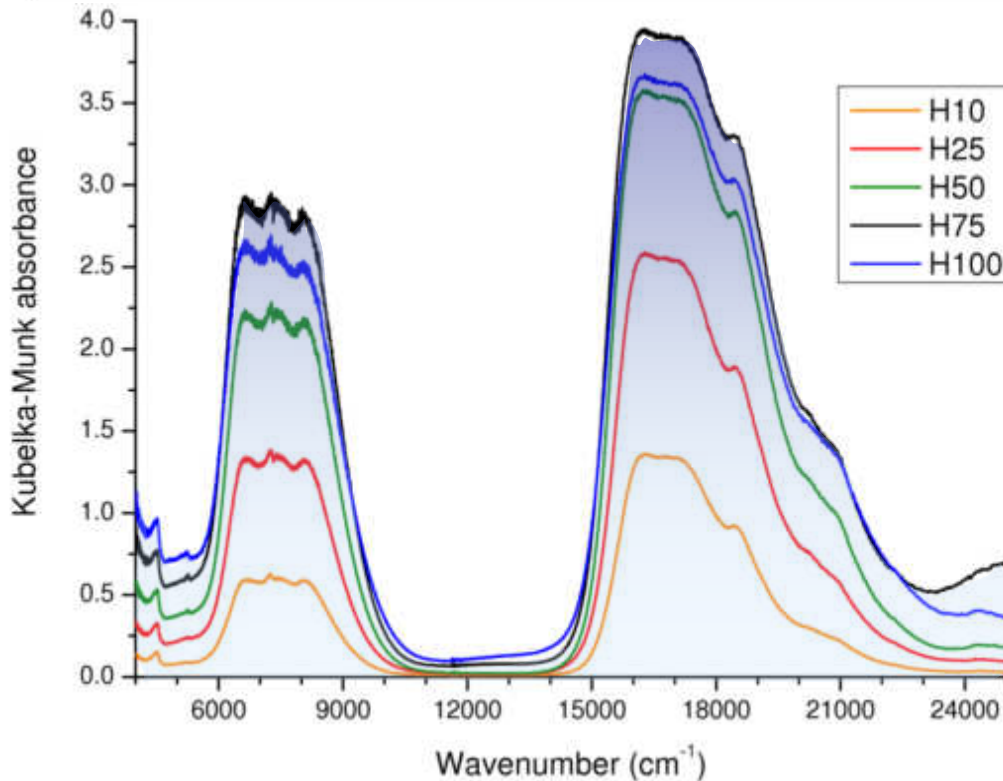
### e3. MELILITE

14000–25000  $\text{cm}^{-1}$ :  ${}^4T_1$  ( ${}^4P$ )  
transition split in three subbands  
+ several spin-forbidden  
transitions at high energy  
( $> 18000 \text{ cm}^{-1}$ )



### e3. MELILITE

Sample label	H10	H25	H50	H75	H100
Nominal cobalt content (apfu)	0.10	0.25	0.50	0.75	1.00
Crystal field strength, $10Dq$ ( $\text{cm}^{-1}$ )	4273	4270	4228	4230	4225
Racah $B_{35}$ parameter ( $\text{cm}^{-1}$ )	752	743	757	750	742
$\langle \text{Co-O} \rangle^{\text{local}}$ ( $\text{\AA}$ )	1.933	1.933	1.936	1.937	1.938



- $10Dq$  decreases  $\rightarrow$  local bond distances elongation;
- Racah  $B_{35} \sim \text{const}$   $\rightarrow$  no change in covalence degree of tetrahedral ligands.

# e3. MELILITE

Point Charge Approximation

$$10Dq = \text{const} \times \langle \text{Co-O} \rangle^{-5}$$

const: effective charge on the ligand (Q) and av. radius of the *d* orbital  $\langle r \rangle^4$

$$\langle \text{Co-O} \rangle_x^{\text{local}} = \langle \text{Co-O} \rangle_{x=1} \times [(10Dq_{\text{Co}})_{x=1} / (10Dq_{\text{Co}})_x]^{1/5}$$

Thus:

$$\varepsilon = (\langle \text{Co-O} \rangle_x^{\text{local}} - \langle \text{Zn-O} \rangle) \times (\langle \text{Co-O} \rangle - \langle \text{Zn-O} \rangle)^{-1}$$

Relaxation coefficient

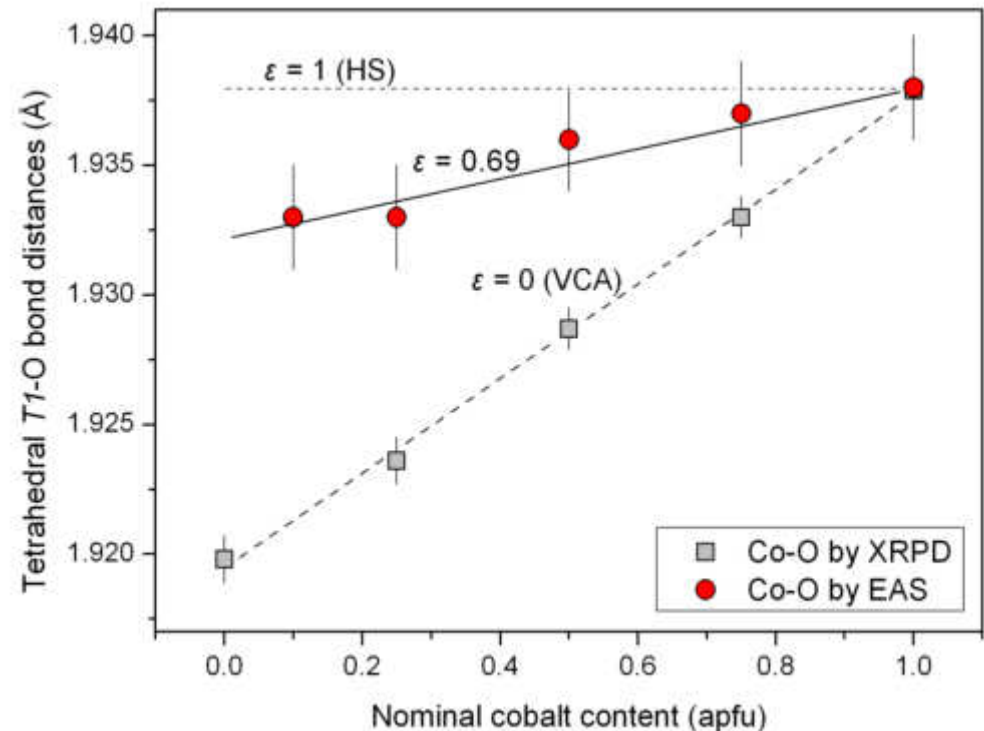
$$\varepsilon(\lim_{x_{\text{Co}} \rightarrow 0}) = 0.69,$$

far from the Vegard's law

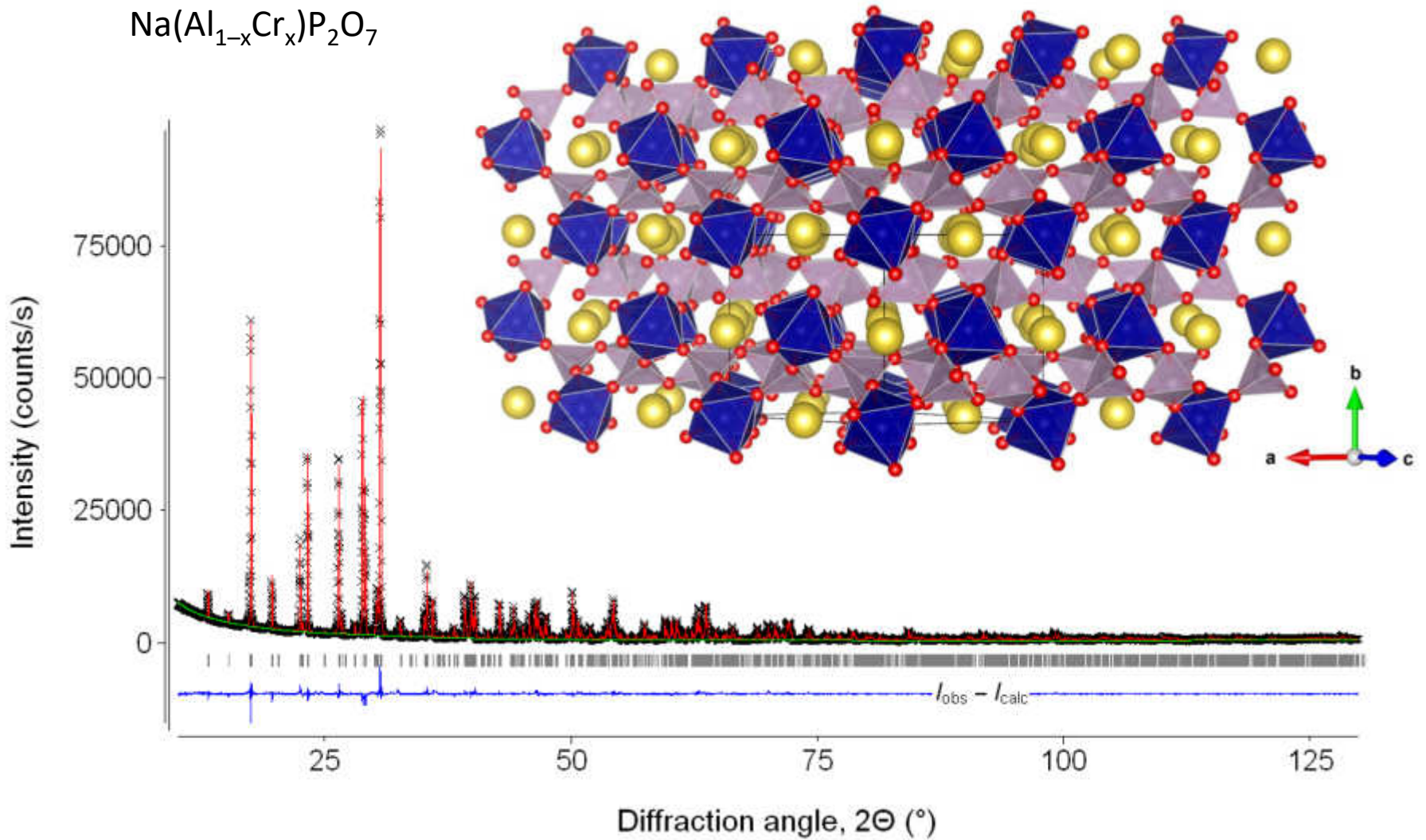
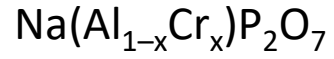
where the structural relaxation

is absent ( $\varepsilon = 0$ )

closer to the HS model ( $\varepsilon = 1$ ).



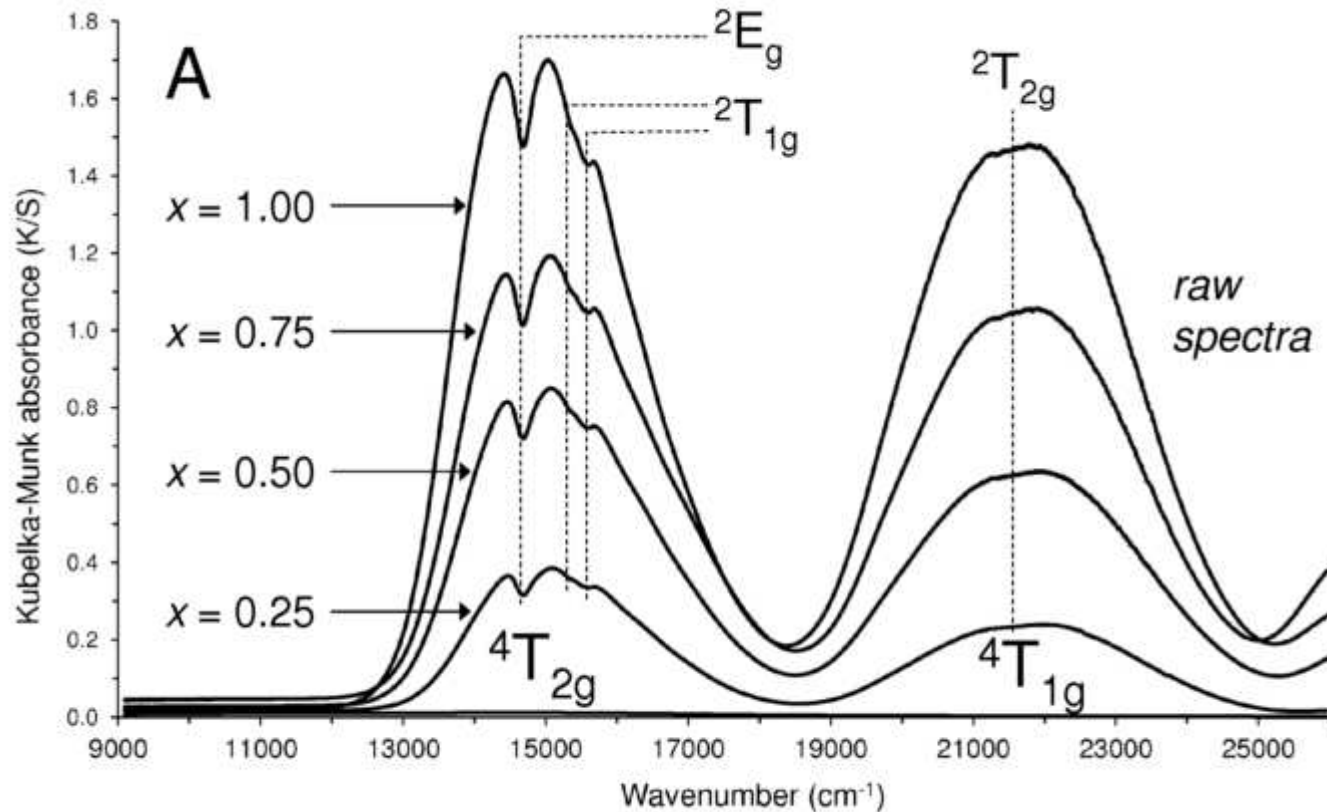
# e4. PYROPHOSPHATE



## e4. PYROPHOSPHATE

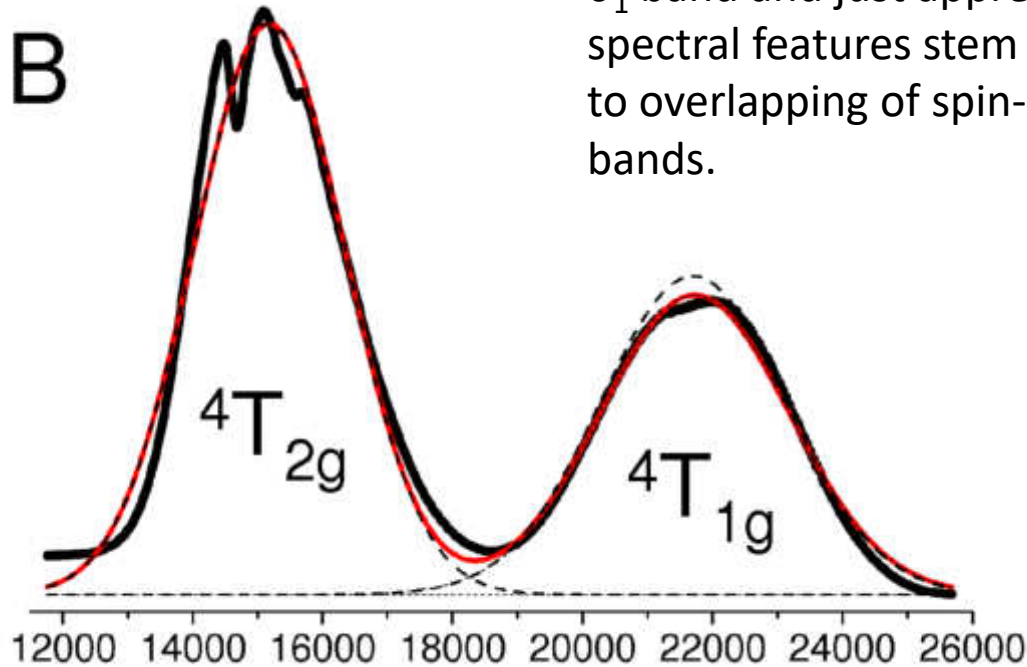
two strong absorbance bands attributed to the  $u_1$  and  $u_2$  transitions of  $\text{Cr}^{3+}$  in octahedral coordination ( $d-d$  electronic transitions):

- band absorbance increase with chromium content;
- band energy tiny shifted.



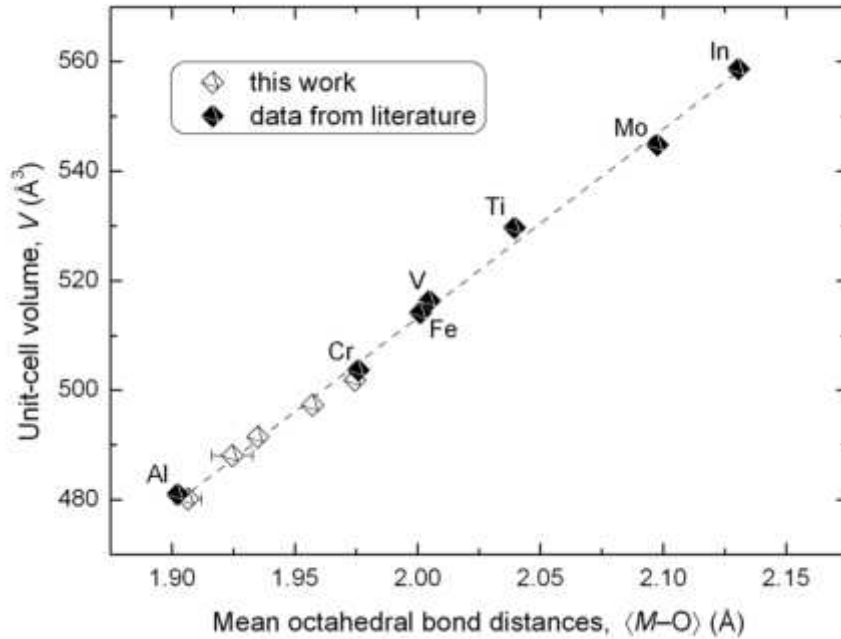
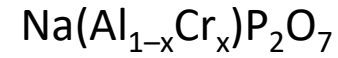
## e4. PYROPHOSPHATE

14,500-15,500  $\text{cm}^{-1}$  and 21,500-22,800  $\text{cm}^{-1}$ : spin-allowed transitions [ ${}^4T_{2g}({}^4F): \nu_1$  and  ${}^4T_{1g}({}^4F): \nu_2$ ].

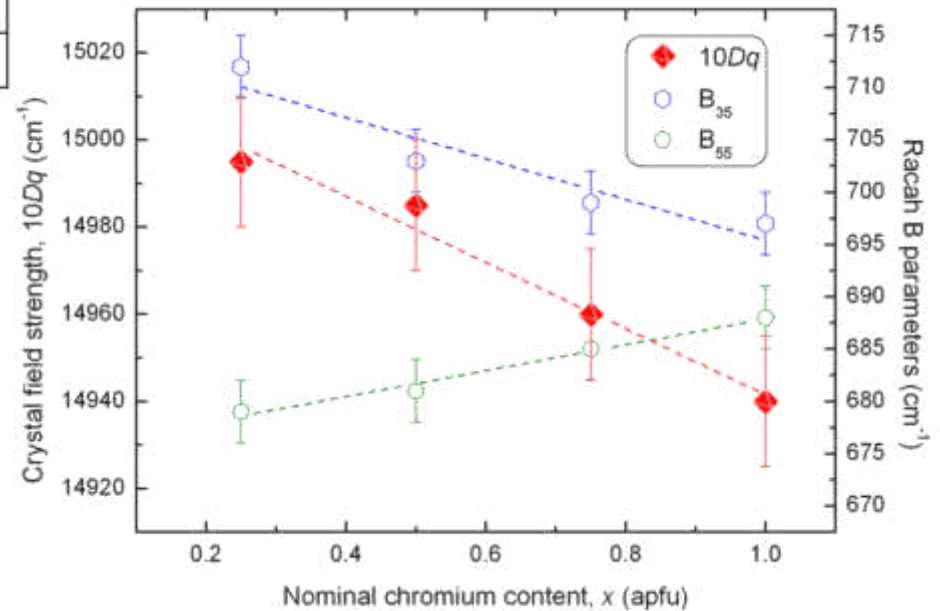


A distinctive feature in pyrophosphate spectra is the occurrence of a sort of notches: conspicuous on the  $\nu_1$  band and just appreciable on the  $\nu_2$  band. These spectral features stem from Fano antiresonance due to overlapping of spin-allowed and spin-forbidden bands.

# e4. PYROPHOSPHATE



- Lattice parameters follow the Vegard's law;
- Mean octahedral bond lengths scale linearly as a function of Cr increasing.



# e4. PYROPHOSPHATE

Point Charge Approximation

$$10Dq = \text{const} \times \langle \text{Cr-O} \rangle^{-5}$$

const: effective charge on the ligand (Q) and av. radius of the *d* orbital  $\langle r \rangle^4$

$$\langle \text{Cr-O} \rangle_x^{\text{local}} = \langle \text{Cr-O} \rangle_{x=1} \times [(10Dq_{\text{Cr}})_{x=1} / (10Dq_{\text{Cr}})_x]^{1/5}$$

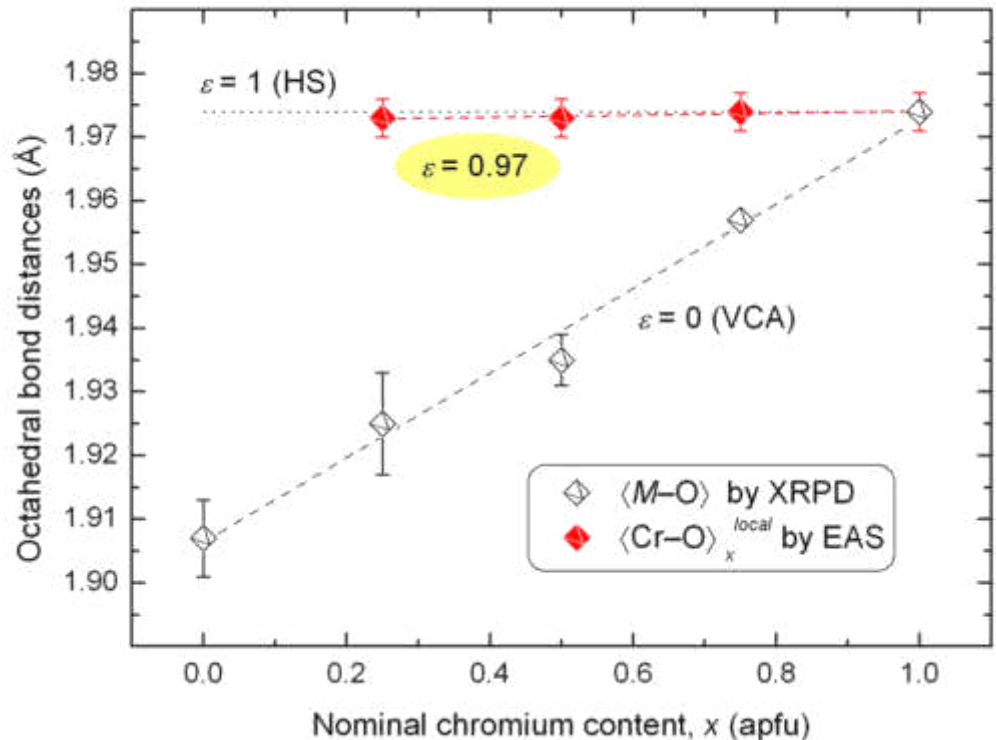
Thus:

$$\varepsilon = (\langle \text{Cr-O} \rangle_x - \langle \text{Al-O} \rangle) \times (\langle \text{Cr-O} \rangle - \langle \text{Al-O} \rangle)^{-1}$$

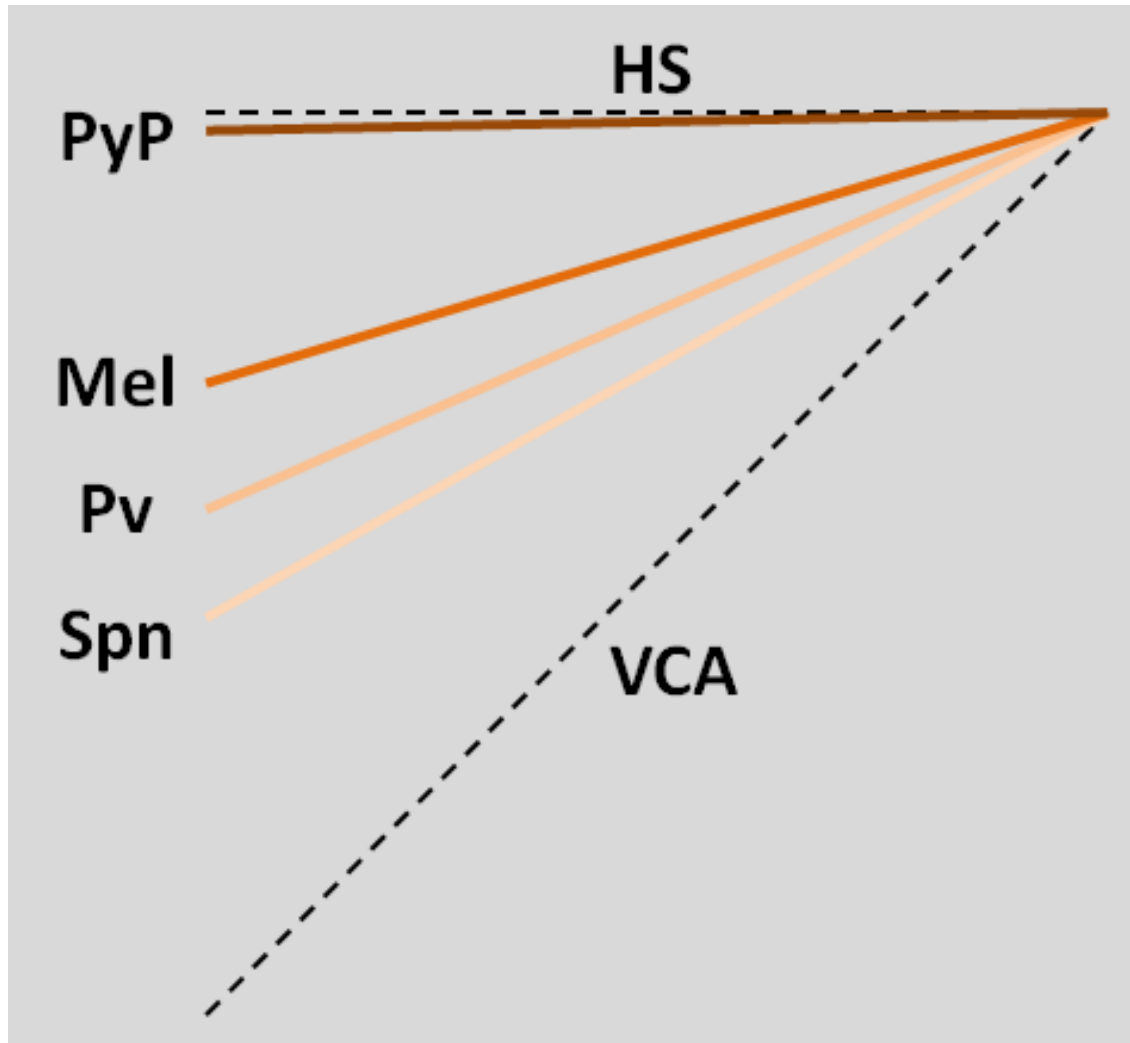
Relaxation coefficient

$$\varepsilon(\lim x_{\text{Cr}} \rightarrow 0) = 0.97,$$

very close to the HS model.



$\epsilon$



## f. REPLACEMENT OF CR<sup>3+</sup> FOR AL<sup>3+</sup> AT OCTAHEDRAL SITE

**2014.** Many studies were devoted to establish the structural relaxation along substitutional solid solutions of minerals and synthetic analogues. Among these studies, the most common and well-documented assessment of structural relaxation is that derived from the octahedral replacement of chromium for aluminium, calculated by means of local distances obtained through EAS, *e.g.*:  
garnet (Taran et al., 2004; Langer et al., 2004)  
perovskite (Cruciani et al., 2009; Ardit et al., 2016)  
spinel (Hålenius *et al.*, 2010)  
clinopyroxene (Taran *et al.*, 2011).

No works explored the possible processes linking in a systematic way the structural features to the relaxation occurring in a given crystal structure.

## f. REPLACEMENT OF CR<sup>3+</sup> FOR AL<sup>3+</sup> AT OCTAHEDRAL SITE

2012. (Urusov & Taran, 2012) from the Point Charge Approximation assumption

$$10Dq = 5/3 \times q \times \langle r^4 \rangle \times \langle Al_{1-x}Cr_x-O \rangle^{-5}$$

$$10Dq = \text{const} \times \langle Al_{1-x}Cr_x-O \rangle^{-5}$$

const: effective charge on the ligand (Q) and av. radius of the *d* orbital  $\langle r \rangle^4$

correlated the octahedral mean bond distances of several chromium minerals and synthetic analogues with their 10*Dq*

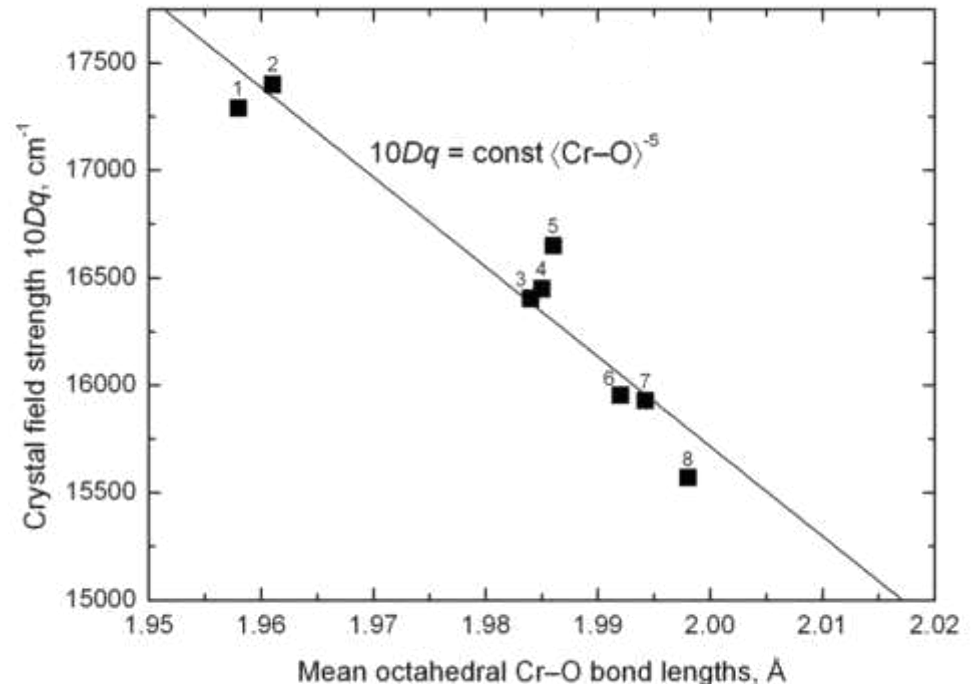
garnet (1, 4, 7)

KCr(SO<sub>4</sub>)<sub>2</sub> · 12H<sub>2</sub>O (2)

perovskite (3)

corundum (5)

pyroxene (6 and 8)

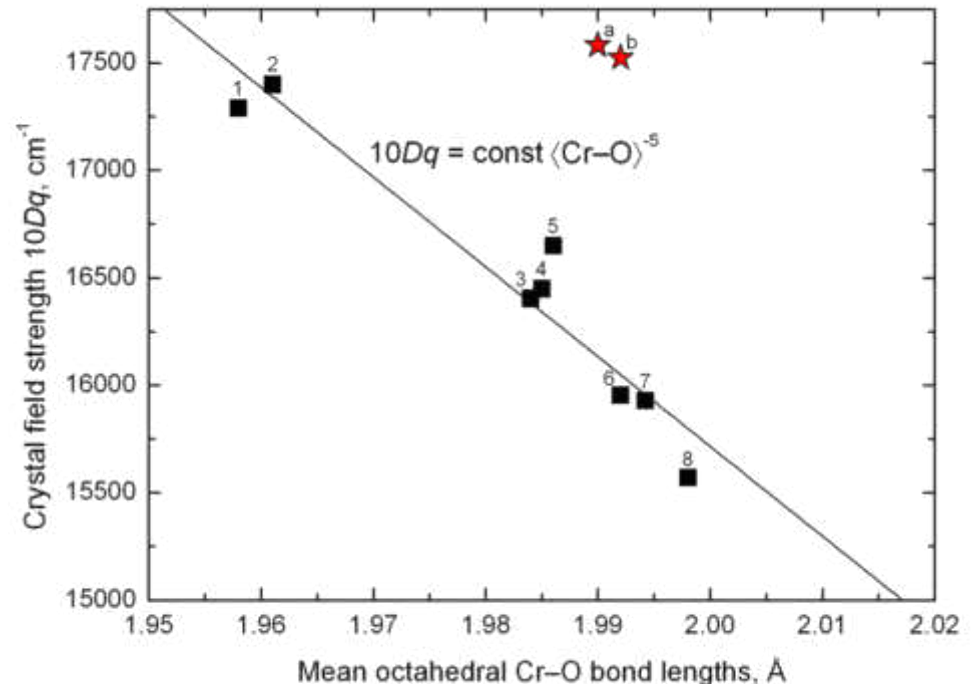


## f. REPLACEMENT OF $\text{Cr}^{3+}$ FOR $\text{Al}^{3+}$ AT OCTAHEDRAL SITE

**2012.** (Urusov & Taran, 2012) Although some slight deviation, the relationship seems satisfied the previous equations.

Nonetheless... whether spinel structure is taken into account...

garnet (1, 4, 7)  
 $\text{KCr}(\text{SO}_4)_2 \cdot 12\text{H}_2\text{O}$  (2)  
perovskite (3)  
corundum (5)  
pyroxene (6 and 8)  
spinel (a and b)



## f. REPLACEMENT OF CR<sup>3+</sup> FOR AL<sup>3+</sup> AT OCTAHEDRAL SITE

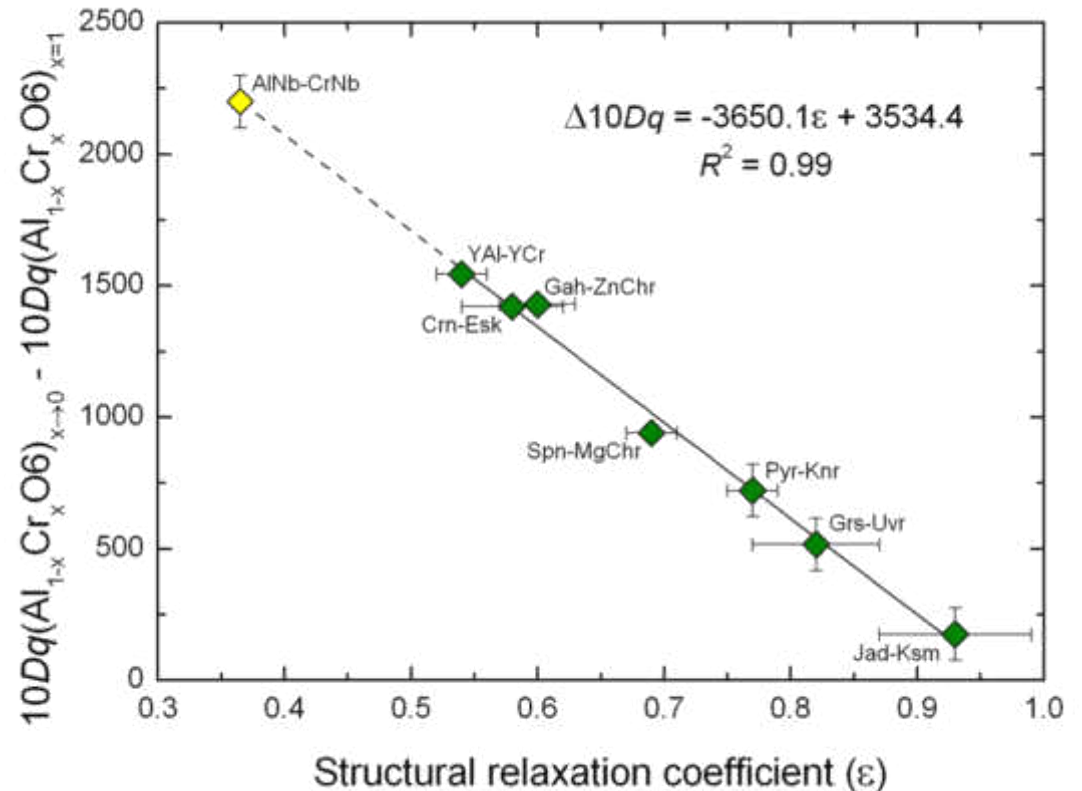
Label	Mineral Name	Structure-type: Formula	$10Dq$ (Al <sub>1-x</sub> Cr <sub>x</sub> O <sub>6</sub> ) <sub>x</sub>	Ref.	$\epsilon$	Ref.	$10Dq$ (Al <sub>1-x</sub> Cr <sub>x</sub> O <sub>6</sub> ) <sub>x→0</sub>	$10Dq$ (Al <sub>1-x</sub> Cr <sub>x</sub> O <sub>6</sub> ) <sub>x=1</sub>	$\Delta 10Dq$
YAl		perovskite: YAlO <sub>3</sub>	17867 $x = 0.02$	Cruciani <i>et al.</i> , 2009	0.54(2)	Cruciani <i>et al.</i> , 2009	17949	16405	1544
YCr		perovskite: YCrO <sub>3</sub>	16405 $x = 1$						
Crn	corundum	corundum: Al <sub>2</sub> O <sub>3</sub>	18100 $x \rightarrow 0$	Poole & Itzel, 1963	0.58(4)	Cruciani <i>et al.</i> , 2009	18100	16680	1420
Esk	eskolaite	corundum: Cr <sub>2</sub> O <sub>3</sub>	16680 $x = 1$						
Gah	gahnite	spinel: ZnAl <sub>2</sub> O <sub>4</sub>	18995 $x = 0.02$	Hålenius <i>et al.</i> , 2010	0.60(3)	Hålenius <i>et al.</i> , 2010	19005	17576	1429
ZnChr	Zn-chromite	spinel: ZnCr <sub>2</sub> O <sub>4</sub>	17576 $x = 0.998$						
Spn	spinel	spinel: MgAl <sub>2</sub> O <sub>4</sub>	18420 $x = 0.037$	Hålenius <i>et al.</i> , 2010	0.69(2)	Hålenius <i>et al.</i> , 2010	18458	17518	940
MgChr	Mg-chromite	spinel: MgCr <sub>2</sub> O <sub>4</sub>	17518 $x = 1$						
Pyr	pyrope	garnet: Mg <sub>3</sub> Al <sub>2</sub> Si <sub>3</sub> O <sub>12</sub>	18008 $x \rightarrow 0$	Taran <i>et al.</i> , 2004	0.77(2)	Taran <i>et al.</i> , 2004	18008	17286	722
Knr	knorringite	garnet: Mg <sub>3</sub> Cr <sub>2</sub> Si <sub>3</sub> O <sub>12</sub>	17286 $x = 1$						
Grs	grossular	garnet: Ca <sub>3</sub> Al <sub>2</sub> Si <sub>3</sub> O <sub>12</sub>	16590 $x = 0.005$	Langer <i>et al.</i> , 2004	0.82(5)	Langer <i>et al.</i> , 2004	16580	16064	516
Uvr	uvarovite	garnet: Ca <sub>3</sub> Cr <sub>2</sub> Si <sub>3</sub> O <sub>12</sub>	16230 $x = 0.745$						
Jad	jadeite	clinopyroxene: NaAlSi <sub>2</sub> O <sub>6</sub>	15740 $x = 0.03$	Khomenko & Platonov, 1985 Taran <i>et al.</i> , 2011	0.93(6)	Taran <i>et al.</i> , 2011	15743	15568	175
Ksm	kosmochlor	clinopyroxene: NaCrSi <sub>2</sub> O <sub>6</sub>	15568 $x = 0.982$						

# f. REPLACEMENT OF CR<sup>3+</sup> FOR AL<sup>3+</sup> AT OCTAHEDRAL SITE

2014.

$$\langle \text{Cr-O} \rangle_x^{\text{local}} = \langle \text{Al}_{1-x}\text{Cr}_x\text{-O} \rangle_{x=1} \times [ (10Dq_{\text{Cr}})_{x=1} / (10Dq_{\text{Cr}})_x ]^{1/5}$$

*the structural relaxation coefficients stemming from the substitution of Cr for Al in isostructural solid solutions inversely scale with the absolute difference between crystal field strengths of end-members  $\Delta 10Dq$*



## f. REPLACEMENT OF CR<sup>3+</sup> FOR AL<sup>3+</sup> AT OCTAHEDRAL SITE

The internal stress exerted by the Cr for Al replacement at octahedral sites provokes a strain, previously described in terms of structural relaxation and quantified with  $\epsilon$ , which can be related to the structural modifications, such as the volumetric cell compression due to regimes of high-pressure.

